Hippocampal cellular and network properties in a mouse model of metachromatic leukodystrophy

Dissertation

zum Erlangen des Doktorgrades (Dr. rer. nat.)

der Mathematisch-Naturwissenschaftlichen Fakultät

der Rheinischen Friedrich-Wilhelms-Universität Bonn

vorgelegt von:

Christina Baars

aus Olpe

Bonn, Februar 2017

Angefertigt mit Genehmigung der
Mathematisch-Naturwissenschaftlichen Fakultät
der Rheinischen Friedrich-Wilhelms Universität Bonn

Erstgutachter: Prof. Dr. Heinz Beck
Zweitgutachter: Prof. Dr. Michael Hofmann

Tag der Promotion: 30.Oktober 2017
Erscheinungsjahr: 2017

Erklärung

Hiermit erkläre ich, dass ich die vorliegende Dissertation selbständig angefertigt habe. Es wurden nur die in der Arbeit ausdrücklich benannten Quellen und Hilfsmittel benutzt. Wörtlich oder sinngemäß übernommenes Gedankengut habe ich als solches kenntlich gemacht.

Ort, Datum Unterschrift

❖ *There are some things you learn best in calm, and some in storm.* ❖

Willa Cather

Ich sage DANKE:
Meinem Doktorvater PROF. DR. HEINZ BECK, für die Möglichkeit und Unterstützung meine Dissertation in seinem Labor durchführen zu können, für seinen Rat & seine Zeit, die er meinem Projekt gewidmet hat.
PROF. DR. MICHAEL HOFMANN für die Übernahme der Begutachtung dieser Arbeit als Zoologe.
Meinem Betreuer DR. THORALF OPITZ für seine allgegenwärtige Unterstützung und sein offenes Ohr.
PROF. DR. HORST BLECKMANN und PD. DR. JOACHIM MOGDANS für einen unproblematischen Einstieg in das wissenschaftliche Arbeiten während meiner Diplomarbeit am Institut für Zoologie in Bonn.
PROF. DR. VOLKMAR GIESELMANN und DR. MATTHIAS ECKHARDT für die Bereitstellung meines Projektes und für die unkomplizierte Zusammenarbeit.
Der AG BECK für diese einzigartige und großartige Zeit, für den Rückhalt zu so manch schwieriger Zeit, für die Schokoladenpausen und die Freitage!
DR. OLIVER BRAGANZA, DR. HOLGER DANNENBERG und DR. ANDRÉ HEINEN für die gründliche und schnelle Korrektur.
Meinen ELTERN UND GESCHWISTERN für ihre stete Unterstützung, sowohl während meiner Studiumsjahre als auch während der Promotion und in der Korrekturphase.
OLIVIA für eine Freundschaft, die dem Labor entsprungen und ebendies lange überleben wird. Schlussendlich HOLGER, für alles das, was mich für die Arbeit gestärkt hat.

Abstract

The human disease of metachromatic leukodystrophy (MLD) is caused by a single or multiple allelic mutations within the gene locus of arylsulfatase A (ASA). This protein is a lysosomal enzyme catalyzing the degradation of sulfatides. A loss in ASA enzyme activity is accompanied by sulfatide accumulation within lysosomal compartments and plasma membranes. Besides galactosyl-ceramide sulfatide is one of the major lipids in oligodendrocytic myelin sheets. In patients suffering MLD, a clear genotype-phenotype correlation can be observed.Affected patients show more or less signs of demyelinisation and a loss in cognitive abilities dependent on clinical subtype and therefore enzyme activity.

To study neuronal cellular mechanisms and physiology in organisms with no ASA enzyme activity, a murine model for MLD has been established. Mice deficient in ASA accumulate sulfatides in glial cells, microglia, and neurons. Furthermore, they exhibit neuromotor deficits and mild behavioural disturbances. Invasive EEG recordings have revealed a marked cortical hyperexcitability, with episodes of spontaneous high-frequency (around 250 Hz) activity. Despite the description of these phenotypic abnormalities, a direct examination on neuronal excitability has been lacking.

In a first subset of experiments we were able to show that even in young mice at an age of 8-12 weeks sulfatide accumulations could be found within hippocampal and adjacent areas.

We have performed field potential, patch-clamp and sharp micrelectrode recordings in hippocampal slices to compare intrinsic, synaptic, and network properties of hippocampal principal cells from ASA-deficient mice and littermate controls. No apparent changes of passive or active membrane properties could be detected in CA1 or CA3 hippocampal principal cells of ASA-deficient mice. Despite the lack of changes in intrinsic excitability, we found evidence of altered network excitability. We recorded slow wave oscillations, so called sharp waves (SPW) in CA1 and CA3 hippocampal subfields, but found no differences in their incidence and amplitude between ASA-deficient mice and littermate controls in either subfield. However, the fraction of SPWs accompanied by high frequency oscillations, so called sharp wave ripple complexes (SPW-R), was significantly increased selectively in the CA3 pyramidal cell region of ASA-deficient mice. These results suggest that ASA deficiency causes a

selectively increased propensity to generate high frequency network activity in CA3. Examination of the excitation-inhibition balance via feedback stimulation revealed no changes in ASA-deficient mice. Additionally experiments in CA3 pyramidal cells were performed to provide an idea of altered presynaptic properties measuring miniature postsynaptic currents. This revealed that presynapses are functionally unaffected in ASA-deficient mice.

The reasons for an increase of high-frequency activity within CA3 subregion could not be identified via electrophysiological measurements of pyramidal cells within CA3 or CA1 region. Further investigations on interneuron activity and function have to be performed to clarify to what extent sulfatate accumulations in interneurons affect hippocampal network activity.

Contents

1. Introduction

In prokaryonts, such as bacteria, nearly all biochemical reactions take place within the cytoplasm. In contrast to prokaryotic cells, eukaryotic cells show cellular compartmentalization. This enables eukaryotic cells to generate separate, membrane delimited compartments for different metabolic processes, termed organelles. Consequently, each organelle contains a distinctive set of metabolic enzymes, metabolites and other signaling molecules (Alberts et al., 2004). Compartmentalization also enables specific determination of the composition of the medium inside organelles, such as the pH. A simple schematic diagram showing the major organelles common to all eukaryotic cells is shown in Fig. 1.1.

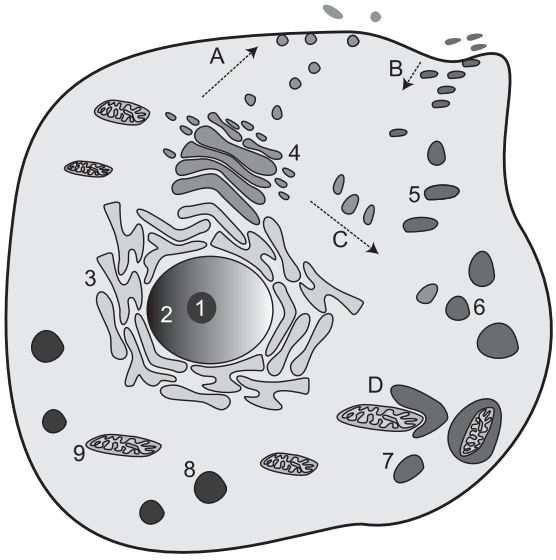

Fig. 1.1.: Scheme of an eukaryotic cell. Main organelles of the cell shown: nucleolus (1), nucleus (2), endoplasmatic reticulum (3), Golgi apparatus (4), endosomes (5), lysosomes (6), autophagosomes (7), peroxisomes (8), mitochondria (9).
A) exocytosis, B) endocytosis, C) transport of vesicles from Golgi apparatus to the endosomes/lysosomes, D) macroautophagy.

1.1. The lysosome

The lysosome of a cell is the sum of all lysosomal compartments. It ensures degradation of cellular content, cholesterol compartmentalization is particularly important in lysosomes. Lysosomes subserve multiple catabolic processes, such as protein degradation, inactivation of pathogenetic organisms, or cholesterol homeostasis. Lysosomes are also responsible to recycle antigens and phagocytosed material.
Catabolism within lysosomes is accomplished by a large family of acidic hydrolases, which are active at low pH, but not at normal intracellular pH. The family of acidic hydrolases contains nucleases, phosphatases, sulfatases, proteases, glykosidases, phospholipases, lysozymes, DNAses and many more, each of which catalyzes specific catabolic reactions (Fig. 1.2).

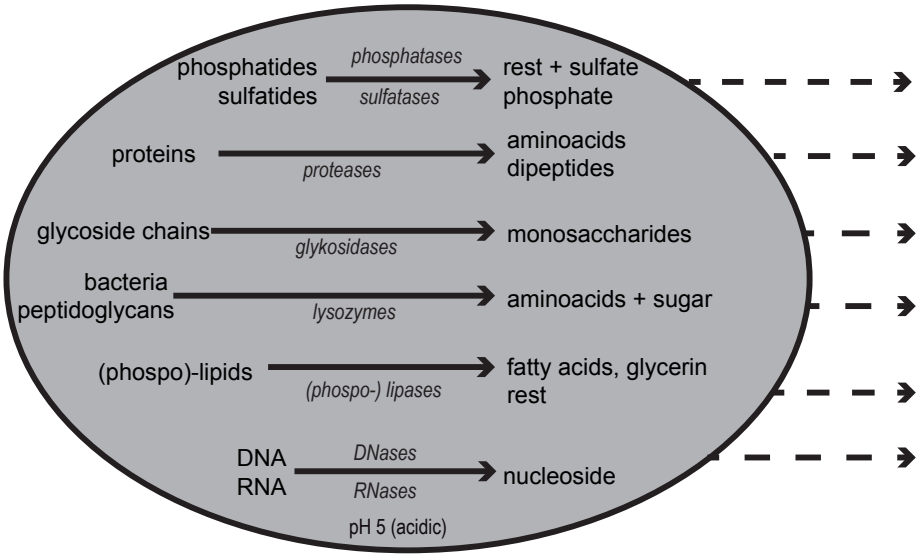

Fig. 1.2.: Scheme of a lysosome and its main catabolic enzymes. Degradation pathways of macromolecules within lysosomes and function of several lysosomal enzymes, while the needed acidic pH is present.

To maintain their acidic pH of ~ 5, lysosomal membranes contain vacuolar-type H^+-ATPases (V-ATPases) which mediate lysosomal proton import.
Cellular and foreign material destined for degradation reaches lysosomes via endocytosis, phagocytosis or autophagy.
Biogenesis of lysosomes involves maturation of early endosomes to form multivesicular

bodies (i.e., late endosomes), followed by fusion to the lysosomes and subsequent lysosome reformation. Accordingly, lysosomal compartments can vary in size (0.1 to 1 µm diameter). Lysosomal enzymes are specifically targeted to lysosomes. As for other cellular proteins, they are translated within the ER and posttranslationally modified within the Golgi apparatus. Subsequently, lysosomal enzymes are tagged with a phosphate at the C6 atom of a terminal mannose molecule (Man6-P). Within the trans-Golgi network membranes contain Man6-P-receptors which bind this tag. In a following reaction clathrin coated vesicles with lysosomal enzymes are formed. Those vesicles maturate by losing their coat to be able to fuse with late endosomes. By fusing with lysosomal compartments, which ensures an acidic environment, the lysosomal enzymes are activated.

1.1.1. Neuronal lysosomes

Besides general lysosomal function like degradation of molecules within cells of different origin, the endo- and lysosomal system in neurons have to overcome additional challenges.

In neuronal tissue, substantial signaling takes place at membranes. Thus, proper composition and maintenance of neuronal membranes is essential for maintained function in the CNS. Synaptic transmission between two neurons requires endo- and exocytosis. Additionally neurons are postmitotic cells, other cells regulate their size via division. Neurons regulate their size via membrane internalization and trafficking (Nixon and Cataldo, 1995).

Neuronal lysosomes are generally concentrated in the soma and are rare in axons (Tsukita and Ishikawa, 1980; Holtzman, 1989; Walkley et al., 2010). Within the soma they are arranged close to the Golgi apparatus and the proximal dendritic area (Parton et al., 1992). To overcome this extreme geometric asymmetry of neurons it demands endosomatic trafficking along the cytoskeleton. Therefore internalized vesicles from axonal sites travel retrogradely along microtubuli towards the soma similar to the retrograde transport of dendritic endocytic organelles internalized at the dendritic tree of the neuron (Parton and Dotti, 1993). At axonal terminals neurotransmitter release and receptor internalization need active endocytosis. At the nerve terminals, restricted regions called synapses, guarantee these processes by membrane internalization and the turnover of membrane components.

Well working endo-and lysosomal compartments are crucial for neuronal function and

alterations thereof lead to numerous diseases (Parton and Dotti, 1993). Many different inherited disorders involve defects in the synthesis, sorting and transport of lysosomal enzymes and most of them show a neuropathological phenotype (Nixon and Cataldo, 1995).

1.1.2. The lysosomal enzyme arylsulfatase A

The mRNA of the arylsulfatase A (ASA) gene is translated into a 507 amino acid long precursor protein which undergoes several post-translational modification within the ER. One modification that is important for sulfatase activity is a posttranslational oxidation of the cystein-69-formylglycine residue. The resulting enzyme is folded within the ER and afterwards transported to the Golgi apparatus. Within this cellular sorting machinery the enzyme is recognized as a lysosomal protein by phosphotransferase which tags the enzyme with a M6-P. Via a M6-P-receptor in a prelysosomal compartment, ASA is transported towards lysosomal compartments.

The ASA enzyme is involved in different catabolic processes within the lysosome. It is a housekeeping enzyme which shows variations of activity in different tissues in a small range. ASA is involved in sphingolipid-metabolism (Fig. 1.3), where it catalyzes the sulfatide breakdown into ceramides and a sulphate group (von Figura et al., 2001). Sulfatide is enriched in the myelin sheath and constitutes four to six percent of all myelin lipids (Norton and Cammer, 1984; Taylor et al., 2004). Together with its precursor substrate GalC it forms one third of all myelin lipids and due to its location within the outer leaflet of plasma membranes, nearly two thirds of myelin surface are built by sulfatides and GalC (Eckhardt, 2008). The activity of the ASA enzyme is increased during myelination processes and does not change after the myelination processes are finished.

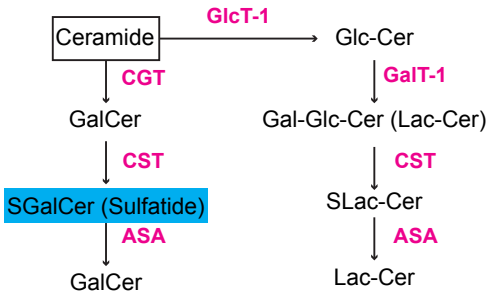

Fig. 1.3.: The Role of ASA in the degradation of sulfatides to achieve functional ceramides. Modified acc. to Eckhardt et al. (2007).

1.2. Lysosomal Storage Diseases

The group of lysosomal storage diseases (LSDs) comprises more than 50 diseases (Grabowski, 2012), which are due to impaired lysosomal function. These disorders are caused by mutations in genes encoding for lysosomal enzymes or transporters (Tab. 1.1). Most of these disorders are inherited autosomal recessively (Hers, 1965). A few, like Morbus Fabry are X-linked recessively inherited. Such diseases occur with an incidence of 1:40,000 to 1:4 Mio (Tab. 1.1).

classification	incidence	affected protein	therapy
lipidoses	one to		
M. Krabbe	$100x10^3$	galactosyl-cerebrosidase	stem cell
MLD	$190x10^3$ *	arylsulfatase A or saposin B	ERT, stem cell
M. Gaucher	$90x10^3$	β-glucocerebrosidase	ERT, SDT
M. Fabry	$100x10^3$ **	α-galactosidase A	ERT
M. Niemann-Pick A+B	$40x10^3$ ***	acid sphingomyelinase	none in human
M. Niemann-Pick C .	$150x10^3$ **	lipid transport enzymes	none
GM_1 -Gangliosidose	N.A.	β-galactosidase	none
Galactosialidoses	$2000x10^3$ *	β-galactosidase + neuraminidase	none
GM_2 -Gangliosidose $\diamond$	$320x10^3$***	β-hexosaminidase A	stem cell
GM_2 -Gangliosidose ∞	$310x10^3$	β-hexosaminidase A+B	stem cell
oligosaccharidoses	one to		
α-Mannosidose	$1000x10^3$	acid, lysosomal α-mannosidoses	nothing safe
Sialidose	$4000x10^3$	α-N-acetylneuraminidase	none
mucopolysaccharidoses	one to		
7 distinct clinical types	$25x10^3$***	11 different proteins ∇	stem cell, ERT

Tab. 1.1.: Classification of lysosomal storage diseases via effected proteins and avalable therapies. Abbreviations used as follows: M.= Morbus, $\diamond$= M. Tay-Sachs; ∞ = M. Sandhoff, ERT = enzyme replacement therapy, stem cell = hematotopic stem cell therapy, SDT = substrate depression therapy, *= only Germans, **= of live birth, ***= in special populations, ∇= absence or malfunctioning of certain enzymes needed to break down molecules called glycosaminoglycans; Modified acc. to Hoffmann and Grau (2004); Meikle et al. (1999); Poupetová et al. (2010); NIH Publication No 03-5115 (2014).

The group of LSDs is characterized by progressive accumulation of nondegraded macromolecules within the cell. A loss of lysosomal function is most often caused by lysosomal hydrolase dysfunction. However, LSDs may also be the result of an impaired transport of molecules into lysosomal compartments (i.e. Niemann Pick C). Moreover, some LSDs are caused by impaired delivery of key lysosmal components towards lysosomes like the impairment of the enzyme N-acetylglucosamine 1-phosphotransferase in

mucolipidosis II which is responsible for the M-6-P tag for lysosomal enzymes (Dierks et al., 2009; Huizing et al., 2008; Ballabio and Gieselmann, 2009).

1.2.1. Lipidoses

A subgroup of lysosomal storage diseases is the group of lipidoses, a group of inherited metabolic disorders which are also known as lipid storage disorders. Patients suffering these disorders store harmful amounts of fatty substrates within various cells and tissues. Those patients either do not produce enough enzymes to break down those lipids or produce enzymes which do not work properly (NIH Publication No 05-2628, 2005).
Lipidoses do not show common phenotypes or symptomatology. Whereas most of them show a neurological phenotype, others do not affect the functionality of the CNS or PNS at all. All diseases offer different subtypes dependent on severity and age of onset. To give an overview of the symptomatology spectrum of single diseases, I will describe a number of key lipidoses in more detail within the following section.
Patients suffering Morbus Gaucher can be divided into 3 clinical subtypes: nonneuropathic, acute infantile neuropathic and chronic neuropathic. The nonneuropathic type is the most common form and patients show first signs early in life or even in young adulthood. The CNS is not affected and patients may live well into adulthood. Children suffering the second type show symptoms at three month of birth and die before the age of two. These children show extensive and progressive brain damage, spasticity, seizures and other neurological impairments. The third form can begin at any time in child- or adulthood and also show severe neurological impairments (NIH Publication No 05-2628, 2005).
Patients suffering Niemann-Pick can also be classified into one of four subtypes (A-D). Not all subtypes show brain involvement or even severe brain damage (type A). Patients suffering Niemann-Pick type B show peripheral neuropathy but generally the brain is not affected (NIH Publication No 05-2628, 2005).
The onset of Fabry disease is in childhood and patients show a buildup of fatty material within the nervous system. They often suffer burning pain in arms and legs but their lifespan is not generally shortend.
The group of gangliosidoses consist of GM1- and GM2-gangliosidoses. In GM1 patients acidic lipids are accumulated in the nerve cells of CNS and PNS. This disease can be divided into three different subtypes. In early infantile GM1 children show severe neurodegeneration, seizures and develop deafness and blindness until the age of one. They

often die before they reach the fourth year of age. Late infantile patients develop first symptoms between their second and third year, show ataxia, seizures and dementia and die early. Patients suffering the adult form show early symptoms between three to 30 years and develop neurological complications which are less severe than those in the other two subtypes.

The GM2-gangliosidoses can be diveded into Tay-Sachs and Sandhoff disease. Both types show first symptoms at an age of six months. Patients suffering Tay-Sachs show deafness, blindness and a loss of mental ability and most often develop seizures within the second year. They die at an age of around four. Children suffering Sandhoff disease show severe neurological symptoms like progressive deteroriation of CNS, early blindness, seizures, spasticity and macrocephaly. Those children most often die before they reach the fourth year.

Most patients suffering Morbus Krabbe develop early symptoms with six months, but in some patients the onset occurs in adulthood. Symptoms like deafness, myoclonic seizures, paralysis and demyelinisation of nerves are due to the buildup of undigested fats which affect the growth of the myelin sheath.

Besides these common lipidoses a few others exist. Those will briefly be listed here: Farbers disease, Wolman disease and cholesteryl ester storage disease.

Since parts of the lysosomal role for cell function were understood in the late 1950s (de Duve, 1963) today a more functional understanding of LSDs like sphingolipidoses has been achieved. Effects have been observed that are due to accumulation of the primary lipid catabolites. However, the disturbances in cellular metabolic processes are not confined to lipid catabolism in most lipidoses.

Accumulation of catabolites within cells can modulate specific intracellular signaling pathways. For instance, psychosine accumulations in M. Krabbe can bind as ligands to intracellular receptors like the TDAG8 receptor (Hannun and Bell, 1989; Ballabio and Gieselmann, 2009), which mediates inhibition of cytokinesis (Tanaka and Webster, 1993; Jatana et al., 2002; Zaka and Wenger, 2004; Ballabio and Gieselmann, 2009). Similarly, changes in receptor response due to a change in receptor sensitivity as well as changed subcellular receptor localization has been demonstrated in Niemann-Pick disease type C for a member of the toll like receptor (TLR) family the TLR-4 (Vainio et al., 2005; Suzuki et al., 2007). This receptor is important for the regulation of the innate immune response in microglia (Ballabio and Gieselmann, 2009). In Niemann-Pick, cytokine production is enhanced and an inflammatory component of the disease arises.

Intracellular Ca^{2+} increases, which are a key modality of intracellular signaling, have also been shown to be altered in some LSDs. A reduced re-uptake of Ca^{2+} into the ER could be seen in GM1- and GM2-gangliosidoses (Nguyen et al., 2002). In M. Gaucher an increase of the intracellular Ca^{2+}-level triggers a variety of responses and lead to a neurotoxic reaction and neuronal cell death (Ballabio and Gieselmann, 2009; Korkotian et al., 1999). Within the ER two ligand-gated Ca^{2+}-channels which release Ca^{2+} into the cytoplasm are known (Ballabio and Gieselmann, 2009), the InsP3- and the ryanodine-receptor. The ryanodine receptor is known to be controlled by cytoplasmic Ca^{2+}-levels. Increased Ca^{2+} opens the receptor and results in further Ca^{2+} release from the ER. Within M. Gaucher the accumulation of glucosylceramide sensitizes this receptor to agonist mediated Ca^{2+} release from the ER. Glutamate stimulation of neurons with accumulated glucosylceramide might induce an increase in cytosolic Ca^{2+} either by opening of ionotropic Ca^{2+}-permeable glutamate receptors or through the increase of InsP3by activation of metabotropic receptors. In both cases the Ca^{2+} increases and triggers Ca^{2+} induced response to glutamate. This enhanced glutamate toxicity results in an increased rate of neuronal apoptosis and neurodegeneration (Ballabio and Gieselmann, 2009; Korkotian et al., 1999).

Additionally secondary effects can occur via altered composition of plasma membranes. Plasma membranes often contain specialized microdomains, so called lipid rafts, which are characterized by a high amount of sphingolipids, such as sulfatides (Simons and Ikonen, 1997; Simons and Toomre, 2000) and cholesterol (Simons and Vaz, 2004).Due to an increase of non-degraded sulfatides, an accumulation within lipid rafts could be the result. Lipid rafts are important for trafficking of ion channels and receptors (Simons and Toomre, 2000). It could also affect localization or the transport of lipid raft associated membrane proteins in neuronal membranes (Eckhardt, 2008; van Zyl et al., 2010).

In a mouse model of M. Gaucher altered lipid biosynthesis was reported (Kacher et al., 2007). As an important cellular process, autophagy is disturbed in many LSDs (Nishino, 2006; Lieberman et al., 2012).

As another aspect of altered cellular processes due to accumulation of macromolecules intracellular trafficking, including endocytosis, could be seen in LSDs. Intracellular sorting events could also be altered, such as membrane flow and receptor-trafficking. In a mouse model of MLD the endocytosis of the M6-P- and transferrin-receptor is en-

hanced, while the recycling rate of both seems to be reduced (Klein et al., 2009).

In summary LSDs are often accompanied by neuronal phenotypes due to lysosomal involvement in vesicle maturation, synaptic release and a disruption of lysosomal trafficking along the axons (Luca et al., 2005).

1.2.2. Sphingolipidoses

Sphingolipidoses are a subgroup of lipidoses and refer to a metabolic dysfunction in sphingolipid metabolism (Fig. 1.4).

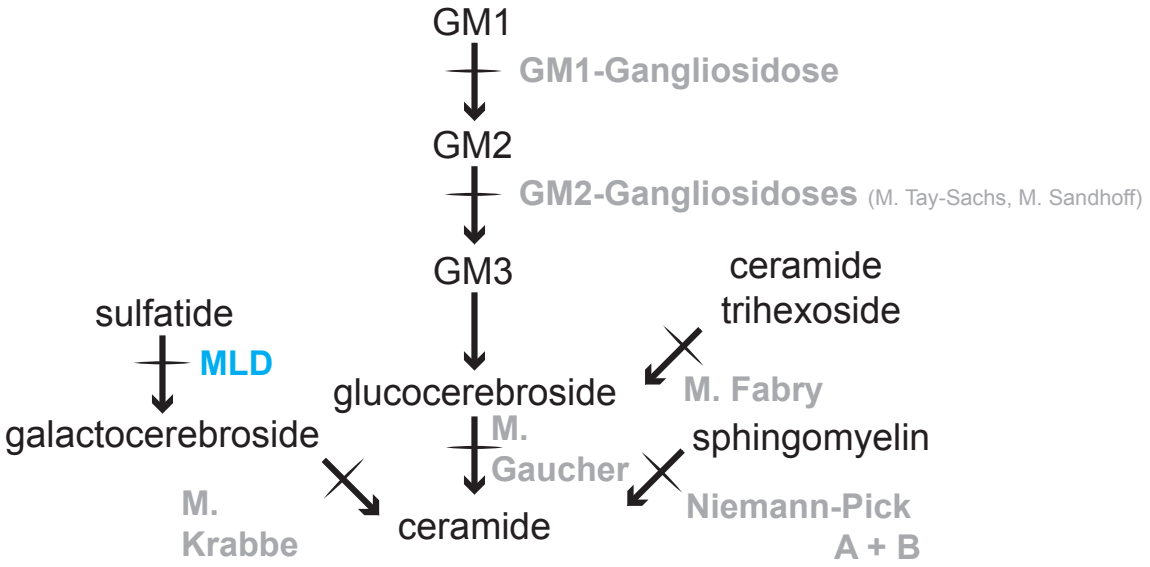

Fig. 1.4.: Sphingolipidoses and affected enzymes in sphingolipid metabolism. Modified acc. to Huckfinne (2010).

The main members of this group are M. Niemann-Pick, M. Fabry , M. Krabbe, M. Gaucher, M. Tay-Sachs and metachromatic leukodystrophy (MLD). The proteins which are affected in these diseases are listed in Table 1.1. M. Krabbe and MLD are also classified as leukodystrophies. This terminology is descriptive and has developed due to the pronounced demyelination and white matter defects in these disorders. It should be noted that the family of leukodystrophies also contain other white matter disorders with very different etiology.
Myelin consists of proteins and lipids. The major proteins are myelin basic protein

(MBP), proteolipid protein (PLP) and myelin and lymphocyte protein (MAL). The major lipids are galactosyl-ceramide (GalC) and sulfatide and are abundant in oligodendrocytes (Yaghootfam et al., 2005).
In M. Krabbe, a disease due to a deficiency or malfunction of galactosyl-ceramidase the amount of GalC is increased, which causes an accumulation of psychosine leading to a destruction of oligodendrocytes. Myelin sheaths of fibers within peripheral and central nervous system are destroyed. Up to 70 different mutations within the gene locus of GalC have been found and a single mutation can lead to a functional loss. This severe neurological disease occurs 1-2 per 100,000 live births (Kohlschütter, 2013).Clinical symptoms of sphingolipidoses differ due to affected lysosomal enzyme and accumulated macromolecules. Since the main topic of this thesis is a mouse model of metachromatic leukodystrophy, the characterstics of this human disorder will be described in more detail in the following.

1.2.3. Metachromatic Leukodystrophy

In the early 1960s Austin et al. reported the clinical picture of MLD together with a deficiency of ASA (Austin et al., 1964). Since then, MLD has been reported to occur between 1 in 40,000 to 1 in 190,000 live births (Gustavson and Hagberg, 1971; Heim et al., 1997; Poorthuis et al., 1999). In most cases, loss-of-function mutations in the human ASA gene are found, which encode the lysosomal enzyme ASA. The functional deficiency in this enzyme leads to an increase of intracellular sulfatide accumulation.

ASA gene and protein

The ASA gene locus has been identified to be on the arm of chromosome 22 band q13 (Kreysing et al., 1990). The human disease of MLD is caused by a single or multiple allelic mutations within this gene locus. The ASA gene consists of eight exons, together spanning 3.3 kbp (Kreysing et al., 1990). The promoter region shows several GC boxes which might act as interaction sites with transcription factor Sp1. Due to polymorphisms and alternative splicing, three different transcripts are the product of transcription processes. The primary transcript is a 2.1 kb-long mRNA which is used for the synthesis of the ASA polypeptide. The other two mRNAs are either 3.7 kb or 4.8 kb long (Gieselmann, 1995).

Within the coding sequence up to 110 different mutations have been reported which can lead to ASA deficiency (Gieselmann, 2008). Most of the occurring mutations are only found in single patients. In Europeans three more common ASA gene mutations have been identified (Tab. 1.2) (von Figura et al., 2001).

mutation characterization	specific description	incidence (%)
splice donor site mutation of exon 2/ intron 2	459+1A → G	15-43
amino acid substitution	Pro426 → Leu	16-25
amino acid substitution	Ile179 → Ser	12

Tab. 1.2.: The Table shows the occurring European ASA gene locus mutations a precise description and their incidence in European MLD patients. Mod. acc. to von Figura et al. (2001).

Some of the ASA gene mutation have been reported to segregate within certain ethnic groups. The most frequently occurring mutations are listed in Table 1.3.

ethnical group	mutation within ASA gene
Alaskan Eskimo and Navajo Indian	single splice donor site mutation
Lebanese	Thr274 → Met substitution
Habbanite Jews	Pro377 → Leu substitution (homozygous)
Japanese	Gly99 → Asp substitution
Arabs	1:8.000 newborns suffer of 5 different mutations

Tab. 1.3.: The Table shows the occuring ASA gene locus mutations a precise description and their incidence in MLD patients of different ethnic groups. Mod. acc. to von Figura et al. (2001).

While most patients with MLD have defects in ASA, some patients have been reported to exhibit mutations in the prosaposin gene (Shapiro et al., 1979; Rafi et al., 1990; Deconinck et al., 2008; Sandhoff et al., 2001; Landrieu et al., 1998). Proteolytic cleavage of this protein gives rise to four different saposins (A-D) (Kretz et al., 1990). Saposins or sphingolipid activator proteins are crucial co-factors for the lysosomal degradation of sphingolipids (Wenger et al., 2013). Since the first description of this deficiency by Shapiro et al. (1979) only a few patients have been described (von Figura et al., 2001).

All ASA gene mutations can be attributed to three major mutation types. Splice site mutations have only been reported four times and thereby represent uncommon muta-

tions. Deletions of single bases occur in exon 1 and 2 and lead to a reading frame shift. Other deletions of single or multiple bp could lead to a frame loss or a frameshift. At least six different deletional mutations, have been reported. Besides the reported deletional mutations a high number of amino acid substitutions have been reported. These mutations occur all over the gene but seem to be clustered within exon 2 (von Figura et al., 2001). These amino acid substitutions have been reported to have differing impact on ASA enzymatic function. The above mentioned amino acid substitution Pro426 → Leu in Europeans does not directly impair the enzymatic activity of ASA. Rather, a loss of lysosomal stability causes rapid degradation of the enzyme. A number of further amino acid substitutions lead to a retention of the enzyme within the ER (von Figura et al., 2001). A further mutation (D335V) causes loss of a negatively charged amino acid residue, which leads to an incorrectly folded enzyme and a loss of enzymatic activity (von Figura et al., 2001). A reduced activity of cysteine protein kinase might lead to a normalized sulfatide metabolism and is discussed as a possible therapy (von Figura et al., 2001).

Clinical subtypes of MLD

In MLD a clear genotype-phenotype correlation can be observed. The above mentioned mutations can be classified into those that do not allow the synthesis of any functional enzyme and those that cause reduced enzymatic activity. Homozygosity for alleles with complete loss of function (null alleles) cause severe forms of MLD with onset in late infancy. Conversely, the presence of two alleles leading to residual enzymatic activity (R alleles) causes MLD with adult onset. Finally, patients with a copy of a null and an R allele present with a juvenile onset form MLD. Even in the less severe adult forms of MLD, the ASA activity has been found to be only about 2-5 % of normal levels (von Figura et al., 2001).

A total of 75 % of patients suffering from MLD show either late infantile or juvenile form, 25 % suffer from adult MLD (Heim et al., 1997; Lugowska et al., 2005; Poorthuis et al., 1999). The most severe form, the late infantile MLD, occurs 1 in 170,000 times in Germany (Zlotogora et al., 1995).

The following section will characterize the clincial features of these three disease phenotypes with differing age of onset in more detail. Children with late infantile MLD show first signs of impaired neurological function between half a year and four years after birth Hagberg (1971) divided this form into four clinical stages. The first stage lasts a few

months up to one year and is characterized by a hypotonia of all four limbs. The gait becomes unsteady and the child requires support to stand or walk. Within this time, deep tendon reflexes may be diminished or absent and progressive polyneuropathy develops. The second stage lasts a few months and is accompanied by the inability to stand, mental regression and deteriorated speech, greyish discoloration of macula, nystagmus, ataxia and truncal titubation. The muscle tone is increased. The third stage shows gradual involvement of the pyramidal system, spastic tetraplegia, pathologic reflexes, extensor plantar reflexes and the child becomes bedridden. In this stage, swallowing deficits, as well as airway obstruction can develop. Nearly 25 % of the children develop epileptic seizures. In the last stage of the disease, the children lose all contact to their environment, become blind and decerebrate. This stage can last several years and leads to death (von Figura et al., 2001). After the first clinical symptoms occur, children suffering late infantile MLD live for on average approximately five years (Fig. 1.5).

Fig. 1.5.: A Belgium girl (†January 2014) shows the severe outcome of late infantile MLD. Photos used with permission of the MLD Foundation (MLD Foundation, 2013).

Children suffering juvenile MLD show first clinical symptoms at an age of four to sixteen years. These symptoms include reduced cognitive and intellectual abilities with impaired school performance and speech. Additional symptoms may include gait disturbances and incontinence. Other prevalent symptoms are behavioral and emotional disturbances (von Figura et al., 2001). Within the first year after disease onset, the patients lose the ability to walk, and may show spastic paresis and cerebellar ataxia. In some cases, extrapyramidal features are predominant. Half of the patients develop

optic atrophy and half of them show seizures. Finally, the patients become bedridden and have to be fed through a tube. The majority of patients suffering this subtype die before they reach an age of 20 years (von Figura et al., 2001).
The adult subtype of MLD covers all patients suffering ASA deficiency with onset of clinical symptoms older than 16 years. Single cases occur with a much later age of onset within the second half of life (Bosch and Hart, 1978). Affected patients often show a gradual decline in intellectual performance, sometimes accompanied by labile emotional states, memory deficits, disorganized thinking, behavioral abnormalities as well as psychiatric symptoms like hallucinations and delusions. Motor symptoms such as clumsiness and progressive spastic paresis have been reported. Patients can additionally suffer of urine and fecal incontinence (von Figura et al., 2001).
Whereas signs of peripheral neuropathy are absent in many cases and epileptic seizures occur less often optic atrophy and signs of bulbar dysfunction have been reported (Gieselmann, 1995). At the final stage patients reach a vegetative state. After onset of the first clinical stages the patients may live on for years up to several decades (von Figura et al., 2001).
The diagnosis of the different subtypes of MLD is based on the observed clinical features. Additionally, diagnosis can be aided by magnetic resonance imaging (MRI) (Fig. 1.6), in which primary features of MLD are present before clinical signs appear. The MRI pictures reveal symmetric decreases of cerebral white matter and with ongoing progress, significant enlargements of the ventricels is observed (von Figura et al., 2001). To distinguish MLD from other disorders like multiple sclerosis (MS) and M. Krabbe a reduced ASA enzyme activity can be determined by sulfatides degredation essays performed either in cultured fibroblasts or peripheral blood leukozytes (Kudoh and Wenger, 1982; von Figura et al., 2001).

Neuronal pathology

The adult form was first described by Alzheimer (1910) who discovered sulfatide accumulation in both gray and white matter of neuronal tissue using post-mortem methylene blue and eosine staining. Due to this characteristic staining pattern the term metachromatic was coined for sulfatide-accumulating tissues. In the following years metachromatic material was also found within non-neuronal tissue (Witte, 1921), for instance in liver, kidney and heart (von Figura et al., 2001; Sandhoff et al., 2002). Furthermore, a metachromatic staining pattern and clinical symptoms of the adult MLD form has been

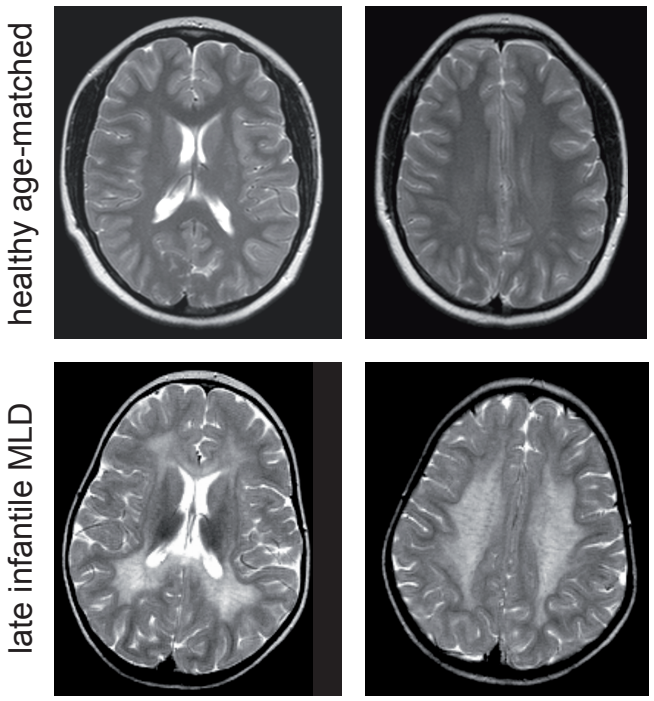

Fig. 1.6.: T2 weighted axial MR images height of lateral ventricles (left) and height of the centrum semiovale (right). Image of a healthy age-matched (upper images) and a child suffering late infantile MLD (lower images). A typical broad signal increase of the central white matter with the MLD-typical tigroid pattern can bee seen. The Pons is also already involved. Pictures courtesy of Inge Kraegeloh-Mann.

described also in late infantile and juvenile patients (von Figura et al., 2001).
A striking feature of MLD in human patients of all subtypes is demyelination within the peripheral and central nervous system. In the CNS, the pronounced white matter degeneration has prompted the clinical designation of MLD as a leukodystrophy (originating from the Greek leuko 'white', dys 'lack of' and troph 'growth'). Within the CNS the reduction in white matter results in a spongy degeneration. Patients suffering late infantile MLD show hallmarks of demyelinisation within the brainstem and spinal cord (von Figura et al., 2001). These symptoms are less prominent in patients suffering juvenile MLD. On a cellular level, sulfatide storage is observed in oligodendroglia, which is thought to be causally related to the white matter demyelination. Additionally to oligodendritic sulfatide storage, sulfatide storage could also be found within grey matter neurons and astroglia, as well as some immune cells (Molander-Melin et al., 2004). Within affected cells, storage of sulfatides is observed within lysosomes and plasma membranes. Neuronal sulfatide storage could be found in different nuclei within the CNS like the ventral cochlear nucleus, pontine nucleus and within hippocampal areas. Additionally to de-

myelination in white matter, an age-dependent loss of neurons within the posterior part of the ventral cochlear nucleus and the nucleus of the trapezoid body could be found in postmortem stained tissue (Wittke et al., 2004). Within the cerebellum an atrophic, severe demyelinisation and prominent gliosis can be detected as well as storage granules and a reduction of Purkinje and granule cells (von Figura et al., 2001). A loss of axonal terminals of climbing and mossy fibers is also part of the neuronal pathology within every subtype (von Figura et al., 2001).
Within the PNS the sural nerves show reduced myelin sheath thickness for all fibers and segmental demyelinisation is a prominent feature. The severity of demyelinisation of the peripheral nerves seemed to be correlated with the onset and duration of the MLD subtype (von Figura et al., 2001).

Therapy of MLD

For a long period of time, treatment of MLD was aimed mainly at easing the symptoms and slowing the progression of MLD. To reduce spasticity and ataxia patients are treated with GABA transaminase inhibitors (Vigabatrin) (von Figura et al., 2001). MLD patients suffering from seizures are treated with antiepileptic drugs, but so far no standardized treatment for this disease is available (von Figura et al., 2001; Krägeloh-Mann et al., 2013).
More recently, the insight that MLD is caused by deficiency in a single enzyme has prompted attempts to replace deficient ASA. One approach to achieve this has been enzyme replacement therapy (Schmandt et al., 2006). In this approach, repeated intravenous injection of recombinant ASA is carried out, rhASA is then thought to be internalized by endocytic receptors which allow transport of this enzyme to the lysosome. This approach was not found efficacious in several transgenic mouse models (Matzner et al., 2005; Consiglio et al., 2001; Sevin et al., 2006; Matzner et al., 2002; Biffi et al., 2004). One potential reason is that rhASA does not directly pass the blood-brain barrier. In mice, this obstacle can be overcome by using an implantable pump system for direct ASA delivery to the CNS. In patients, this is not possible. In addition, enzyme replacement therapy has also been successfully used in sphingolipidoses like M. Gaucher type I or M. Fabry (Beck, 2010; Lachmann, 2011; Brown et al., 2014). This indicates the enzyme replacement therapy can alleviate CNS symptoms, even though the enzyme itself very likely does not enter the CNS.
Also viral-mediated gene therapy in ASA null mice (Sevin et al., 2006; Consiglio et

al., 2001) and gene therapy in ASA null mice using hematopoietic stem cells (HSTC-therapy; Biffi et al. (2004, 2008) and could be used for patients within early stages of the disease.
Allogenic hematopoietic stem cell transplantation (HSCT) is the transplantation of multipotent hematopoietic stem cells from a donor. The used cells are usually derived from bone marrow, peripheral blood, or umbilical cord blood.
The idea to use HSCT in MLD arised due to the use of enzyme-proficient hematopoietic progeny cells which can migrate to the affected tissues and scavenge sulfatides and cross-correct the resident cells even within the CNS (Souillet et al., 2003; Biffi et al., 2008). In clinical trials HSCT fails to provide consistent benefits in MLD patients.
Another therapeutical approach works via lentiviral-based (LV) HSC gene-therapy. Within a first trial (Cartier et al., 2009), it was tested if LVs could transduce human HSCs in clinically relevant settings with the efficiency required for application to MLD gene therapy. The experimenters collected bone marrow from the patients according to a standard procedure. HST were afterwards purified and cultured. Within the medium they were exposed to cytokines and purified vector for infection with the LVs. In a last step the infected cells were harvested, washed and purified for patient infusion. The solution was infused intravenously through a central catheter. Three patients of late infantile MLD were treated for 1.5-2 years accompanied by reduced progress of the disease. Within the trial the cells induced extensive and supraphysiological expression of the functional human ASA gene throughout the HSC progeny, which in turn mediated widespread cross-correction of CNS and PNS (Biffi et al., 2013).

Animal model of human MLD

To evaluate how neuronal storage and demyelinsation affect CNS function, and to investigate why memory and learning are affected in MLD, murine models are required.To this end, mice lacking ASA gene expression were generated (Hess et al., 1996). This ASA null mouse has been extensively evaluated with respect to its usefulness as a model for MLD.

Sulfatide storage

Hess et al. (1996) found an increased sulfatide storage in several nuclei of the brainstem, diencephalon, spinal chord and in the cerebellum, whereas no lysosomal storage could be observed within Purkinje cells in ASA null mice. Later studies within the limbic system

showed that sulfatides were also stored within hippocampal neurons (Molander-Melin et al., 2004; Wittke et al., 2004). White matter within the CNS also showed stored sulfatide either in fine clusters adjacent to myelinated fibers or large clusters within swollen cells interspersed within the white matter (Hess et al., 1996). The small clusters are likely related to sulfatide accumulation within oligodendrocyte proscesses, larger clusters reflect astrocytic and microglial sulfatide accumulation (Hess et al., 1996). In addition to sulfatide storage, myelinated axons in different areas of the CNS are affected in a age-related manner. For instance, myelinated axons in the optic nerve and corpus callosum of ASA null mice showed a reduction in cross-sectional area at an age of 12-24 months. In addition, progressive neuron loss has been demonstrated in some areas in ASA null mice, such as the acoustic ganglion. Acoustic ganglion cells were reduced in number in eight to eleven months old, but not six months old ASA null mice. However, evidence of gross demyelination is missing, independent of age (Hess et al., 1996; Gieselmann et al., 1998). In Schwann cells of the PNS, sulfatide storage was also found, but demyelination was not observed at all (Hess et al., 1996). In mice older than 18 months 20% of peripheral nerves show degeneration (Gieselmann et al., 1998).

Behavior

A number of behavioral and motor abnormalities have been described in ASA null mice. Mice with an age of 10-14 months, at which substantial CNS sulfatide accumulation is present, showed hyperactivity in the home cage (D'Hooge et al., 2001). However, mice start showing deficits in motor coordination at $\sim$ 12 months, evidenced by subtle disturbances in gait pattern (Stroobants et al., 2008) and a significant decrease in performance in the rotarod motor test (Hess et al., 1996; D'Hooge et al., 2001).

Spatial learning was adversely affected in ASA null mice from an age of 12 months. Both the acquisition of platform position in the Morris water maze, as well as the recall of platform position in a probe trial were impaired in adult mice, older than one year (Hess et al., 1996; Gieselmann et al., 1998; D'Hooge et al., 2001). In a T-maze delayed alternation task that predominatly tests working memory, both ASA null and heterozygous mice fully acquired the task (Faldini et al., 2011). The authors describe a difference in the speed with which this task is acquired. However, due to the very low numbers of employed animals in a highly variable behavioral task, this result has to be treated with caution. At two years of age, ASA null mice showed severe motor deficits in the rotarod test with a complete loss of ability to perform the test. Additionally, the

ability to swim was lost, so that learning and memory tests that rely on motor behavior could no longer be carried out (Hess et al., 1996; Gieselmann et al., 1998). Taken together, the results in ASA null mice indicate a progressive phenotype with emerging behavioral, motor and memory deficits that is consistent with symptoms of human MLD. These results could hint towards progression in incipient symptoms of ASA deficiency like the loss of walking ability which could also been seen in late infantile MLD-patients (von Figura et al., 2001). Within the last category the learning abilities of ASA null mice were tested. These results coincided with the strong cognitive symptoms of late infantile MLD-patients (Gieselmann, 1995; von Figura et al., 2001). Within the second year of life ASA null mice showed a slow-frequency tremor while walking. As within the human disease of late infantile MLD the murine model showed progression within neurological/behavioral symptoms like tremor of the head and learning difficulties (Hess et al., 1996; Gieselmann et al., 1998).

General condition

In summary, the ASA deficient mice show many features of human MLD, in particular in aged mice. It should be noted, however, that some aspects of pathology seem to be less pronounced in the mouse model compared to human MLD. This may be considered surprising since the severity of ASA loss in the mouse model resembles the early-onset infantile form of MLD. For instance, white matter damage emerges only late in ASA deficient mice, and mice in general do not show strongly reduced life spans. The reasons for this milder phenotype are unknown. One hypothesis that has been advanced to explain this difference is that the metabolic pathways of sulfatide might be different in mice. In particular, alternative sulfatide pathways independent of ASA activity have been reported in rodents (Tempesta et al., 1994). In addition, there might be difference in the accumulation of toxic metabolites. For instance, lysosulfatide, a toxic derivative of sulfatide, and a potent inhibitor to proteinkinase C (Hannun and Bell, 1989), might be present at higher levels in human MLD patients (Toda et al., 1990; Hess et al., 1996).

Electrophysiology

Electrophysiological data on ASA null mice is scarce. One study has addressed the levels of hippocampal synaptic long-term potentiation and short-term plasticity in 11 month old animals. These experiments revealed impaired hippocampal synaptic plasticity in ASA null mice. No other differences in basal excitability and short-term plasticity were

observed (Faldini et al., 2011). In 2007, Eckhardt et al. investigated *in-vivo* cortical EEG recordings of ASA null mice at different ages (Eckhardt et al., 2007). In younger animals at an age of 8-10 weeks basal EEG activity was not changed between ASA null and healthy littermates. However ASA null mice showed abnormal episodes of spontaneous discharges and polyspikes which were increased in transgenic mice, which accumulated a bigger amount of sulfatides. Power-analysis of the spontaneous discharges showed that these events were associated with an increase of power in different frequency bands (delta-, theta-, alpha- and beta-bands). The incidence of these events was decreased in older animals at an age of 5-6 months (Eckhardt et al., 2007). The presence of cortical hyperexcitability is in agreement with the increased incidence of epileptic seizures in MLD, which is particularly high in the infantile form (von Figura et al., 2001).
Indirect evidence for an involvement of sulfatides in modulating neuronal excitability comes from several studies showing that sulfatide application within the extracellular and intracellular solution is capable of modulating ion channel properties *in vitro* (Chi and Qi, 2006; Lingwood et al., 2004).

1.3. The Hippocampus

1.3.1. Hippocampal anatomy

The medial temporal lobe of mammals includes a system that is essential for the formation of declarative memory (Bunsey and Eichenbaum, 1996; Squire, 1992; Squire et al., 2004) as well as for spatial declaration (O'Keefe and Dostrovsky, 1971; O'Keefe, 1976; Moser et al., 2008). The system consists of a crescent -like structure, the hippocampal formation and the adjacent perirhinal, entorhinal, and parahippocampal cortices. The hippocampal formation is composed of the dentate gyrus, the cornu ammonis (CA) the subiculum, the presubiculum, the parasubiculum and the entorhinal cortex (Amaral and Lavenex, 2007). The cornu ammonis region in rodents consists of three subregions CA1-CA3 (Fig. 1.7).

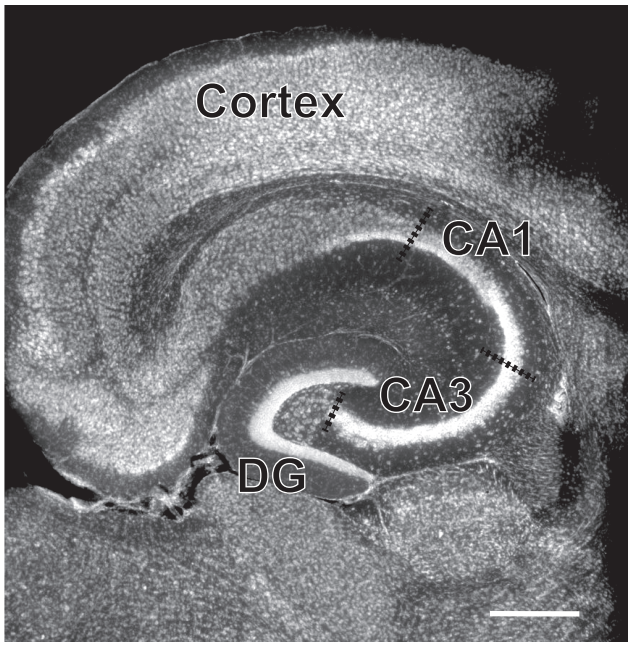

Fig. 1.7.: Nissl-staining of a transverse murine brain slice. Hippocampal and cortical areas are indicated. DG=dentate gyrus, CA3 and CA1. Scale bar (lower right corner) is 500 µm long.

The three layered hippocampus receives information from different cortical structures (Fig. 1.8). Information from excitatory cells in layer II of the six-layered entorhinal cortex reaches the dentate gyrus (DG) granule cells via the perforant path (Steward and Scoville, 1976; Witter et al., 1989; Witter, 1993). As a first computational step this information is processed within the DG. The efferent projections of the DG are solely

from granule cells and called mossy fibers. These non-myelinated axons (Schmidt-Hieber et al., 2008) terminate onto the CA3 pyramidal cells (Blackstad et al., 1970) in a zone called stratum lucidum (s.l.). Axonal collaterals of CA3 pyramidal cells contact other CA3 pyramidal cells and therefore lead to a strong recurrent excitation within the CA3 subregion. The target of CA3 axons are pyramidal cells located within the CA1 stratum oriens (s.o.) and stratum radiatum (s.r.) either ipsilaterally via the Schaffer collaterals or contralaterally via commissural projections (Ishizuka et al., 1990; Amaral et al., 1990). CA3 neurons can project backwards to the dentate gyrus (Li et al., 1994; Scharfman, 2007).
The principal glutamatergic cells in the CA1 region are CA1 pyramidal cells. From CA1 information is conveyed to both the subiculum and to layer V of the entorhinal cortex (Amaral and Witter, 1989; Witter et al., 1989; Witter, 1993). Apart from this, a fraction of the perforant path that originates in entorhinal cortex layer III gives rise to the direct pathway (also referred to as the temporo-ammonic pathway; Steward and Scoville (1976)) that innervates the CA1 pyramidal cells on their apical tuft dendrites (Amaral and Witter, 1989).
Which excitatory input has the bigger impact on CA3 pyramidal cells depends in part on the location of the neuron. Cells lying closer to the hilus most often recieve excitatory input from mossy fibers which terminate on their apical and basal dendrites (Blackstad et al., 1970). Those pyramidal cells have short apical dendrites, which do not reach stratum lacunosum moleculare (s.l.m.) (Amaral et al., 1990). In contrast CA3 pyramidal cells lying close to CA1 region, have dendrites that span through s.r. and s.l.m., where mossy fiber input terminates at the proximal portion of the apical dendrites (Blackstad et al., 1970).

The basal dendrites of CA1 pyramidal cells extend into s.o. and their apical dendritic tree branches into s.r. and s.l.m.. The dendrites in s.o. and s.r. are therefore mainly innervated by excitatory inputs from CA3, whereas the distal apical tuft in s.l.m. receives excitatory input from the entorhinal cortex. Additionally the CA1 region receives excitatory inputs from the nucleus reuniens of the thalamus and the basolateral nucleus of the amygdala. These projections terminate in s.l.m. (Wouterlood et al., 1990), or in s.r. and s.o. respectively (Amaral and Lavenex, 2007; Pikkarainen et al., 1999; Kemppainen et al., 2002).
The myelinated axons of CA1 pyramidal cells either originate at the soma or a basal den-

drite (Thome et al., 2014), pass through s.o. and travel in a fiber bundle, the alveus, to innervate targets in the subiculum and the entorhinal cortex .
Recurrent connections by CA3 axon-collaterals are formed extensively within CA3 region. Axon-collaterals diverge within s.o. and s.r. and contact apical and basal dendrites of other pyramidal cells and interneurons before projecting out of the region. In previous studies it had been shown that 30 - 70 % of all CA3 pyramidal cell are connected to other pyramidal cells within CA3 (Li et al., 1994). In contrast to CA3 pyramidal cells CA1 pyramidal cells have fewer axon collaterals within CA1. These local axon collaterals mainly terminate inside the alveus and s.o., and rarely enter s.r. (Knowles and Schwartzkroin, 1981; Amaral et al., 1991).

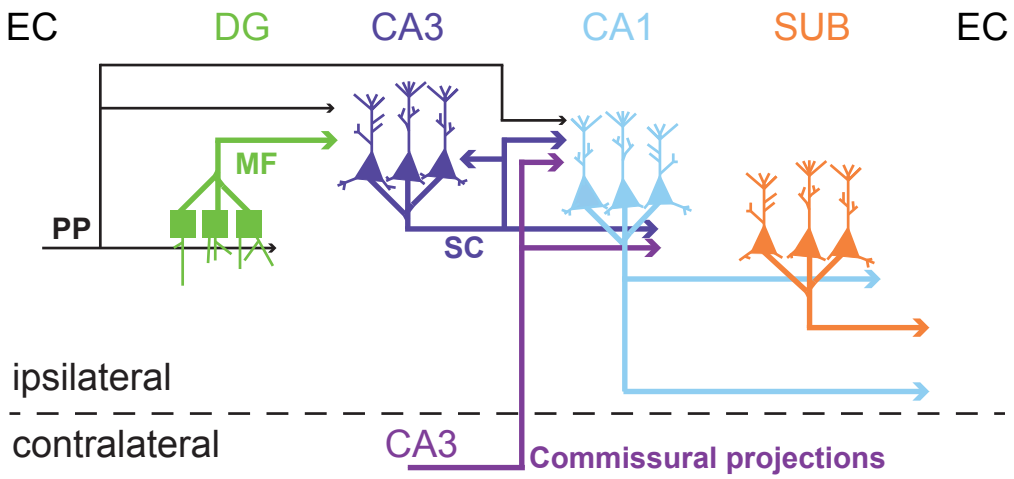

Fig. 1.8.: Scheme of the hippocampal circuitry. The abbreviations are used for the main excitatory pathways. Information from the entorhinal cortex (EC) reaches the hippocampus via the perforant path (PP, black arrows). The granule cells (green) of the dentate gyrus (DG) target CA3 pyramidal neurons (purple) via the mossy fiber pathway. From CA3 information is conveyed to CA1 (blue) via the unmyelinated Schaffer collaterals. Both CA1 and the subiculum (SUB) project to the EC. Adapted from Amaral and Witter (1989); Amaral and Lavenex (2007).

As recordings in this study were performed in the CA1 and CA3 subfields of the hippocampus, the functional anatomy of these regions will be described in more detail.

1.3.2. CA3 and CA1 pyramidal cell

Cell morphology

The CA regions of the hippocampus are three layered structures. The somata of the excitatory pyramidal cells are located in the pyramidal cell layer (stratum pyramidale). CA1 and CA3 pyramidal cells have pyramidal-shaped somata and show both basal and apical dendrites. Pyramidal neurons of CA3 have bigger somata than in CA1 and their apical dendrites bifurcate close to the soma (Fig. 1.9). The total length and the organization of the dendrites are heterogeneous among CA3 pyramidal cells. Next to the hilus, CA3 pyramidal cells are smaller than those located more distally towards the CA1 region (Amaral et al., 1990). CA3 pyramidal cell basal dendrites extend into stratum oriens. The apical dendrites exhibit a short apical trunk, located in stratum lucidum, which is decorated with complex excrescences that constitute the targets for mossy fibers. In s.r., the trunk usually branches into two or more secondary dendrites, which elaborate apical oblique dendrites. Finally, in s.l.m., distal but not proximal CA3 pyramidal cells form apical tuft dendrites that receive direct perforant path inputs (Ishizuka et al., 1995; Henze et al., 1996). CA3 pyramidal cells receive their major excitatory input either from GCs via the mossy fibers,which terminate in the s.l. close to the pyramidal cell layer. Furthermore, they receive a direct input from the lateral EC via the perforant path, a connection termed the temporoammonic pathway. Finally, a major pathway derives from other, ipsilateral or contralateral CA3 pyramidal cells, termed the associational/commissural input (Bennett et al., 1994).

Firing behavior of CA1 and CA3 pyramidal cells

The knowledge about intrinsic firing properties leads to the comprehension how voltage gated channels contribute to action potential (AP) firing. Channels within neuronal membranes influence passive as well as active properties like AP threshold, afterhyperpolarization (AHP), spike afterdepolarization (spike ADP) and AP-firing mode.
In hippocampal pyramidal cells APs are typically followed by an ADP (Wong and Prince, 1981; Jung et al., 2001; Metz et al., 2005). The ADP is mediated by voltage-gated Na^+- or Ca^{2+}-channels but also requires K^+ channels to limit repolarization (Spruston, 2008; Yue, 2004). Variation of ADP size contributes to differences between regular-spiking (RS) and intrinsically bursting (IB) neurons (Metz et al., 2005). Additionally the ADP is regulated by intrinsic membrane properties (Yue et al., 2005; Golomb et al.,

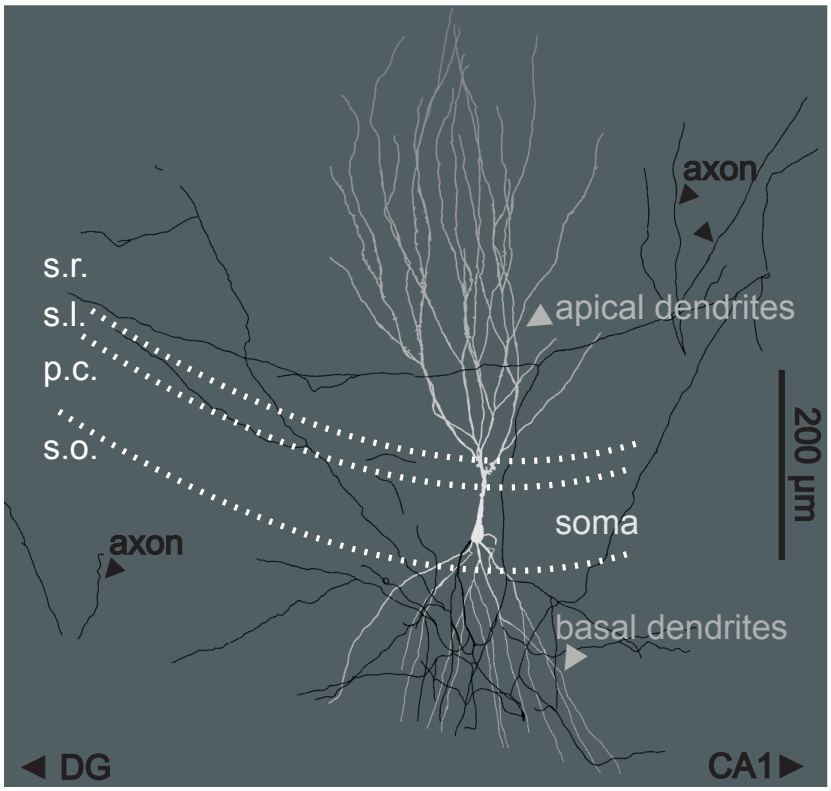

Fig. 1.9.: Reconstructed CA3 pyramidal cell with its dendritic arbor (light grey) and partly reconstructed axonal network (black). Hippocampal subregions are indicated with dashed lines. Left to the cell DG would be situated, right handside CA1 network continued.

2006; Yaari et al., 2007). *In vitro* , some pyramidal cells respond to somatic current injection with a regular spiking pattern that shows spike-frequency adaptation, whereas other pyramidal cells exhibit intrinsic burst firing (Connors and Gutnick, 1990; Staff et al., 2000).

Besides morphological differences, CA3 and CA1 pyramidal cells show differences in firing behavior. As a hallmark feature CA3 pyramidal cells show a much greater tendency to burst spontaneously or follow brief intracellular current pulses (Wong and Prince, 1978; Schwartzkroin and Prince, 1978). This tendency of intrinsic bursting in CA3 seems to be important to generate epileptiform discharges in slices (Schwartzkroin and Prince, 1977, 1978, 1980).

This bursting is accompanied by smaller (Ca^{2+} dependent) spikes later in the waveform (Wong and Prince, 1981), which are caused by an ADP following a single AP and mediated by a Ca^{2+}-current. CA3 pyramidal cells close to the CA1 region tend more often to fire intrinsic bursts, which could be due to a longer initial apical dendrite. It is known, that L-type voltage gated Ca^{2+} channels are clustered with high density at

the base of major dendrites of CA3 pyramidal cells (Westenbroek et al., 1990). This might cause a large Ca^{2+} influx during burst firing. Burst firing in CA3 pyramidal cells can be blocked via the use of Mn^{2+} (Wong and Prince, 1981). The AHP also depends on Ca^{2+} influx and seems to play a role in termination of CA3 pyramidal cell bursting (Wong and Prince, 1981). The area of CA3 pyramidal cell ADPs is bigger than in CA1 pyramidal cells (Wong and Prince, 1981), which might depend on M-Type K^+-channels Yue (2004, 2006).
CA3 pyramidal cells have longer average time constants than within CA1. The reason might be a higher specific resistivity of the CA3 plasma membrane (Wong and Prince, 1981).
In contrast to pyramidal cells of the CA3 region those lying in CA1 region exhibit a regular spiking behavior during direct somatic current injections (Staff et al., 2000). Within hippocampal slice preparations all pyramidal cells are non-bursters and show a nonlinear IV-relationship (Wong and Prince, 1981). Single APs show fast rising rates, great amplitudes and wide half-widths (Staff et al., 2000).

1.3.3. Inhibitory hippocampal microcircuits

The activity of excitatory neurons in the hippocampal formation is controlled by a wide variety of interneurons. Interneurons in the hippocampus are diverse, and have been classified into more than 20 different subtypes (Freund and Buzsáki, 1996). Conceptually, hippocampal interneurons are integrated into two fundamental inhibitory circuit motifs, termed feed forward and feed back inhibition. Feed forward inhibition denotes an inhibitory circuit in which an extrinsic excitatory afferent activates both excitatory and inhibitory cells. The inhibitory cells then locally inhibit the excitatory neurons. Feed back inhibitory circuits are mediated via axon collaterals of glutamatergic neurons that activate local interneurons, which then inhibit glutamatergic neurons within the same hippocampal area. Both feed back and feed forward inhibition are mediated by multiple types of interneurons. One major defining feature of interneuron types is the location where they generate inhibition onto pyramidal cells. Several types of interneurons produce strong, perisomatic inhibition. Axoaxonic interneurons express parvalbumin (PV^+), and characteristically contact the axon initial segment of CA1 and CA3 pyramidal neurons (Somogyi, 1977). Basket cells that express the immunocytochemical marker parvalbumin (PV^+ BC) display a dense axonal arbor within the pyramidal cell layer and predominant inhibitory synaptic contacts onto pyramidal cell somata. This type of in-

terneuron is readily identifiable by its fast-spiking behavior. A second type of basket cell, the regular firing basket cell, also innervates pyramidal cells perisomatically, but is positive for cholecystokinin (CCK^+ BC).

Interneurons in s.l.m., the so-called L-M interneurons, get their excitatory input either from PP- or MF-terminals. They modulate the influence of EC or DG to the CA3 region thereby providing a strong feed forward-inhibition of CA3 pyramidal cells (Lacaille and Schwartzkroin, 1988; Williams et al., 1994). Collectively, perisomatic inhibitory inputs, due to their location, provide a strong control over action potential generation of pyramidal neurons.

Dendritic targeting interneurons (DTIs) also recieve their input from different hippocampal and cortical structures. Unlike spiny s.l. interneurons which mediate feed forward inhibition in pyramidal cells, spiny OLM-interneurons in CA3 and CA1 mediate feed back inhibition. The dendrites of these interneurons in CA3 are located within all layers except s.l.m. whereas the dendrites within the CA1 subregion are horizontally oriented and restricted to s.o. The laminar distribution of the dendrites in CA3 and CA1 overlaps that of recurrent collaterals of local pyramidal cells (Freund and Buzsáki, 1996; Hájos et al., 2013). These collaterals target the apical dendritic tuft of CA3 pyramidal cells aligned with the entorhinal cortical input (Klausberger and Somogyi, 2008). It was described previously that each granule cell makes more connections with spiny interneurons in CA3 s.l. than with pyramidal cells (Acsády et al., 1998). Therefore DG activation drives an enormous number of interneurons which mediate feed forward inhibition in CA3, Lawrence and McBain (2003) concluded that the DG controls the excitability of CA3. A loss of inhibition in CA3 region therefore leads to a change in inhibition-excitation balance and epileptiform activity can arise (Treviño et al., 2011).

1.3.4. Oscillations in the healthy brain

In 1924, Hans Berger performed the first human electroencephalographic (EEG) recording revealing an 8 to 12 Hz rhythm, today known as the alpha waves of Berger (Berger, 1929). Since this time, different cortical brain oscillations have been detected with the help of surface EEGs. Ever since, scientists try to understand the network and cellular mechanisms underlying neocortical and hippocampal oscillations.
Within this chapter we will introduce the recording methods, electrophysiological characteristics, and behavioral relevance of the most prominent hippocampal oscillations. The mammalian hippocampal network shows different oscillatory activity with regard to frequency and functional behavioral states.
To study the physiological properties of hippocampal oscillations and their behavioral correlations in vivo researchers frequently use rodents, mostly mice and rats, as model organisms. Using intracranial recordings of local field potentials (LFP) in rodents, certain oscillation frequencies and patterns were found to be highly correlated to different phases of sleep, memory encoding or consolidation, and awake attention phases. Therefore, brain oscillations are thought to play a critical role in neuronal information trafficking and memory function

Theta activity

One rhythmic oscillation associated with a particular brain state is the theta oscillation, which has a frequency range between 4-8 Hz. The theta rhythm is actually not really sinusoidal, but has a rather saw-tooth like appearance with a fast rise time and a slower decrease (and superimposed phase coupled gamma oscillations) (Buzsáki et al., 1985). Theta waves have initially been hypothesized to have their origin in subcortical regions and could be measured in hippocampal areas which receive direct input from the medial septum (Vanderwolf, 1969).
Hippocampal theta oscillations can be measured in behavioral states of arousal (Green and Arduini, 1954), locomotion, especially during spatial navigation and exploration (Vanderwolf, 1969), as well as during REM sleep (Jouvet, 1969). Furthermore, theta oscillations play a role for processing novelty and spatial representation (O'Keefe and Recce, 1993; Jeewajee et al., 2008). In 1971, O'Keefe and Dostrovsky described the existence of the so called place cells for the first time in rats (O'Keefe and Dostrovsky, 1971). They showed that cells of the CA1 pyramidal cell layer fire selectively at one or

even more locations within the environment of the animal. Different place cells show different firing locations and place fields (O'Keefe, 1976; Moser et al., 2015). Together with grid cells in the entorhinal cortex (Hafting et al., 2005) and the neuronal ability for synaptic plasticity, they seemed to play a critical role for the formation of declarative memory (Moser et al., 2015). The firing sequences of place cells are not only simply related to their current locations, but can also integrate contextual information (see Dupret et al. (2010) for goal related reorganization of CA1 firing fields). Interestingly, during rest or sleep directly after exploration sessions, place cell assemblies can be activated at the same order as they fired during the previous exploration sessions, but on a compressed time scale in so-called replay events (Pavlides and Winson, 1989; Wilson and McNaughton, 1994; Foster and Wilson, 2006; O'Neill et al., 2006). Furthermore, place cell firing advances to more and more earlier phases of subsequent theta cycles while traversing its place field, a phenomenon called phase precession (O'Keefe and Recce, 1993). Thus, hippocampal theta oscillations can provide a temporal structure for processing of information related to episodic memory.

Gamma activity

Hippocampal network oscillations between 25-100 Hz are called gamma oscillations (Colgin, 2016). They correlate to a variety of behaviors and can be divided into slow and fast gamma oscillations. In contrast to other neuronal oscillations they show a lower amplitude (Buzsáki, 1984; Csicsvari et al., 2003).
Slow gamma oscillations show frequencies between 25-55 Hz and are thought to be driven by CA3 input, whereas fast gamma is named after oscillations around 60-100Hz (Colgin et al., 2009; Belluscio et al., 2012) and is associated with inputs from the entorhinal cortex. Consistent with the termination of entorhinal cortex fibers on the one hand, and Schaffer collateral fibers on the other hand, fast gamma oscillations can be measured primarily within s.l.m., slow gamma primarily within s.r. of CA1. Besides these location preferences in the hippocampus, gamma is a neuronal network oscillation which can also be recorded in multiple other brain regions outside the hippocampal formation (Colgin, 2016).
Several types of hippocampal fast spiking interneurons show gamma phase locked firing (Tukker et al., 2007). Additionally, freely behaving rats show a coupling of gamma amplitude to theta phase. Therefore it is stated that excitation at a particular theta phase triggers gamma onset by inducing gamma-frequency bursting interneurons. The impact

of slow gamma for memory function has been investigated in several studies (Treves and Rolls, 1992; Brun et al., 2002; Steffenach et al., 2002; Nakazawa et al., 2002). These scientist stated that slow gamma is needed for memory retrieval. They hypothesized that memories are stored within the hippocampal region of CA3 and the slow gamma recorded in CA1 might be entrained by inputs from CA3 (Colgin et al., 2009; Belluscio et al., 2012). In 2010, Shirvalkar et al. investigated slow gamma and theta oscillations in rats and were able to show a comodulation between these two oscillations, which predicted successful memory retrieval (Shirvalkar et al., 2010).
While performing a spatial alternation task or linear track running gamma frequency increases. Therefore, it has been hypothesized that one function of fast gamma is the encoding of current sensory information (Ahmed and Mehta, 2012; Zheng et al., 2015). Another study stated that fast gamma shows a correlation to working memory (Yamamoto et al., 2014).

SPW-R complexes

In addition to the rhythmic oscillations mentioned above, another transient oscillation occurs during phases of behavioral immobility and sleep. The most synchronous network activity pattern within the pyramidal cell layers (Chrobak and Buzsáki, 1994), the so called 'sharp wave ripple complex' (SPW-R complex, Foster and Wilson (2006); Diba and Buzsáki (2007)), is a transient hippocampal oscillation. During slow wave sleep the number of SPW-R complexes reaches its peak (Mölle et al., 2006). If this activity is blocked during memory formation in vivo via low-frequency electrical stimulation, animals will perform subsequent spatial memory tasks worse than sham implanted controls (Girardeau et al., 2009; Jadhav et al., 2012).
It was also shown that the sequences are replayed during subsequent SPW-Rs in the same or reverse order that the cells show during experience (Wilson and McNaughton, 1994; Foster and Wilson, 2006; Diba and Buzsáki, 2007). This replay strengthens memory consolidation and recall and might also influence the future behavior of the animal. Due to their role in place cell activity SPW-Rs are thought to ensure memory consolidation and memory transfer from the CA3 region into the neocortex (Buzsáki, 1986, 1989; Siapas and Wilson, 1998; Ólafsdóttir et al., 2016).
SPWs are slow wave events which can be detected in a frequency range of 1-50 Hz and last between 30 and 100 ms. They show a slow potential shift most often superimposed by fast (around 150 - 200 Hz) local network oscillations (ripples) (Fig. 1.10; O'Keefe

(1976); O'Keefe and Conway (1978); Kanamori (1986); Buzsáki (1986); Suzuki and Smith (1988); Buzsáki et al. (1992); Chrobak et al. (2000)). SPWs occur spontaneously within layers of DG, CA3, CA1, and subiculum (Buzsáki, 1986; Maier et al., 2003). This activity was first discovered by (Jouvet et al., 1959) who measured it in the ventral hippocampus of cats. It is generated intrinsically within the CA3 pyramidal cell layer and is transmitted to other hippocampal areas via back-propagation and the Schaffer collateral pathway. SPWs reflect a transient synchronized network population activity event, which is reflected as a sink of net current due to synchronous AP generation of the principal cells, which are thought be synchronized via local interneurons.

Ripple activity reflects unit activity which can only be recorded within the principle

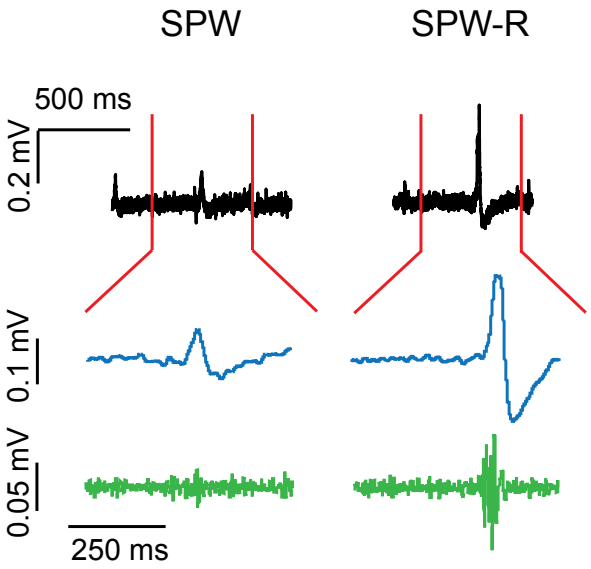

Fig. 1.10.: Examples of field potential recordings in the wide band without post-hoc filtering (black traces), after application of a 1-50 Hz bandpass filter (blue traces) and a 150-300 Hz bandpass filter (green traces), in murine hippocampal slices. The left part show recordings with one sharp wave (SPW), the right recording showes simultaneous sharp wave and ripple events (SPW-R).

cell layers of the hippocampus (Buzsáki et al., 1992) and it still remains unclear which cellular properties are responsible for these extracellularly recorded events. They are non-disease associated high-frequency oscillations (HFO) (Buzsáki, 1989). Other HFOs like ultrafast ripples (200 - 600 Hz) occur during epileptic brain states (Gulyás and Freund, 2014).

1.3.5. Oscillations in ASA null mice

ASA null mice show an increase in neuronal network activity within cortical EEG recordings (Eckhardt et al., 2007). In this study, young animals at an age of 8-10 weeks showed a striking increase in high frequency activity occuring in short bursts. We therefore speculated that these patterns might be related to hippocampal network activities like ripples. Inspired by these experiments we decided to study high-frequency hippocampal network oscillations like SPW-R events in hippocampal slices of ASA null mice.
Since Buzsaki, 1986 first reported SPW-Rs, investigations have been performed to validate these extracellular recording methods in vitro and in vivo (O'Keefe and Conway, 1978; Csicsvari et al., 2000). In contrast to the SPW-R activity observed in vivo, recordings in vitro show more regularly occurring events with stable amplitudes (Buzsáki and Chrobak, 2005). An easy way to study this HFO is therefore given by the use of acute brain slice preparations under the premise that these oscillations need a minimum of network size and/or connectivity (Schlingloff et al., 2014). In vitro, population events are typically initiated in the hippocampal CA3 region, and spread to the DG, CA1 region and subiculum (Papatheodoropoulos and Kostopoulos, 2002; Kubota et al., 2003; Maier et al., 2003; Kano et al., 2005; Nimmrich et al., 2005). Based on these experiments we used hippocampal slices for our experiments to study basic properties of SPW-R within ASA null and wildtype-control animals.

1.4. Key questions

Considering physiological high-frequency oscillations in hippocampus and the discovery of Eckhardt et al. (2007) which describes cortical high-frequency activity in young ASA null mice (see 1.2.3) we were interested if we were able to

- detect an increase in high-frequency activity in acute hippocampal slices
  → if this is the case: are neuronal intrinsic properties (of CA3 pyramidal cells) affected?
  → Do those changes have an influence on excitation-inhibition balance within the hippocampal network?

Other questions arise when sulfatide accumulation is investigated

- Do ASA null mice accumulate sulfatides within hippocampal and cortical layers at an age of 8-12 weeks?
  → Are cellular intrinsic properties of CA3 pyramidal cells changed?

In the end these questions were investigated to achieve a more precise picture of how the deficiency of ASA influences neuronal function. A better understanding of this might lead to an improvement in therapy and treatment of MLD-patients.

2. Materials and Methods

2.1. Animals

All animal experiments were performed in accordance with the regulations of the local animal care and use committee. ASA wildtype-control and ASA null mice were provided by Dr. Matthias Eckhardt (Department of Biochemistry, University of Bonn, Germany).

2.1.1. Arylsulfatase null mice

The generation of ASA null mice has been previously described (Hess et al., 1996). The replacement vector encompassed 6 kb of 5' flanking upstream sequence, the entire coding sequence of the ASA gene and additional 2 kb of 3' flanking downstream sequence of the ASA locus. A neo cassette was placed into the coding sequence of exon 4 thereby disrupting the open reading frame (Fig. 2.1.). The replacement vector was linearized with the endonuclease *NotI* and introduced into E14-1 ES cells via electroporation. G418 and gancyclovir resistant colonies were selected and screened by Southern blot analysis of *EcoRI* -digested DNA, hybridized with external 3' probe. Homologous recombination was confirmed by *NsiI* digestion and hybridization with a 5' probe. Correctly targeted clones were identified and injected into blastocytes of C57BL/6J mice. Chimeric male mice were bred with wildtype C57BL/6J females and offspring was analyzed by Southern blot. Mice heterozygous for ASA gene were mated to obtain ASA null mice which are fertile with litter size comparable to wildtype-control animals.

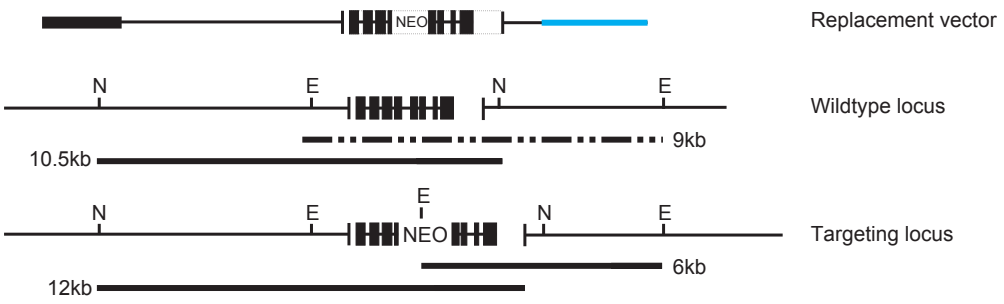

Fig. 2.1.: Structure of the replacement vector and targeted ASA locus. The genome of ASA is shown by boxes, open parts are 5' or 3' untranslated regions, solid parts are coding sequences. The tk gene is a herpex simplex virus thymidine kinase gene. Bluesript plasmid vector is shown as a blue bar. The wildtype locus is shown underneath, N and E indicate *Nsi*I and *Eco*RI sites. The position of the external probes used to detect the targeted locus is shown in the 5' and 3' end. Size of the fragments (9 and 10.5 kb) hybridizing to these probes is indicated by the bars below. The last scheme shows the recombined locus which alters size of DNA fragments to 6 and 12 kb. Mod. acc. to (Hess et al., 1996).

Male ASA null mice and their wildtype littermates were used either at an age of 8-12 weeks or 5-6 months.

2.1.2. Genotyping

DNA extraction

Tail tips were cut from three weeks old mice and put into 1.5 ml eppendorf-tubes. To each tube 750 µl lysis buffer with 100 µg/ml proteinase K was added and incubated at 55 ℃ in a shaking water bath over night. Then 250 µl of 6 M NaCl was added and incubated for 5 min. The lysate was centrifuged (10 min at 13.000 rpm, room temperature) and 750 µl of the resulting supernatant without top phase was transferred into a new tube. For DNA precipitation, 500 µl isopropanol was added followed by thorough mixing and centrifugation (10 min at 13.000 rpm). The resulting pellet containing precipitated DNA was washed with 70 % ethanol and left to air-dry for 5 to 10 min. Finally, DNA was dissolved in 200-300 µl H_2O or TE buffer (10 mM Tris/HCl pH 8.0/1 mM EDTA) and stored either at 4 ℃ for short term storage or at -20 ℃ for long term storage.

PCR protocol

For genotyping of ASA wildtype-control and null mice the PCR reaction tube contained the following:

- 1 µl DNA (100-300 ng/µl),
- 0.2 pmol ASA sense primer (L-3548, sequence TAGGGTGGAAGTTACCCTAGA),
- 0.2 pmol ASA antisense primer (L-3549, sequence TGACCCAGGCCTTGTTCC-CAT),
- 0.2 pmol neo primer (L-3549, sequence GGAGAGGCTATTCGGCTATGAC),
- 10 µl DNA polymerase (REDTaq®, Sigma-Aldrich, Munich, Germany),
- 8.4 µl H_2O to reach the reaction volume of 20 µl.

The following standard PCR protocol was used: The PCR mixture was initially heated to 94 ℃ for 180 s to ensure an initial denaturation. The PCR consisted of 32 cycles of denaturation (30 s at 94 ℃), annealing (30 s at 56 ℃), and strand elongation (60 s at 72 ℃) and was followed by a final elongation step (180 s at 72 ℃) to ensure that any remaining single-stranded DNA was fully extended. To stop PCR reaction the solution was stored at 4℃ until DNA fragment electrophoresis on a 1 % agarose gel (100 bp ladder as size marker). For analysis DNA bands were identified according to Tab. 2.1.

genotype	expected band size (bp)
ASA wildtype-control	480
ASA null	1100
ASA heterozygot	480 + 1100

Tab. 2.1.: Expected band size after PCR of ASA wildtype-control, heterozygous, null animals.

2.2. Preparation of hippocampal slices

For preparation of horizontal hippocampal slices animals were deeply anesthetized with ketamine (100 mg/kg; Pfizer, Berlin, Germany) and xylazine (15 mg/kg; Bayer, Leverkusen, Germany) and then decapitated. The brain was quickly removed and transferred to ice-cold sucrose artificial cerebrospinal fluid (sucrose ACSF, for composition see Tab.

2.2). Horizontal slices (300, 400, 450 or 500 µm thick, depending on the experiment) were prepared with a vibrating microslicer (Leica VT 1200 S; Wetzlar, Germany) in sucrose ACSF and then gradually rewarmed to 35 ℃ for 30 min. Afterwards slices were either kept at room temperature in oxygenated (5 % CO_2 - 95 % O_2) normal or modified ACSF (for composition see Tab. 2.2), depending on the experiment.

2.3. Sulfatide accumulation

2.3.1. Alcian-blue staining

As described by Schott et al. (2001) tissue accumulation of sulfatides can be visualized by staining with alcian blue. Selected 300 µm thick horizontal slices from 8-12 weeks old ASA null and littermate control mice were fixed in Bouin solution (Sigma-Aldrich, Munich, Germany; diluted 1:3 with phosphate buffered saline), or 4 % paraformaldehyde (PFA) in phosphate buffered saline. After fixation, tissue was incubated with alcian blue (Alcian blue; Sigma-Aldrich, Munich, Germany). For staining the tissue was equilibrated with dye-free vehicle (25 mM Na-acetate buffer, pH 5.7, supplemented with 0.3 M MgCl and 1 % PFA) for 48 h, incubated with the dye solution (0.05 % Alcian blue) for 2-3 weeks under continuous shaking and rinsed in dye-free vehicle for 48 h. As a second staining, cells were stained with a biomarker for neurons. We used primary the peroxidase-coupled secondary antibody anti-NeuN. For this staining slices were washed with TBS and incubated in 0.3 % H_2O_2 at room temperature. Afterwards slices were again washed with TBS and incubated in 5 % NGS (normal goat serum) and 1 % BSA (bovine serum albumin) for 30 min up to 2 h. at room temperature. The diluted primary antibody (1:500; polyclonal mouse anti NeuN; MAB377; Chemicon, Merck KGaA, Darmstadt, Germany) was incubated over night at 4℃. Afterwards slices were washed with TBS and the secondary antibody (biotin conjugated goat anti mouse; 1:400; in 5 % NGA and 1 % BSA) was incubated for 1.5 h. After 75 min. an avidin-biotin complex (ABC; VECTASTAIN ABC Kit; Vector Laboratories, Burlingame, USA) solution was prepared and incubated for 30 min. In between slices were washed with TBS. The incubated ABC solution was added to the slices and incubated for 1 h at room temperature. The incubated slices were washed once with TBS and were finally incubated with a DAB-substrate solution (0.5 %) and H_2O_2 at room temperature. The chemical process was stopped by washing the slices at the point a well stained structure

could be seen. After staining the tissue was post-fixed with 2 % OsO for 3 h, then dehydrated and embedded in paraffin. Microtome sections (7 µm thick) of the tissue were mounted with DePeX (Serva, Heidelberg, Germany) and stored in the dark at 4 ℃.

2.3.2. Electrospray ionization mass spectroscopy

Horizontal hippocampal slices (500 µm thick) of ASA null and littermate control mice were prepared and micro-dissected into DG, CA3, CA1, and neocortex. The tissue fragments were then transferred into cryo-tubes and frozen in liquid nitrogen. To prepare lipids for ESI-MS, tissue samples were thawed and homogenized in ice-cold TBS. After saving 20 µl for protein analysis, (protein content was quantified using the BCA Protein Assay Reagent method ;Pierce, Rockford, USA) the remaining homogenate was centrifuged (100,000 x g) for 1 h at 4 ℃ to separate the cytosol from the membrane fractions which accumulate in the pellet. This pellet was dispersed in a mixture of chloroform and methanol (2:1) and homogenized again. This homogenate was stirred for 4 h at 60 ℃ and then centrifuged (1000-1300 RPM) for 10 min at 4 ℃. The resulting supernatant was transferred into a new pyrex tube and the pellet was washed with a 1:1 mixture of chloroform and methanol and centrifuged again. This second supernatant was merged with the first one and dried by heating in a water bath to 50 ℃ and additionally injecting nitrogen. To emulsify glycerophospholipids the whole extract was dissolved in methanol (5 min sonication) before 4 µM sodium hydroxide was added (2 h stirring at 37 ℃). By adding glacial acetic acid the hydrolysis was stopped and lipids were dried by heating in a water bath to 50 ℃ and additionally injecting nitrogen. To desalinate this lipid fraction it was again dissolved in methanol and added to a silica-column (LiChrospher 100 RP-18 (5 m); Merck, Darmstadt, Germany). After washing off the unbound lipids with H_2O, lipids were eluted with methanol and chloroform. These lipids were dried by heating in a water bath to 50 ℃ and additionally injecting nitrogen. The prepared lipids were purified using a silica-column (LiChroCART 125-4 Si-60; Merck, Darmstadt, Germany) and then transferred into an electrospray capillary at 4000 V with argon as collision gas. The settings of the ESI were the following:

- Flow Rate 400 l/min
- Nebulizer Pressure 40 psi

- Drying gas flow 9 l/min
- Gas temperature 365 ℃
- Column Temperature 30 ℃
- Runtime 10 min

The linear range which allows a direct conversion of signal intensity to lipid concentration lies between 0-8 x 10^7, thus signal strength should fall within 2-7 x 10^7. The calibration was done with C12:0-sulfatide (stock 200 µM, M=722.6 g/mol), intensities of target and spike should be located at the same values. For analysis of changes in neuronal sulfatide-storage the ratio of C18:0 and C24:1 sulfatides were evaluated in ASA null mice and healthy littermates.

2.4. Electrophysiology

2.4.1. Field potential recordings

For field potential recordings, 450µm thick hippocampal slices were placed in a Haas-type interface chamber (35 ± 1℃) and perfused with normal ACSF (for composition see Tab. 2.2) for at least 20 min (flow-rate 2.5 ml/min) before electrode placement. Field potentials for assessing SPW-R activity were recorded with tungsten electrodes (1 MΩ, TM33A10OKT; WPI, Sarasota, USA) which were positioned in the pyramidal cell layer of hippocampal CA1 and CA3 subregions 2 h after slice preparation.
AC-coupled signals were low-pass filtered at 1 kHz (cut-off) and amplified 100-fold using an AxoClamp 2B (Molecular Devices, Sunnyvale, USA) followed by a BF-48DGX differential amplifier/filter module (npi electronic GmbH, Tamm, Germany). Line-frequency pick-up was removed with a humbug device (Digitimer Ltd, Hertfordshire, England) before signals were digitized at a sampling rate of 10 kHz (Digidata 1322A; Axon Instruments, Sunnyvale, USA) and stored on hard disk (pClamp V. 8.2; Molecular Devices, Sunnyvale, USA).

2.4.2. Patch-clamp recordings

For whole-cell patch-clamp recordings, 300 µm thick slices were submerged in a chamber and continuously perfused with mACSF (for composition see Tab. 2.2). Pyramidal

cells in the CA3 region were visualized with DIC optics using a Zeiss upright microscope (Axioskop 2 FS; Goettingen, Germany) equipped with a water immersion objective (Olympus 60x/NA 0.9; Tokyo, Japan) and a video camera (Hamamatsu Photonics Deutschland GmbH, Herrsching, Germany). Additionally, the microscope featured epifluorescence (100 W Mercury lamp, Zeiss filter set 09: excitation filter 450-490 nm, beam splitter 510 nm, emission filter 515 nm) that was used to identify neuronal morphology. Patch pipettes (4-7 MΩ) were pulled from borosilicate glass on a vertical puller (PP-830; Narishige, Tokyo, Japan) and filled with intracellular solution depending on the type of experiment (see Tab. 2.3). Current-clamp recordings were performed using bridge balance circuitry and capacitance compensation of a BVC-700A amplifier (Dagan Corporation, Minneapolis, USA). Signals were low-pass filtered at 10 kHz, sampled at 100 kHz (Digidata 1440A; Molecular Devices, Sunnyvale, USA), and stored on hard disk (pClamp V. 9.0; Molecular Devices, Sunnyvale, USA). Voltage-clamp recordings were obtained using an Axopatch 200B amplifier (Molecular Devices, Sunnyvale, USA). low-pass filtered at 10 kHz, digitized at a sampling rate of 100 kHz (Digidata 1440A; Molecular Devices, Sunnyvale, USA) and stored on hard disk (pClamp V. 9.0; Molecular Devices, Sunnyvale, USA). The series resistance was smaller than 15 MΩ, and was compensated by 50-80 %, resulting in a voltage error smaller than 3 mV for all measurements.

Miniature inhibitory or excitatory postsynaptic currents (mIPSCs or mEPSCs, respectively) were recorded from CA3 pyramidal cells in the extracellular presence of 500 nM tetrodotoxin (TTX, Tab. 2.4) to block action potential generation. For mIPSCs, cells were held at a membrane potential of 0 mV (liquid junction potential-corrected) while glutamatergic neurotransmission was blocked with 50 µM (2R)-amino-5-phosphonovaleric acid (AP-V) and 10 µM 6-cyano-7-nitroquinoxaline-2,3-dione (CNQX). For mEPSCs, cells were held at -85 mV (liquid junction potential-corrected) while GABAergic neurotransmission was blocked with 500 nM 2-(3-Carboxypropyl)-3-amino-6-(4 methoxyphenyl) pyridaziniumbromid (GABAzine). Signals were low-pass filtered on-line at 1 kHz and analyzed with a custom routine programmed in IGOR-Pro (V 5.02; Wavemetrics, Lake Oswego, USA). To evoke IPSCs and EPSCs in CA3 region a monopolar glass pipette was placed within the CA1 s.r. for stimulation with square pulses of constant current (50 % of current-amplitude used for maximal IPSC amplitude, 0.1 ms pulse duration, 5 pulses
at 1, 5, 10 and 30 Hz, repeated 5 times every 30 s). To gain the maximal IPSC ampli-

tude we recorded an input-output curve with square pulses of currents between 5 and 150 µA. By holding the CA3 pyramidal cell at a membrane potential of -40 mV, compound postsynaptic currents with both an excitatory and inhibitory component could be recorded. For the isolated measurement of the excitatory component, inhibitory transmission was blocked by 10 µM GABAzine. Later, the inhibitory component could be evaluated by subtracting the excitatory component from the compound signal. To avoid the occurrence of synaptic plasticity by the repeated stimulations, 40 µM AP-V was present throughout these measurements.

2.4.3. Sharp microelectrode recordings

For intracellular sharp microelectrode recordings, 400 µm thick hippocampal slices were placed in a Haas-type interface chamber (35 ± 1°C) and perfused with normal ACSF (see Tab. 2.2). Microelectrodes (90-110 MΩ) were pulled from borosilicate glass on a Flaming-Brown type micropipette puller (P-97; Sutter Instruments, Novato CA, USA) and filled with 3.5 M potassium acetate. An active bridge circuit in the amplifier (Axoclamp 2B; Molecular Devices, Sunnyvale, USA) allowed simultaneous injection of current and measurement of membrane potential. After stabilization of neurons, different protocols were applied to assess intrinsic properties of pyramidal cells within CA1 area. Bridge balance was carefully adjusted before each measurement and experiments were discarded if it changes by more than 10 %. The signals were filtered on-line at 10 kHz, digitized at a sampling rate of 100 kHz and stored on hard disk (pClamp V. 8; Molecular Devices, Sunnyvale, USA).

2.5. Analysis

2.5.1. SPW-R activity

Data were analyzed with a custom routine programmed in IGOR-Pro (IGOR Pro V. 5.2). For SPW-detection, extracellular recordings were low-pass filtered at 50 Hz and SPWs were detected as voltage deflections of 3 times standard deviation (SD) above baseline value with a minimal duration of 20 ms defined by the time points when the trace crossed 0 mV level. The baseline was taken from signal sections between detected SPWs. Ripples were detected by the same IGOR-Pro routine as two consecutive negative deflections in the 150-300 Hz band-pass filtered signal exceeding a threshold of

4 times SD of baseline. The extracted events were inspected by eye, if the oscillations showed more than two cycles they were confirmed as ripple-events. Only ripples occuring coincidental with SPWs were included in the analysis for genotype comparison.

2.5.2. Current clamp data analysis

Passive membrane properties

Membrane potential deflections due to intracellular injection of small hyperpolarizing current steps (-10 to -50 pA) were used to calculate passive properties. Resting membrane potential (RMP in mV) was determined as the mean baseline-value of all sweeps before current injection onset. Membrane resistance (Rm in MΩ) was calculated from steady state membrane voltage deflection (mV) and corresponding injected current (pA) with Ohm's law.
Membrane time constant (τ) was calculated after fitting the decay of the evoked hyperpolarizing voltage (A) to the following equation:

$$f(t) = \sum_{i=1}^{n} A_i e^{-t/\tau_i} + C_m \tag{2.1}$$

The capacity of the membrane (C_m) was calculated subsequently as the quotient of τ and R_m:

$$C_m = \tau / R_m \tag{2.2}$$

Action potential morphology

A series of square-pulse current injections (lasting 500 ms) with increasing amplitude were applied to the cell. The first action potential (AP) occurring during the
first 50 ms of the current injection was selected and described quantitatively by determining its threshold, amplitude and halfwidth. The AP threshold was determined as the voltage at which the slope of the membrane potential (calculated as the first derivative of the recorded voltage-signal) exceeded 15 mV/ms (Sekerli et al., 2004). For the AP amplitude we determined the maximal membrane potential reached during the AP and for halfwidth we measured the duration of the AP at the voltage level halfway between

AP threshold and AP peak. Repetitive firing was examined using prolonged current injections (500 ms). Input-output relations were obtained with an automatic AP detection routine programmed in IGOR-Pro, which counted APs per sweep.
Many neurons show a reduction in the firing frequency during long depolarization. This spike adaptation was examined using prolonged (500 ms) depolarizing current injections of an amplitude which elicited six to seven APs per sweep. As an additional criterion, the first AP had to occur within 50 ms after current injection onset. The recording protocol was repeated up to 10 times for statistical robustness and the interval between consecutive APs (inter-spike inteval, ISI) was calculated. A spike adaptation index (SAI) which quantitatively describes spike adaptation was calculated by the following equation:

$$SAI = 1 - (ISI_{\text{min}}/ISI_{\text{n}}) \tag{2.3}$$

where ISI_{min} is the smallest ISI in a given sweep and ISI_n is the n^{th} ISI within that sweep. Large SAI values indicate strong spike adaptation.
AP afterpotentials like the fast afterhypolarizing potential (fAHP) and the afterdepolarizing potential (spike ADP) play a critical role in shaping neuronal firing patterns (Brown and Randall, 2009).
Brief (3 ms) depolarizing current injections were used to elicit single action potentials in conjunction with a spike ADP. The active component of the spike ADP was determined by subtracting the passive return of membrane voltage, elicited by a just subthreshold depolarizing current step, from the voltage waveform following an AP. The magnitude of the spike ADP was calculated as the integer of the voltage waveform from the fAHP to the point at which the membrane potential returned to baseline
(Clampfit V. 8; Molecular Devices, Sunnyvale, USA).

2.5.3. Miniature inhibitory postsynaptic currents

Miniature inhibitory postsynaptic currents (mIPSCs) were detected with an IGOR-Pro routine which calculated the sliding difference between two adjacent time windows of 0.5 ms duration each. Detection threshold was set to a difference of 5 pA between the mean current amplitude within each window. All detected mIPSCs were assessed by visual inspection to manually reject noise artifacts. To evaluate mIPSC kinetics, all events of a single cell were averaged and the decay of that average was fitted to a monoexponential function rendering the decay time constant τ. Histograms of mIPSC

amplitude and frequency were constructed by analyzing 5 min of gap free recording for each cell.

2.5.4. Miniature excitatory postsynaptic currents

For miniature excitatory postsynaptic current (mEPSC) detection, the first derivative of current traces (dI/dt) and its standard deviation (SD) of the entire current recording (10 min) were calculated. Then events with dI/dt >5 x SD were detected but only accepted for further analysis if their amplitude exceeded 5 x SD of the pre-event baseline (3 ms) and their decay time constant was 5-15 ms (as assessed with a mono-exponential fit). To evaluate mEPSC kinetics, all events of a single cell were averaged and the decay of that average was fitted to a monoexponential function yielding the decay time constant τ. Histograms of mEPSC amplitude and frequency were constructed by analyzing 10 min of gap free recording for each cell.

2.5.5. Evoked postsynaptic currents

For each neuron, an excitation/inhibition ratio was calculated using peak amplitudes of the isolated excitatory and inhibitory components of the electrically evoked postsynaptic currents. To estimate short-term plasticity, the peak amplitude of the first and fifth evoked current in a sweep was measured and their ratio calculated. This analysis was performed for all the different stimulation frequencies using Clampfit V. 10.2 (Molecular Devices, Sunnyvale, USA).

2.5.6. Statistics

All values are given as arithmetic mean ± standard error of the mean (SEM), unless otherwise noted. Statistical significance was tested using appropriate tests in Prism4 (GraphPad Software, San Diego, USA) as indicated in the Results section.

2.6. Immunohistochemistry and confocal imaging

CA3 pyramidal cells were recorded with an intracellular solution (see Tab. 2.3.) containing 0.3 % biocytin (Sigma-Aldrich, Munich, Germany) for at least 30 min. After the experiment slices were transferred to 4 % PFA for at least 24 h. For fluorescent labelling

and post-hoc reconstruction of the CA3 morphology, the slices were washed three times with 0.1 M phosphate-buffer and 0.05 M Tris-buffered saline (TBS) at room temperature for 10 min each. Subsequently, slices were incubated with Streptavidin-Alexa Fluor 488 conjugate (1:500, Life technologies, Darmstadt, Germany) in TBS for 2 h in the dark. After washing the slices three times for 5 min in 0.1 M phosphate-buffer, they were embedded in Vectashield mounting medium (Vector Labs, Peterborough, United Kingdom) and kept at 4 ℃ in the dark. Images were acquired with a confocal microscope (Nikon Eclipse T_i; Tokyo, Japan) using Nikon imaging software (NIS-Elements-AR). Maximum intensity projections of confocal image stacks were performed with imageJ software (NIH, Bethesda, USA). Pyramidal cell morphology was reconstructed using Corel Draw® 12 (Corel Corporation, Ottawa, Canada). Fig. 2.2 and 2.3 illustrate some example cells of either ASA wildtype-control or ASA null mice, respectively.

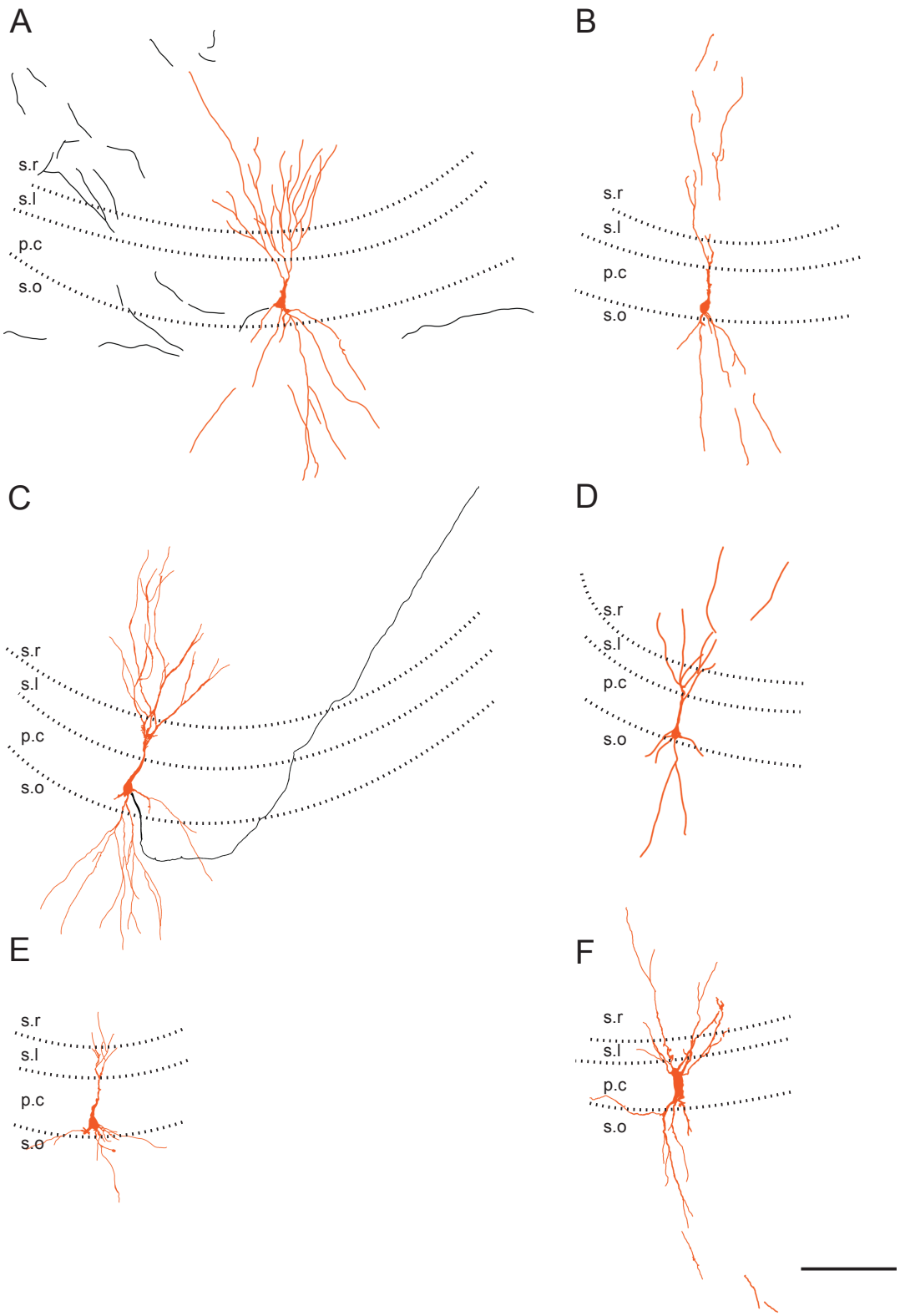

Fig. 2.2.: Reconstructed CA3 pyramidal cells of ASA wildtype-control slices
These cells had been filled with biocytin during whole cell measurements. Somata and dendrites are shown in orange, axons (if present) are shown in black. The hippocampal layers are indicated by the dashed lines. In all cases DG is located to the left, and CA1 region to the right. The scale bar in the right lower corner indicates 200 µm.

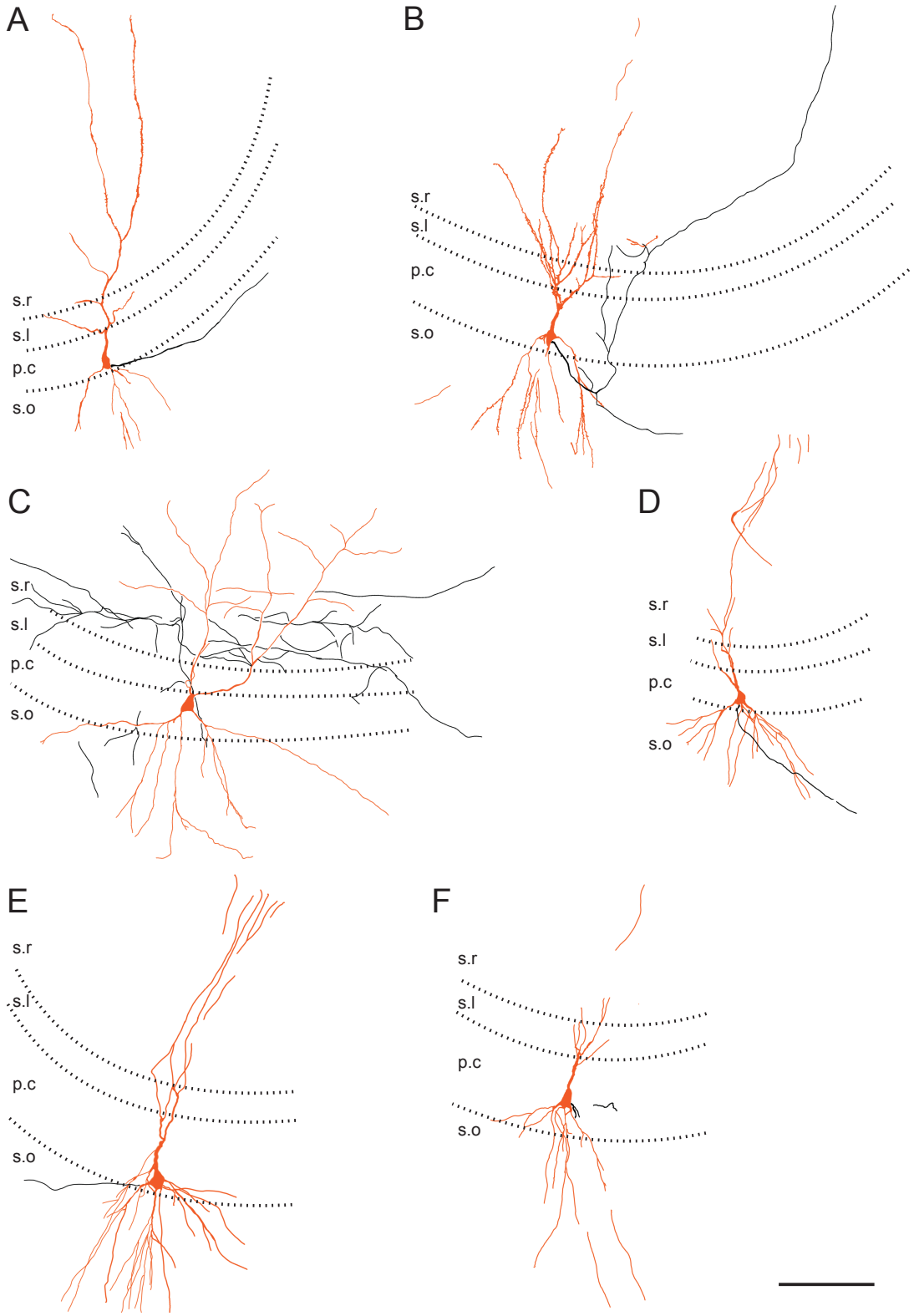

Fig. 2.3.: CA3 pyramidal cells from ASA null slices, reconstructed after staining
These cells had been filled with biocytin during whole cell measurements. Somata and dendrites are shown in orange, axons (if present) are shown in black. The hippocampal layers are indicated by the dashed lines. In all cases DG is left of the cell, whereas CA1 region would be located at the right handside. The scale bar in the right lower corner indicates 200 µm.

2.7. Solutions

2.7.1. Solutions for slice preparation and maintenance

Chemical	Sucrose ACSF	Normal ACSF	Modified ACSF (mACSF)
Sucrose	100		
NaCl	60	125	125
Na_2CO_3	26	26	26
KCl	2.5	3.5	3
Na_2HPO_4	1.25	1.25	1.25
$MgCl_2$	5	2	1.3
$CaCl_2$	1	2	2.5
D-glucose	20	15	15

Tab. 2.2.: All concentrations are given in mM. Osmolality of all three solutions: 295-305 mosmol/kg. pH 7.4 (when saturated with 95% O2/5% CO2.) All chemicals from Sigma-Aldrich (Munich, Germany).

2.7.2. Pipette solutions for whole-cell patch-clamp recording

Chemical	Current clamp *	Voltage clamp**	Miniature EPSC
potassium gluconate	140		
$MgCl_2$	0.5	0.5	3
phosphocreatine disodium salt	5	5	5
EGTA	0.16	0.16	0.16
HEPES	5	5	5
cesium methansulfonate		120	120
QX-314		5	

Tab. 2.3.: All concentrations are given in mM. Osmolality: 282 mosmol/kg (adjusted with sucrose). pH 7.4 (adjusted with *KOH or **CsOH). All chemicals from Sigma-Aldrich (Munich, Germany). For morphological analysis 50 µM Alexa Fluor 488 hydrazide (Invitrogen, Life Technologies GmbH, Darmstadt, Germany) and 0.3% biocytin (Sigma-Aldrich, Munich, Germany) were added. Abbreviations: HEPES (4-(2-hydroxyethyl)-1-piperazineethanesulfonic acid); EGTA (ethylene glycol tetraacetic acid).
*The liquid junction potential of this solution was -13 mV. Without correction potentials would be 13 mV more positive.
**For all voltage-clamp experiments, voltages were corrected for a liquid junction potential of -15 mV. Without correction potentials would be 15 mV more positive.

2.7.3. Specific inhibitors for pharmacological experiments

chemical	Stock concentration	Final concentration
tetrodotoxin (TTX) citrate	1 nm	500 nM
(2R)-amino-5-phosphonovaleric acid (AP-V)	No stock	50 µM
6-cyano-7-nitroquinoxaline-2,3-dione (CNQX) disodium salt	10 mM	10 µM
2-(3-Carboxypropyl)-3-amino-6-(4 methoxyphenyl)pyridaziniumbromid (GABAzine)	10 mM	10 µM

Tab. 2.4.: Specific inhibitors for pharmacological experiments. For stocks, substances were dissolved in ddH_2O, aliquoted, and stored at -20 ℃ until use. All chemicals from Tocris.

3. Results

3.1. Sulfatide storage in CNS

ASA null mice show an increased incidence of brief episodes of aberrant high-frequency cortical activity at an age of 8-10 weeks (Eckhardt et al., 2007). To see if ASA deficiency is associated with sulfatide storage within the murine brain at these early adult timepoints, we performed alcian blue stainings, which detect predominantly lysosomal accumulation of sulfatide (see chapter 2.3.1). In our experiments ASA null mice at an age of 8-12 weeks showed very discrete alcian blue labeling in the cell layers of DG and the hippocampal CA regions, as well as in cortical neurons of ASA null mice, but not in littermate controls (Fig. 3.1, 3.2).

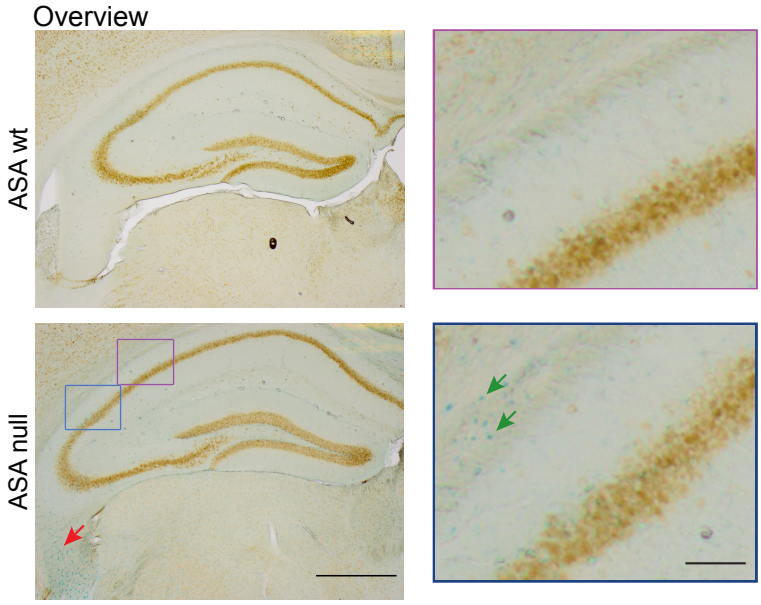

Fig. 3.1.: Alcian-blue staining of horizontal , hippocampal slices
Top pictures show a slice of an ASA wildtype-control, bottom pictures show one of an ASA null animal. Whereas slices from ASA wildtype mice were devoid of any alcian blue staining, ASA null slices showed distinct blue deposits within the fimbria (red arrow) and the alveus (purple and blue rectangle; see close ups at right side). The light-brown staining is caused by NeuN-staining of neuronal structures. Scale bar is 400 µm for left pictures and 50 µm for right close ups.

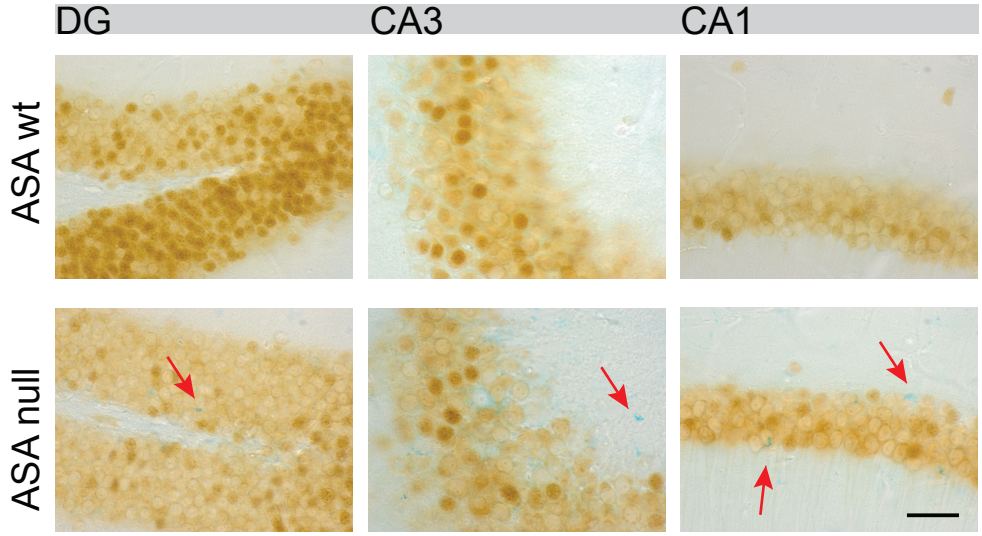

Fig. 3.2.: Alcian-blue staining within adjacent hippocampal areas
Top pictures show a slice of an ASA wildtype-control, bottom pictures show one of an ASA null animal. Alcian blue staining is absent in ASA wildtype-control slices whereas it could be found within all hippocampal areas, (DG, CA3 and CA1; prominent spots are marked with a red arrow) in ASA null mice. The light-brown staining is caused by NeuN-staining of neuronal structures. Scale bar in the lower right panel applies for all pictures and represents 25 µm.

Alcian blue staining could also be clearly seen within fiber tracts of the hippocampus, most notably the fimbria (Fig: 3.3).

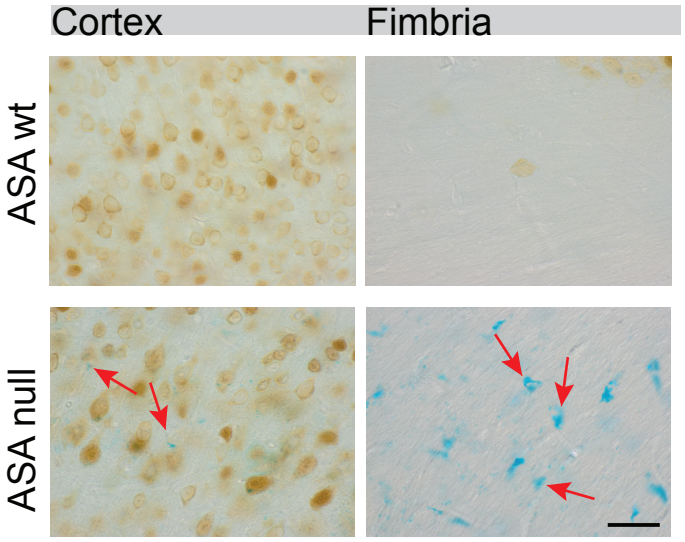

Fig. 3.3.: Alcian blue staining in cortex and fimbria
Photographs of brain slices containing cortex (left) and fimbria (right) stained with alcian blue. Top pictures show stained tissue of ASA wildtype-control animal, bottom pictures show stained tissue of ASA null animal. Example alcian blue stained spots are marked with red arrows . No alcian blue staining could be found within ASA wildtype-control mice whereas ASA null tissue shows numerous alcian blue stained structures in neocortex as well as in fimbria. The light-brown staining is caused by NeuN-staining of neuronal structures. Scale bar is 25 µm.

To quantify total sulfatide storage in neural tissue, electrospray ionization-mass spectroscopy (ESI-MS) was performed for different hippocampal and cortical areas. Because quantification of absolute sulfatide levels is difficult, we co-determined three different sulfatide species (18:0, 24:1 and 12:0 sulfatide). These differ in their distribution. C18:0 sulfatide can be found in grey matter (Eckhardt, 2008) whereas the sulfatide: C24:1 is the most abundant sulfatide within myelin (van Zyl et al., 2010). C12:0 sulfatide is equally distributed amongst the different neural cell types. Thus, determining the ratio of C18:0 or C24:1 vs. C12:0 sulfatide can yield information about changes in neuronal or glial sulfatides in ASA null mice.

We therefore calculated the ratio of 18:0 and 24:1 sulfatides, yielding a value that increases with neuronal sulfatide storage. These calculations were performed in the hippocampal areas DG, CA3 and CA1 (Fig. 3.4) as well as in fimbria, corpus callosum (CC) and cortex (Fig. 3.4). The amount of neuronal sulfatide was significantly higher for ASA null compared to ASA wildtype-control mice in DG and CA1 (Mann-Whitney U test, $p=0.026$ and $p=0.0087$, respectively), but not in CA3 region (Mann-Whitney U test, $p=0.2403$). Within measured other brain areas (CC, neocortex and fimbria) the ratio of C18:0 to C24:1 sulfatide was significantly increased within the Corpus callosum (CC) for ASA null mice compared to ASA wildtype-control mice (Mann-Whitney U test,

p= 0.0060; Fig. 3.4). The other cortical areas did not show a significant difference (Mann-Whitney U test; fimbria: p=0.0640; neocortex: p=0.6004).

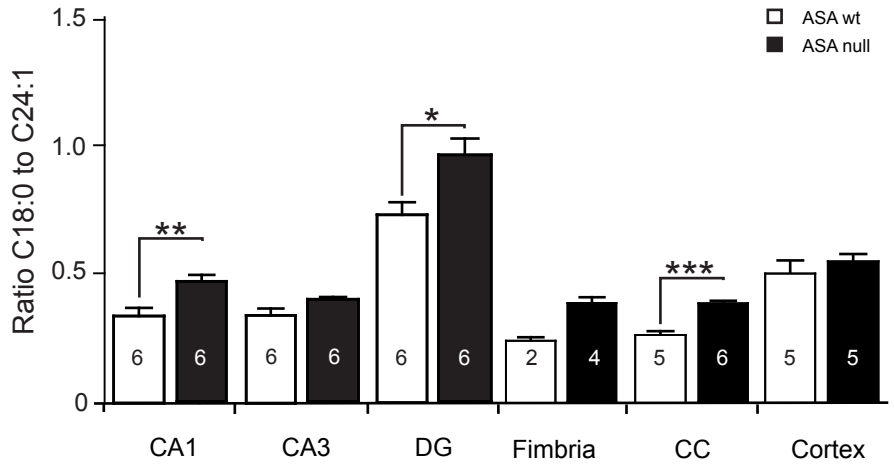

Fig. 3.4.: Plasmalemma storage of sulfatide as determined by EMI-MS results for different brain regions
Plasmalemma sulfatide levels in different hippocampal and other brain areas, quantified as ratio of C18:0 to C24:1 sulfatides. Genotypes are identified by filling color (see legend within the graphs) and numbers of measured animals are indicated within each bar. $*$, $**$ and $***$ indicate $p < 0.05$, 0.01 and 0.001, respectively

3.2. SPW-R complexes

Eckhardt et al. (2007) showed that ASA null mice at an age of 8-10 weeks show an increase in spontaneous discharges and polyspikes in cortical EEG recordings *in vivo* . Because we observed sulfatide accumulation within the hippocampus, we hypothesized that abnormal network activity might also occur in the hippocampus.

To test this idea, we obtained field potential recordings in CA3 and CA1 pyramidal cell layers of 8-12 weeks old ASA wildtype-control and ASA null (as described in chapter 2.4.1). We observed SPW-R complexes in both wildtype-control and ASA-null mice. SPW-Rs consisted of two components: a fast ripple oscillation (150-300 Hz) superimposed on a slower SPW. Ripple oscillations were defined as oscillations with more than one sinusoidal oscillation. The sharp-wave and ripple components can be separated by band-pass filtering (Fig. 3.5). Example traces of 5 s duration are shown in Fig. 3.5 A and B as the uppermost trace (black). After bandpass-filtering between 1-50 Hz slow events, corresponding to SPWs can be detected (dark gray traces in Fig. 3.5 A, B, SPWs indicated by #). Single representative SPWs are shown in the insets of Fig.

3.5 A and B (labeled with SPW). Ripple events were isolated by bandpass-filtering the original recording between 150-300 Hz (lowest trace, light gray in 3.5 A, B). A single ripple oscillation is shown in the inset of Fig. 3.5 B (labeled with SPW-R). SPW-Rs are indicated within all traces.

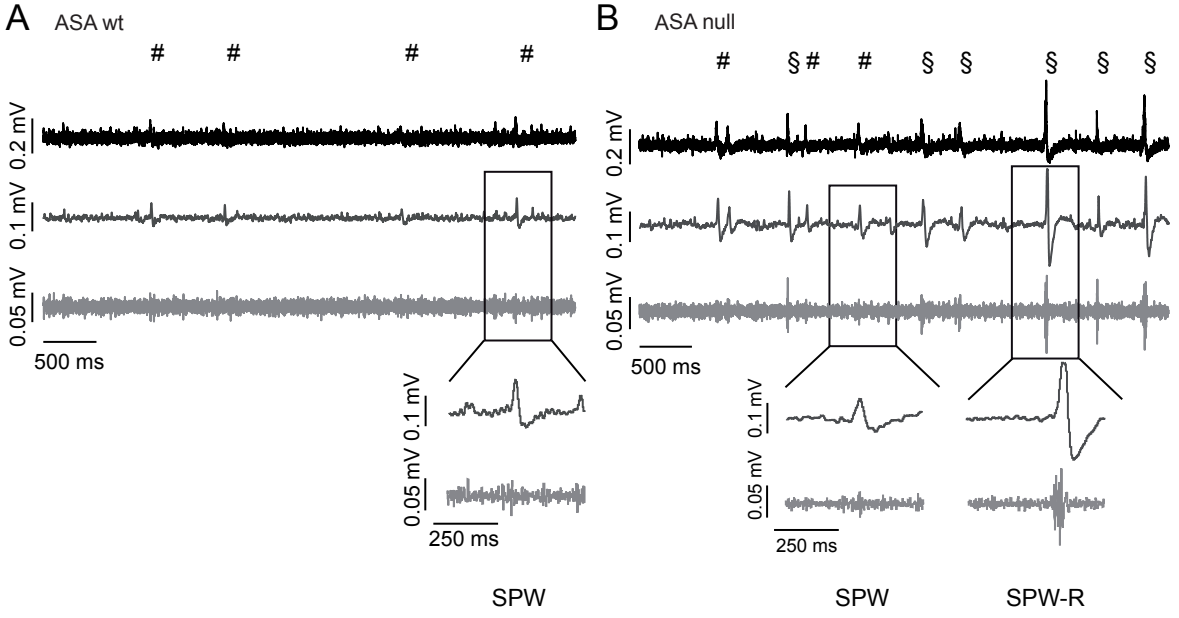

Fig. 3.5.: Representative SPW-R complex recordings in an ASA wildtype-control and an ASA null slice

Examples of field potential recordings in the wide band without post-hoc filtering (top), after application of a 1-50 Hz bandpass filter (middle) and a 150-300 Hz bandpass filter (bottom), for ASA wildtype-control (A) and ASA null mice (B) *in vitro*. # mark sharp wave events (SPWs), § mark simultaneous SPWs and ripple events (SPW-R).

Following band-pass filtering, SPWs and SPW-Rs were detected as described before (see chapter 2.5.1) in gap-free field potential recordings of 5 minutes duration. The frequency of SPWs was not altered between the two genotypes (Fig. 3.6 A; Two-Way ANOVA with Bonferroni's post-test, $p=0.1033$).
Although SPW frequency was significantly higher in CA3 region compared to CA1 region in both genotypes (Two-Way ANOVA, $p<0.0001$, with Bonferroni's post-test positive).

Regarding SPW-amplitude (Fig. 3.6 B), higher, not significant amplitudes were found for SPWs recorded in CA3 compared to CA1 region (Two-Way ANOVA, $p<0.0266$, with Bonferroni's test: not significant).

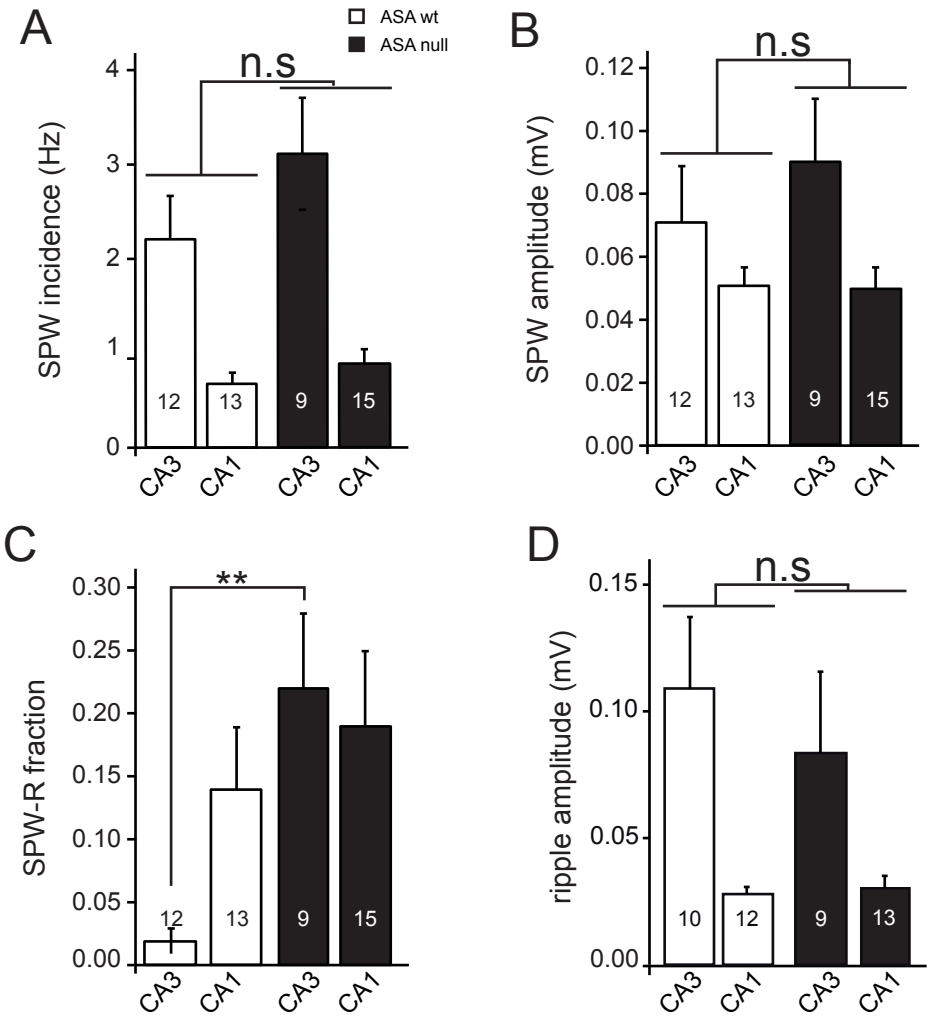

Fig. 3.6.: SPW-R properties in ASA wildtype-control and ASA null slices
Calculated SPW-R properties in CA3 and CA1 pyramidal cell layer in wildtype-control (white bars) and null (black bars) mice. A: SPW incidence in Hz, B: peak SPW amplitude in mV, C: fraction of SPWs accompanied by ripple events, the significant difference between ASA wildtype-control and null slices in CA3 region is indicated with two stars, D: peak ripple amplitude (mV). All bar graphs show mean values ± SEM, n-numbers shown in bars. SPW-incidence, -amplitude and ripple amplitude were tested with Two-Way ANOVA followed by Bonferroni's post-test, SPW-R fraction was tested with Kruskal-Wallis test (non-parametric test) followed by Dunn's multiple comparison test. $*$, $**$ and $***$ indicate $p < 0.05$, 0.01 and 0.001, respectively.

In a further step we analyzed simultaneously occurring SPWs and ripple events and calculated the fraction of all SPWs accompanied with ripple events (Fig. 3.6 C). A significant enhancement of SPW-Rs could be found in ASA null animals within the CA3 region (Kruskal-Wallis test, p=0.0026, Dunn's multiple comparison test: significant) but not within CA1 region (Dunn's multiple comparison test: not significant). The analysis of ripple oscillation amplitude (Fig. 3.6 D) showed no differences between wildtype-

control and null slices, neither in CA3 nor in CA1 subregion (p=0.6307, Bonferroni's test: not significant) .

3.3. Synaptic properties of CA3 pyramidal cells

These results indicate that there is a significant up-regulation in the capability of the CA3 region to generate ripple oscillations. Ripple oscillations are thought to arise as a consequence of a high-frequency phase shifted discharge of pyramidal cell ensembles. Thus, both differences in synaptic drive and differences in the intrinsic properties of CA3 pyramidal cells can underlie augmented ripple oscillations. We first examined synaptic transmission in the CA3 region by recording miniature postsynaptic EPSCs and IPSCs.

3.3.1. Miniature inhibitory postsynaptic currents

To examine spontaneous, AP-independent mIPSCs, voltage-clamp measurements were obtained from CA3 pyramidal cells in the presence of the sodium channel blocker TTX (500 nM). Miniature IPSCs were recorded at a holding potential of 0 mV for 5 min (Fig: 3.7 A). When the cumulative probability of mIPSC amplitudes was plotted over all cells for both genotypes, the distributions proved to be different (gray line for wildtype-control and black line for null cells; Kolmogorov Smirnov test, p=0.012 , 3.7 C). However, when the mean mIPSC amplitudes were calculated for each cell and then averaged, no differences between wildtype-control and ASA null group could be found (unpaired t-test: p=0.836, Fig. 3.7 C, inset). The same type of analysis was applied to inter-event intervals. Also here, significant differences in the distribution of all IEIs between the two genotypes were detected (gray line for wildtype-control and black line for null cells; Kolmogorov Smirnov test, p=0.213 , Fig. 3.7 D). When mIPSC frequencies were calculated per cell and averaged, however, no differences between wildtype-control and ASA null groups were detected (unpaired t-test: p=0.914, Fig. 3.7 D, inset). The kinetics of these miniature IPSCs were unaltered. We averaged all detected mIPSCs in an individual cell, and subsequently fit the decay of the averaged mIPSC with a monoexponential function. The time constant τ of the mIPSC was not different between wildtype-control and ASA null mice (black bar) (unpaired t-test, p=0.620, Fig. 3.7 B).
Even though differences in mIPSC properties were detected using the Kolmogorov Smirnov test on mIPSCs acquired over all cells, there was a clear lack of changes when

considering the average IPSC amplitudes and frequencies. We thus interpret these results as a lack of biologically significant changes in mIPSC properties.

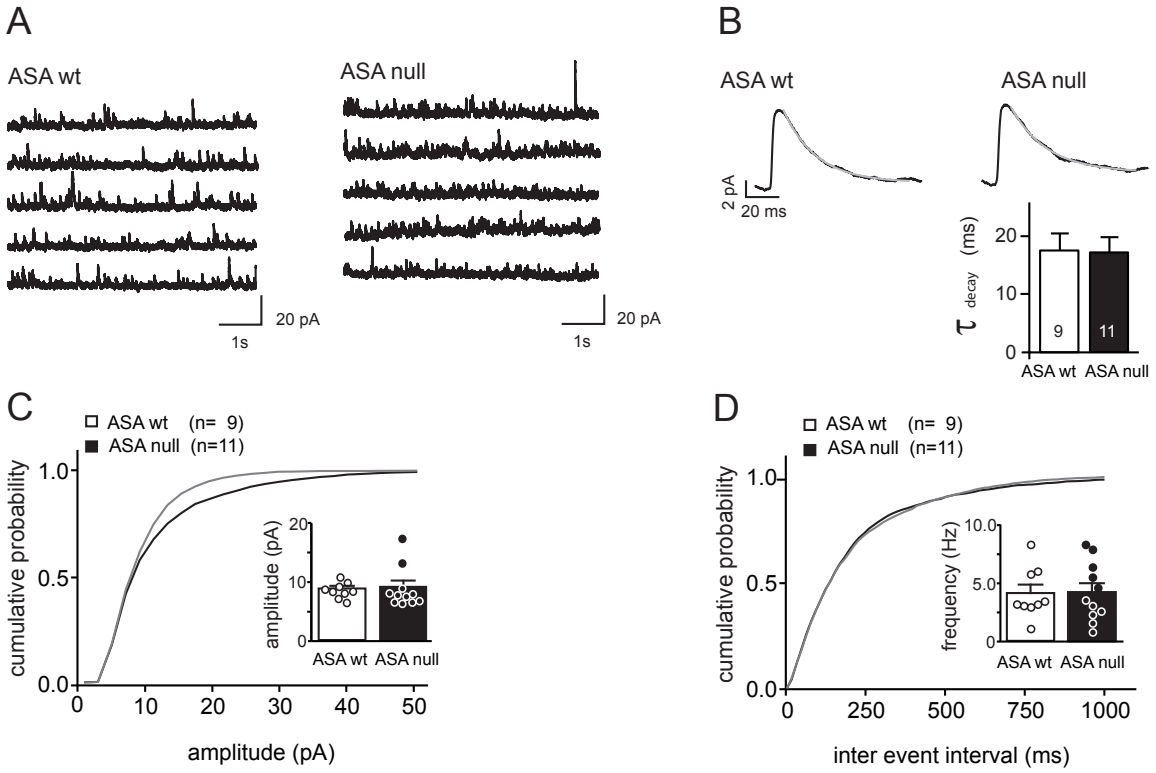

Fig. 3.7.: Properties of miniature inhibitory postsynaptic currents (mIPSCs)
A: Example recording for wildtype-control (left) and null (right) cells. B: Kinetic parameters of measured cells, averaged mIPSC (black trace) and fitted decay (gray trace) shown for one wildtype-control (left) and one null cell (right), bar graph at the bottom shows results for calculated tau decay (ms) for wildtype-control (white bar) and null cells (black bar). C: Cumulative probability plot for mIPSC amplitude in pA of wildtype-control (gray line) and null (black line) cells and additionally bar graph of mIPSC amplitude with inserted mean mIPSC amplitude per cell (circles) for both genotypes. D: Cumulative probability plot for mIPSC inter event interval in ms of wildtype-control (gray line) and null (black line) cells and additionally bar graph of mIPSC frequency in Hz with inserted mean mIPSC frequency per cell (circles) for both genotypes. All bar graphs show mean values ± SEM.

3.3.2. Miniature excitatory postsynaptic currents

Additionally to inhibitory synaptic function, miniature EPSCs were recorded at a holding potential of -85 mV for 10 min (Fig. 3.8 A). We plotted the cumulative probability of all mEPSC amplitudes from all cells (at least 50 events per cell). We were not able to see genotype-dependent differences between the resulting distributions (gray line for wildtype-control cells and black line for null cells; Kolmogorov-Smirnov test, p=0.783, Fig. 3.8 C). The direct comparison of average mEPSC amplitudes also showed

no differences (unpaired t-test, p=0.512, Fig. 3.8 C, inset). Next, we plotted all interevent intervals as a cumulative probability distribution (Fig. 3.8 D). We could detect differences between wildtype-control (gray line) and null cell (black line) distributions (Kolmogorov-Smirnov test test, p=2.597e^{-10}). However, an analysis of average mEPSC frequency did not show differences between wildtype-control and null cells (unpaired t-test, p=0.265, Fig. 3.8 D, inset).

We next examined the mEPSC decay kinetics by fitting the decay of average EPSCs obtained from individual cells with a monoexponential equation. The resulting time constant τ was not different between wildtype-control and ASA null mice (unpaired t-test, p=0.549, Fig. 3.8 B). Similar to mIPSCs, these results suggest that robust changes in mEPSCs are not present in ASA null mice.

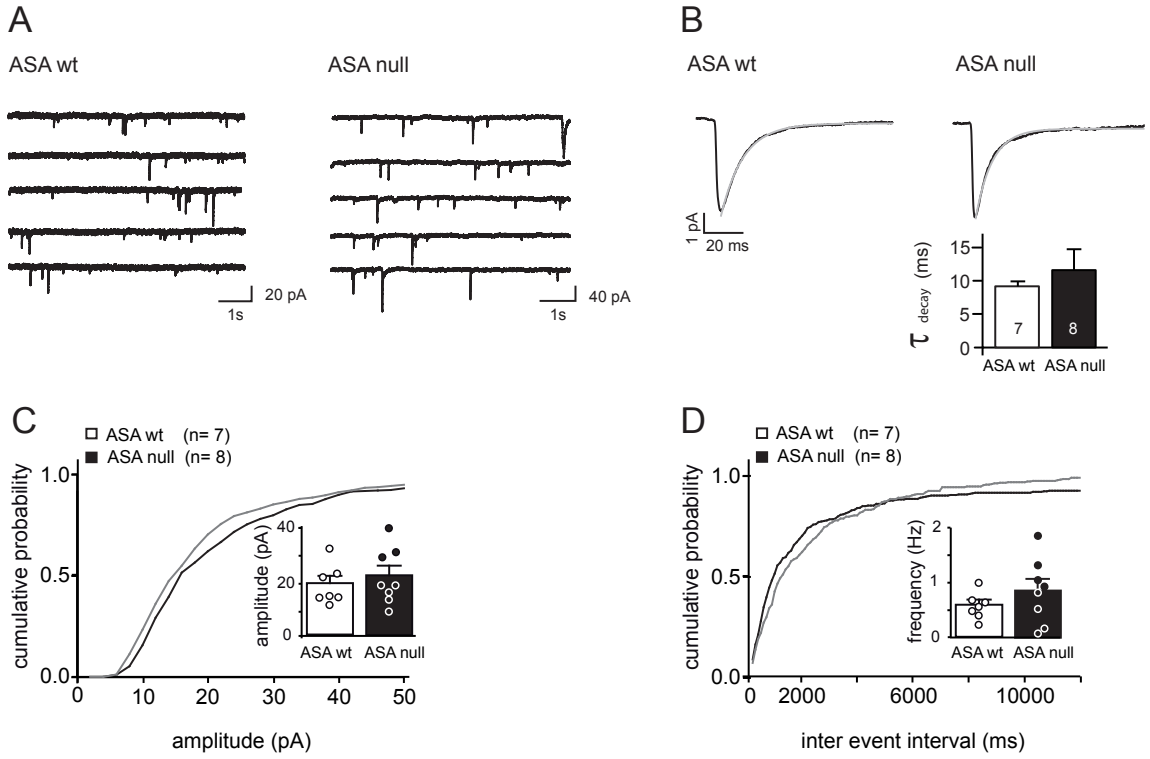

Fig. 3.8.: Properties of miniature excitatory postsynaptic currents (mEPSCs)
A: Example recording for wildtype-control (left) and null (right) cells. B: Kinetic parameters of measured cells, averaged mEPSC shown for one wildtype-control and one null cell, bar graph shows mean ± SEM τ decay (ms) for wildtype-control (white bar) and null (black bar) cells. C: Cumulative probability plot for mEPSC amplitude (pA) of wildtype-control (gray line) and null (black line) cells. Bar graph of mEPSC shows mean ± SEM amplitude with inserted mean mEPSC amplitude per cell (circles) for both genotypes. D: Cumulative probability plot for mEPSC inter event interval (ms) of wildtype-control (gray line) and null (black line) cells. Bar graph shows mean ± SEM of mEPSC frequency (Hz) with inserted mean mEPSC frequency per cell (circles) for both genotypes.

3.3.3. AP-dependent transmitter release

The previous experiments suggest that the properties of excitatory and inhibitory synapses are not fundamentally altered due to sulfatide storage in DG and CA1. However, these experiments have addressed only action potential-independent release, and do not exclude changes in action potential-dependent release. We therefore performed an additional set of experiments to examine whether there might be changes in action potential-dependent neurotransmitter release. Because both feed back inhibition and recurrent excitation are thought to modulate SPW-Rs, we designed an experiment that allows us to examine recurrent excitation and inhibition in the CA3 region. To activate recurrent excitation and inhibition, we electrically stimulated the axons of the CA3 pyramidal neurons (the Schaffer collaterals) with a glass pipette placed within the CA1 stratum radiatum. This leads to antidromic activation of a subset of CA3 neurons, and synaptic activation both of CA3 interneurons and CA3 pyramidal neurons via recurrent collaterals. We then recorded stimulation-evoked PSCs in CA3 pyramidal cells.

Evoked postsynaptic currents of single and train stimulation protocols were measured at a holding potential of -55 mV before (Fig. 3.9 B, top traces) and after the wash-in of GABAzine (10 μM) (Fig. 3.9 B, middle traces). Subtraction between those two resulting recordings (Fig. 3.9 B, bottom trace) yielded the isolated inhibitory currents (due to feed back activation). Measured IPSCs were the result of evoked feed back inhibition due to activated CA3 interneurons. Measured EPSCs should reflect activity of excitatory axon collaterals of CA3 pyramidal cells. The ratio of excitation to inhibition was quantified as the ratio of either EPSC/IPSC amplitudes (Fig. 3.9 C, left axis; white bar for wildtype-control and black bar for null cells) or EPSC/IPSC areas (Fig. 3.9 C, right axis; white bar for wildtype-control and black bar for null cells). No differences of excitation/inhibition balance between genotypes could be detected (amplitude: unpaired t-test p=0.416; area: unpaired t-test p=0.672 with Welsh correction).

To assess short-term plasticity of IPSCs we calculated the ratio of the first and fifth IPSC amplitude ($IPSC_5/IPSC_1$) in a train of 5 stimuli (Fig. 3.9 D, upper recording for example wildtype-control cell and lower recording for example null cell) at different frequencies (Fig. 3.9 E, white bars for wildtype-control cells and black bars for null cells). No differences could be found between ASA wildtype-control and null cells neither for low: 1, 5 and 10 Hz, nor for higher frequencies (30 Hz; Tab. 3.1 middle column). Short-term plasticity of EPSCs was examined in the same manner as for IPSCs (Fig.

3.9 F, upper recording for example wildtype-control cell and lower recording for example null cell). No difference could be found (Fig. 3.9 G) between ASA wildtype-control (white bars) and null cells (black bars) neither for low: 1,5 and 10 Hz, nor for higher frequencies (30 Hz; Tab. 3.1 right column).

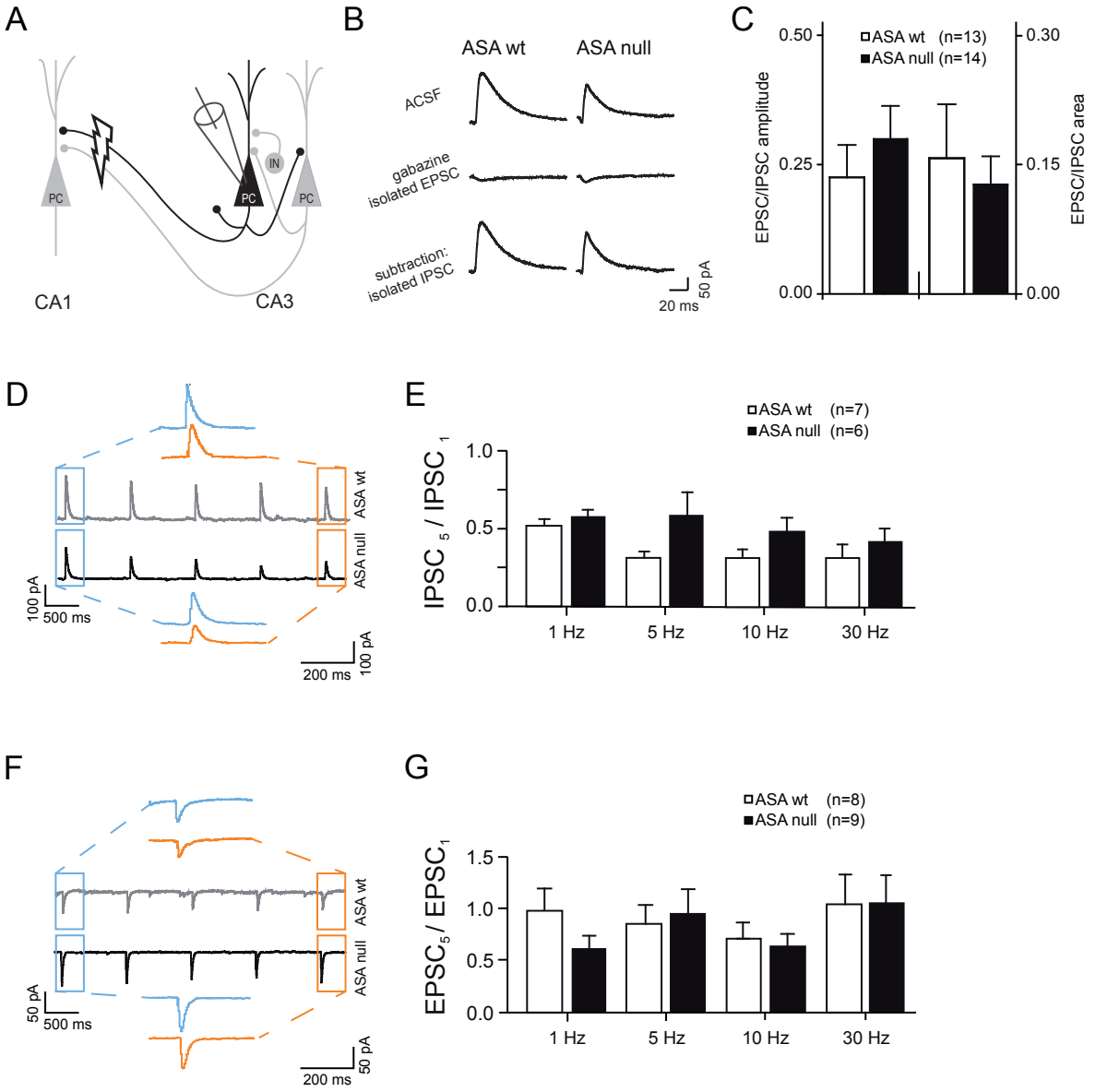

Fig. 3.9.: Postsynaptic currents (PSCs) evoked by Schaffer collateral stimulation in CA3 pyramidal cells

A: Scheme of stimulation configuration and involved cells. B: Example traces of measured evoked postsynaptic current in one ASA wildtype-control (left) and one null (right) cell during single stimulation (upper traces) while holding the cell at -55 mV, after isolation of EPSC by application of GABAzine (10 μM) wash-in (middle traces) and calculated IPSC component (lower trace). C: Calculated ratio of measured EPSC to IPSC amplitude (left) and area (right) of measured cells in ASA wildtype-control (white bars) and null (black bars) animals. D: IPSC example traces for 5 Hz train stimulation with extracted first (blue traces) and fifth (orange traces) evoked inhibitory current. E: Amplitude ratio of fifth to first IPSC calculated for ASA wildtype-control and null cells during 1 Hz, 5 Hz, 10 Hz and 30 Hz stimulation trains. F: EPSC example traces for 5 Hz train stimulation with extracted first (blue traces) and fifth (orange traces) evoked excitatory current. G: Amplitude-ratio of fifth to first EPSC calculated for ASA wildtype-control and null cells during 1, 5, 10 and 30 Hz stimulation trains. All bar graphs show mean values ± SEM.

frequency (Hz)	IPSC ratio	EPSC ratio
1	0.366	0.199
5	0.073	0.962
10	0.101	0.814
30	0.445	1.000

Tab. 3.1.: P-values for short term plasticity
P-values for tested ratios of fifth to first stimulation of either evoked IPSCs or EPSCs. All values were calculated using Mann-Whitney U test.

3.4. Intrinsic properties of hippocampal pyramidal cells

So far no changes in synaptic properties of CA3 pyramidal cells could be detected. A change in intrinsic passive and active properties of those cells seemed to be responsible for an increase in hippocampal network activity as seen in CA3 SPW-R recordings *in vitro* . To assess this we performed current-clamp recordings of CA3 pyramidal cells and microelectrode recording techniques in CA1 pyramidal cells.
As part of our experiments we studied CA1 pyramidal cells since in EMI-MS we were able to detect an increase in neuronal sulfatides within CA1 region. Even though we showed that SPW-R complexes are not altered within this CA1 area we wanted to record if sulfatide accumulations within CA1 excitatory neurons might alter intrinsic properties of these neurons.

3.4.1. Unaltered passive properties of pyramidal cells in ASA null mice

Current clamp measurements allowed us to examine passive and active membrane properties of recorded pyramidal cells. Passive membrane properties were examined via long 500 ms (CA3) or 150 ms (CA1) hyperpolarizing current pulses of low amplitudes.

CA3

None of the calculated parameters like resting membrane potential (RMP in mV), membrane resistance (MΩ), membrane capacitance (pF) and time constant (τ) showed differences between wildtype-control and null cells during physiologic bivalent cation concentrations (Tab. 3.2 first row).

bivalent cations (mM)	genotype	RMP (mV)	τ(ms)	R_M (MΩ)	C_M (pF)
2.6 Ca^{2+} & 1.3 Mg^{2+}	ASA wt	-68.73 ± 0.45	44.26 ± 5.05	187.88 ± 15.94	236.17 ± 19.37
	ASA null	-69.43 ± 1.00	54.26 ± 5.43	232.68 ± 26.14	246.55 ± 20.38
1.3 Ca^{2+} & 1.3 Mg^{2+}	ASA wt	-72.21 ± 0.72	56.56 ± 3.82	240.34 ± 19.29	247.52 ± 20.21
	ASA null	-71.68 ± 0.90	61.62 ± 4.50	298.87 ± 26.96	241.90 ± 11.91
1.0 Ca^{2+} & 1.0 Mg^{2+}	ASA wt	-70.48 ± 0.84	53.62 ± 6.99	213.91 ± 23.73	261.86 ± 31.47
	ASA null	-69.40 ± 0.71	61.73 ± 4.88	249.29 ± 19.61	253.57 ± 15.42

Tab. 3.2.: Passive properties of CA3 pyramidal cells
Mean ± SEM values of passive membrane properties of measured CA3 pyramidal cells dependent on their genotype and bivalent cationic concentrations in the extracellular solution. RMP= resting membrane potential (in mV), τ= time constant (in ms), R_M= membrane resistance (in MΩ) and C_M= membrane capacitance (in pF).

Changes in plasma membrane composition due to a potential increase of sulfatide storage within the outer membrane-leaflet might have an influence on ionic surface screening. Sulfatides are negatively loaded and therefore might disrupt ionic surface screening if they are massively stored within this leaflet. We therefore hypothesized that different concentrations of cationic bivalents might reveal a changed amount of stored sulfatides in ASA null compared to ASA wildtype-control cells. To investigate, if different cationic ion-concentrations would lead to changes in intrinsic properties we applied ACSF with different calcium- and magnesium-concentrations. We additionally injected hyperpolarizing currents of 500 ms duration and low amplitude via the somatic electrode and analyzed passive properties. The assumption that lower bivalent concentrations might reveal the differences in passive properties could not be confirmed. None of the investigated properties was significantly altered due to bivalent cation changes in comparison between genotypes (unpaired t-test).

As mentioned above, we also examined CA1 pyramidal cells. Employing sharp microelectrode technique we were able to establish stable measurements in cells of slices from either young (8-12 weeks) or older mice (5-6 months) of both genotypes. Passive membrane properties were examined via 150 ms long hyperpolarizing current pulses of low amplitudes (-50 pA, -80 pA and -110 pA). None of the calculated parameters like RMP (mV), R_m (MΩ), C_m (pF), and τ (ms) showed differences between wildtype-control and null cells of either young or older animals (Tab. 3.3, unpaired t-test).

Age	n	genotype	RMP (mV)	τ(ms)	R_M (MΩ)	C_M (pF)
8-12	8	ASA wt	-71.70 ± 1.4	9.00 ± 0.6	65.30 ± 5.1	141.00 ± 9.0
weeks	8	ASA null	-74.70 ± 1.3	11.10 ± 1.1	77.00 ± 5.2	146.00 ± 13.0
5-6	7	ASA wt	-70.03 ± 5.5	16.89 ± 11.5	61.72 ± 23.1	202.52 ± 72.4
months	7	ASA null	-70.88 ± 1.8	12.73 ± 0.5	59.61 ± 32.6	150.07 ± 28.3

Tab. 3.3.: Passive properties of CA1 pyramidal cells
Mean ± SEM of passive membrane properties of CA1 pyramidal cells dependent on their genotype and age. RMP= resting membrane potential (in mV), τ= time constant (in ms), R_M= membrane resistance (in MΩ) and C_M= membrane capacitance (in pF).

3.4.2. Unaltered firing properties of pyramidal neurons in ASA null mice

Like passive properties, values which characterize cells while an AP is fired due to a depolarizing sodium influx or other intrinsic properties might be changed as a result of sulfatide storage within membranes. Those intrinsic firing properties were examined by injecting either long or short depolarizing current steps. We next determined how the amount of different extracellular cationic bivalents influences the active properties. Parameters of single APs like threshold, amplitude and halfwidth or ADP parameters like amplitude and area were analyzed. These examinations should provide evidence if voltage-gated channels are impaired as a result of plasma membrane sulfatide storage.

Action potential properties for CA3 pyramidal cells

All values determined for single cells were measured by applying repetitive long current injections (5-8 repetitions) of 500 ms. Example traces for a wildtype-control (upper traces) and a null cell (lower traces) are shown in Fig. 3.10 A. We analyzed the first AP occurring in a time-window 50 ms after pulse onset (Fig. 3.10 A, enlarged first AP). Action potential threshold time was determined (Fig. 3.10 A, below enlarged AP) as the voltage at the timepoint at which the first derivative exceeds a value of 15 mV/ms (Fig. 3.10 A, dashed vertical line). The average value for each cell was plotted in a scatterplot to give a better overview of outliner cells and the effect of changed bivalent concentration and genotype (Fig. 3.10 B, C, D). As part of the analysis we also had a look at the mean of all cells for each condition and dependent of genotype. The data were compared for each genotype and bivalent concentration with unpaired t-tests and no significant differences could be revealed (Tab. 3.4).

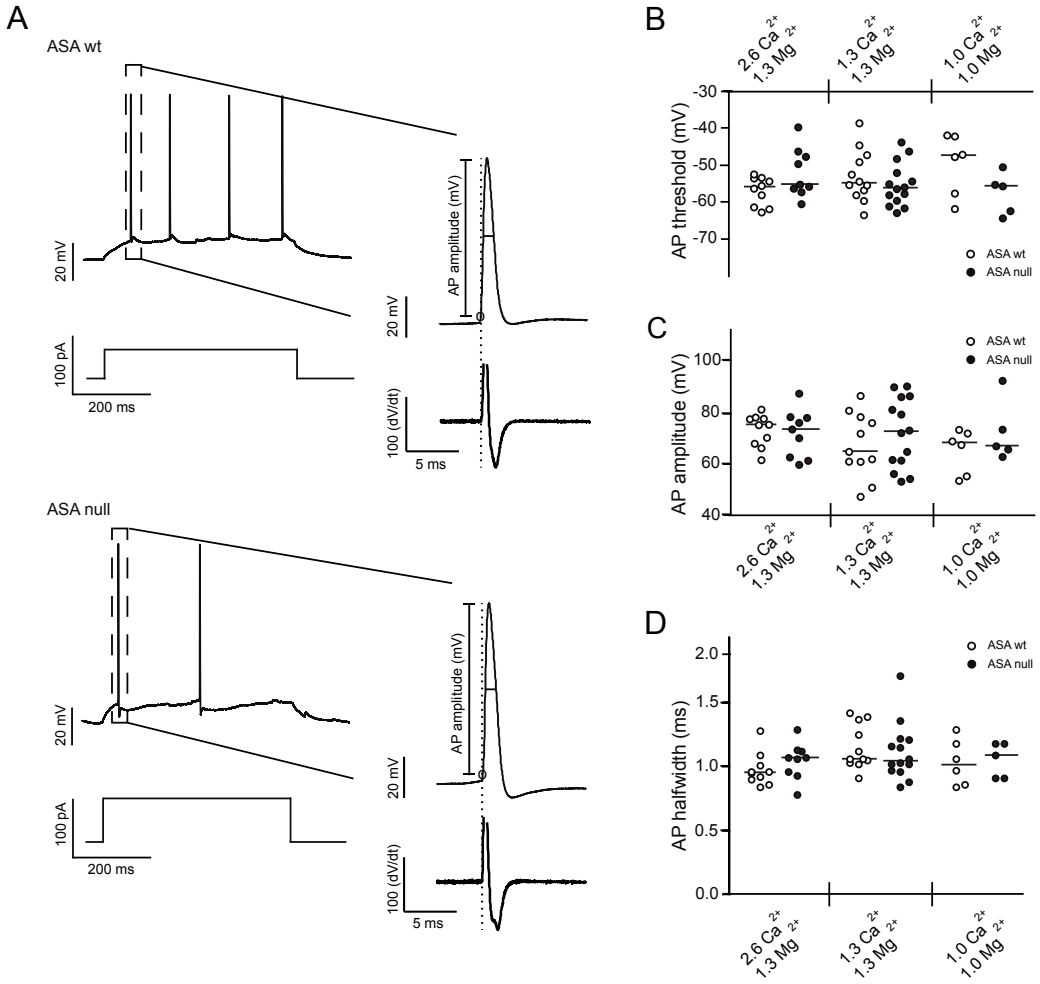

Fig. 3.10.: Properties of current-injection evoked action potentials (APs) measured in CA3 pyramidal cells dependent on extracellular bivalent concentrations
A: Example traces of wildtype-control (top) and null (bottom) cell during 500 ms depolarizing current injection causing an AP 50 ms after injection onset. Augmented section shows original trace (top) with calculated parameters and first derivative (bottom) to set timepoint of threshold. B, C, D: Calculated AP properties for wildtype-control (white circles) and null (black circles) cells dependent on extracellular bivalent concentrations. B: AP threshold in mV. C: AP amplitude in mV and D: AP halfwidth in ms.

bivalent cations (mM)	p-value
AP threshold	
2.6 Ca^{2+} + 1.3 Mg^{2+}	0.0609
1.3 Ca^{2+} + 1.3 Mg^{2+}	0.3676
1.0 Ca^{2+} + 1.0 Mg^{2+}	0.1026
AP amplitude	
2.6 Ca^{2+} + 1.3 Mg^{2+}	0.7460
1.3 Ca^{2+} + 1.3 Mg^{2+}	0.3701
1.0 Ca^{2+} + 1.0 Mg^{2+}	0.2734
AP halfwidth	
2.6 Ca^{2+} + 1.3 Mg^{2+}	0.2873
1.3 Ca^{2+} + 1.3 Mg^{2+}	0.6364
1.0 Ca^{2+} + 1.0 Mg^{2+}	0.8371

Tab. 3.4.: P-values for CA3 AP parameters
The different extracellular bivalent cation concentrations and resulting AP threshold, amplitude and halfwidth were compared for the two genotypes. Resulting values were tested with unpaired t-tests and no differences between the genotypes could be detected.

Action potential properties for CA1 pyramidal cells

Measurements were performed in both younger and older animals to see, if an increased age correlates with an increased neuronal sulfatide storage and progressive physiological changes. While doing repetitive long pulse current injections (500 ms) we analyzed the first AP occurring in a time window 50 ms after stimulation onset (depicted as dashed box and magnified in the inset at the right side of Fig. 3.11 A).

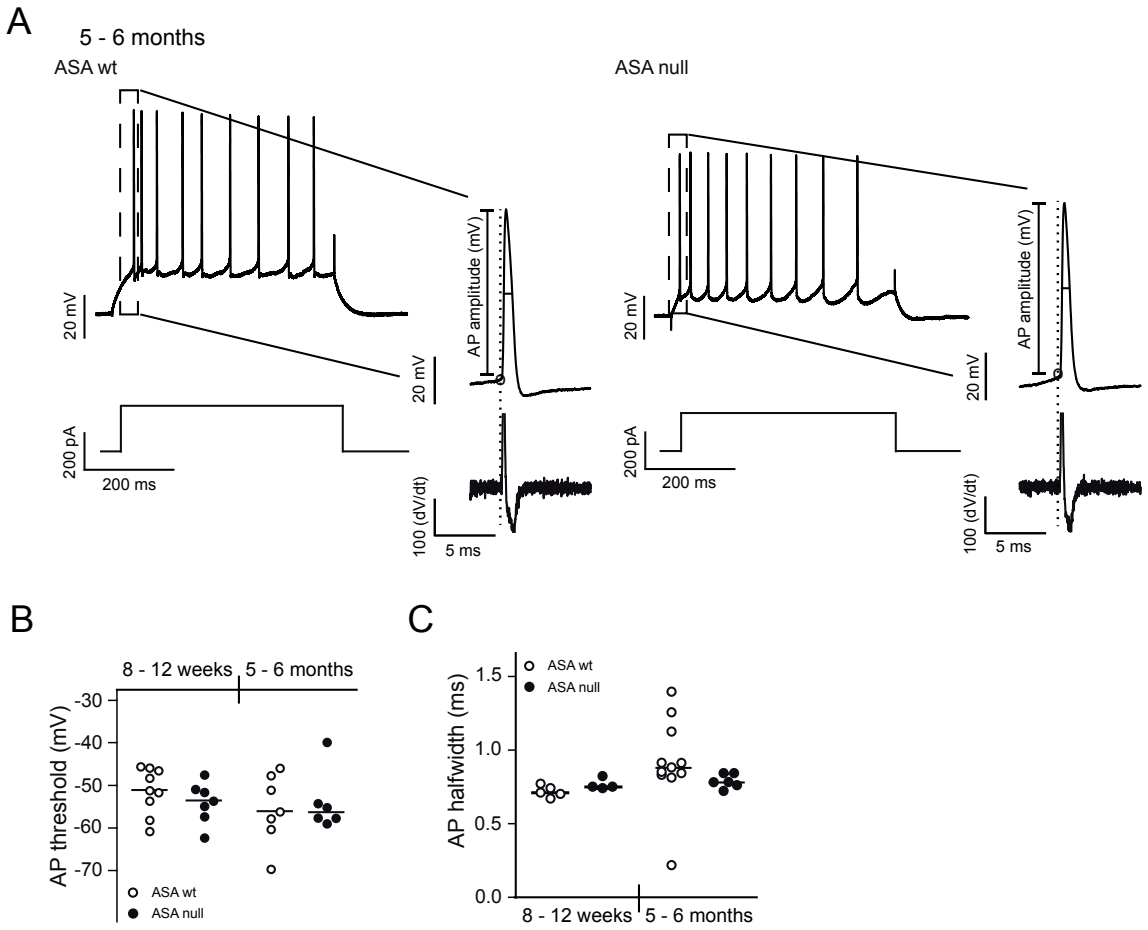

Fig. 3.11.: Properties of action potentials (APs) evoked by current-injection in CA1 pyramidal cells A: Example traces of a wildtype-control (left) and a null (right) cell during 500 ms depolarizing current injection causing an AP 50 ms after injection onset. Augmented section shows original trace (top) with calculated parameters and first derivative (bottom) to set timepoint of threshold. B, C: Calculated AP-properties for wildtype-control (white circles) and null (black circles) cells dependent on age (see x-axis labeling). B: AP threshold in mV. C: AP halfwidth in ms.

No changes between genotypes could be detected in animals at an age of 8-12 weeks (Tab. 3.5). This was also the case for cells measured in older animals with an age of 5-6 months (Tab. 3.5).

age	p-value
AP threshold	
8 - 12 weeks	0.312
5 - 6 months	0.716
AP halfwidth	
8 - 12 weeks	0.105
5 - 6 months	0.337

Tab. 3.5.: P-values for tested CA1 AP parameters
AP threshold and AP halfwidth were tested for young and old ASA wildtype-control and null animals with unpaired t-tests. No differences between the genotypes could be detected.

ADP in CA3 pyramidal cells

An additional influx of calcium ions influences potassium efflux. This is the reason why a hyperpolarization followed by a second depolarization (ADP) could often be seen after an AP. To investigate this spike ADP, single APs, triggered by short current injections of 3 ms duration were examined (Fig. 3.12 A). ADP amplitude and area were calculated as described before (see chapter 2.5.2). ADP amplitude and area did not seem to depend on extracellular bivalent cation concentration and did not differ between ASA wildtype-control and null cells (Fig. 3.12 B, C; Tab. 3.6). Independently of genotype, ADP area and amplitude differed a lot at normal bivalent concentrations of 2.6 mM Ca^{2+} and 1.3 mM Mg^{2+} (SD wildtype-control cells = 119.4, null cells = 155.8), whereas lower bivalent concentrations like 1.3 mM Ca^{2+} and 1.3 mM Mg^{2+} did not show as high SD values (wildtype-control cells = 50.21, null cells = 44.88).

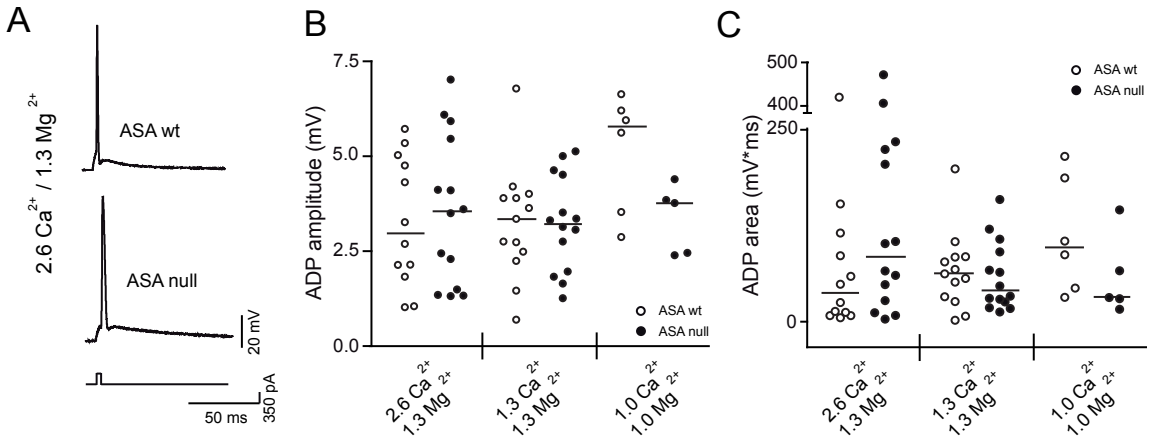

Fig. 3.12.: Properties of ADPs of CA3 pyramidal cells
A: Example traces of ASA wildtype-control (top) and null (bottom) cell during short current injection (3 ms) protocol, while current injection results in a single AP. B, C: Calculated ADP properties for wildtype-control (white circles) and null (black circles) cells dependent on extracellular bivalent concentrations (see x-axis labeling). B: ADP amplitude in mV. C: ADP area in mV x ms.

bivalent cations (mM)	p-value
ADP amplitude	
2.6 Ca^{2+} + 1.3 Mg^{2+}	0.682
1.3 Ca^{2+} + 1.3 Mg^{2+}	0.972
1.0 Ca^{2+} + 1.0 Mg^{2+}	0.052
ADP area	
2.6 Ca^{2+} + 1.3 Mg^{2+}	0.262
1.3 Ca^{2+} + 1.3 Mg^{2+}	0.704
1.0 Ca^{2+} + 1.0 Mg^{2+}	0.210

Tab. 3.6.: Results of tested CA3 ADP parameters
To see if calculated ADP properties show any differences we tested all data sets with an unpaired t-test. No differences could be detected.

CA3 pyramidal cell repetitive firing behavior

To investigate the inactivation states of voltage-gated sodium channels we performed experiments on pyramidal cells via current-clamp techniques and injected long pulse currents with increasing amplitudes in ASA wildtype-control and null cells (Fig. 3.13 A, B).

We examined repetitive firing properties for analyzing gain (Fig. 3.14 A, B, C) and spike adaptation (Fig. 3.16) using long current pulses with increasing (gain) or constant amplitudes (jitter).

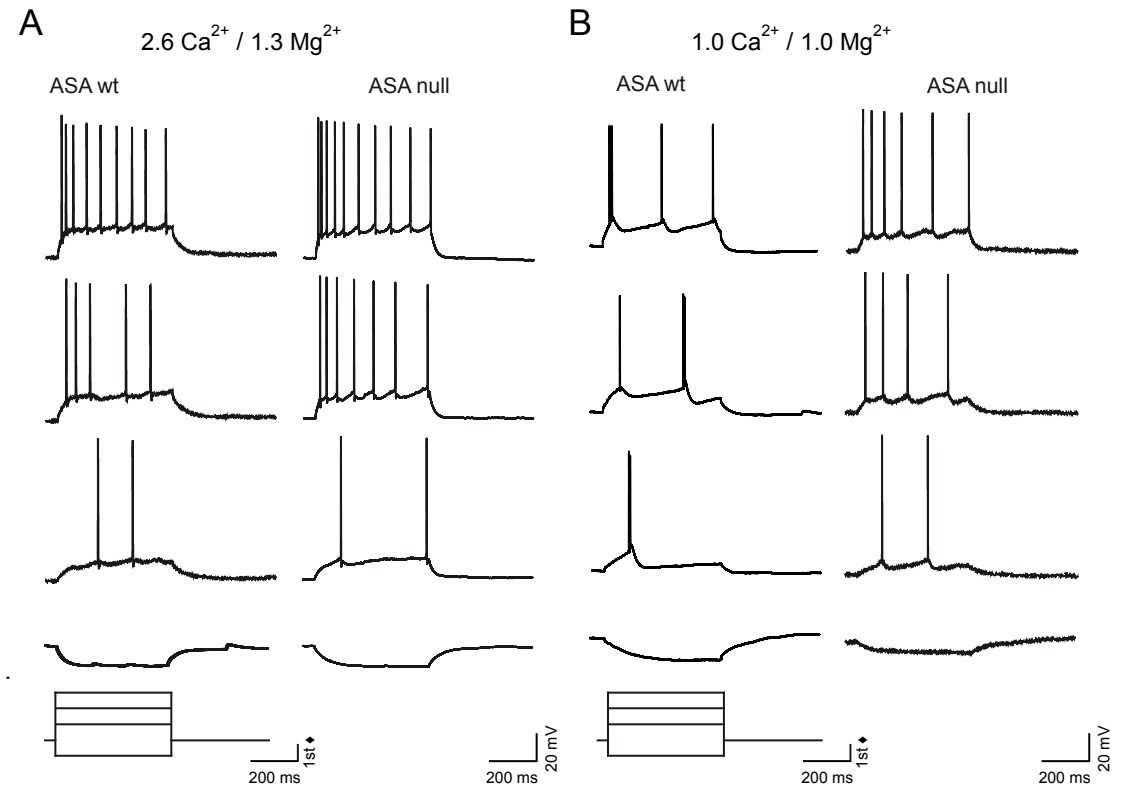

Fig. 3.13.: Firing behavior of CA3 pyramidal cells during long current injections
A: Recordings with extracellular bivalent concentrations of 2.6 mM Ca^{2+} and 1.3 mM Mg^{2+} and B: of 1.0 mM Ca^{2+} and 1.0 mM Mg^{2+}. Example traces for ASA wildtype-control (left) and null (right) cells. Recordings are shown for triple - (uppermost), double- (second) and single- (third) threshold stimulation as well as for a single hyperpolarizing current injection (bottom trace).

For the gain analysis we plotted the firing rate (Hz) as a function of injected current depending on extracellular bivalent cation concentration (Fig. 3.14 A, B and C) and found a significant decrease of firing rate for higher stimulus amplitudes in null cells under 2.6 mM Ca^{2+} and 1.3 mM Mg^{2+} condition compared with the firing rate of wildtype cells (Fig. 3.14 A). For the other two extracellular bivalent cation concentrations used we could not find a difference (Fig. 3.14 B, C). Additionally to gain analysis, we investigated regular (light gray), doublet (gray) and and burst firing behavior (black) of CA3 pyramidal cells (Fig. 3.14 D) during long current injections. With decreasing extracellular bivalent concentrations the tendency for CA3 pyramidal cells of both genotypes to fire doublets or even bursts of APs is increased.

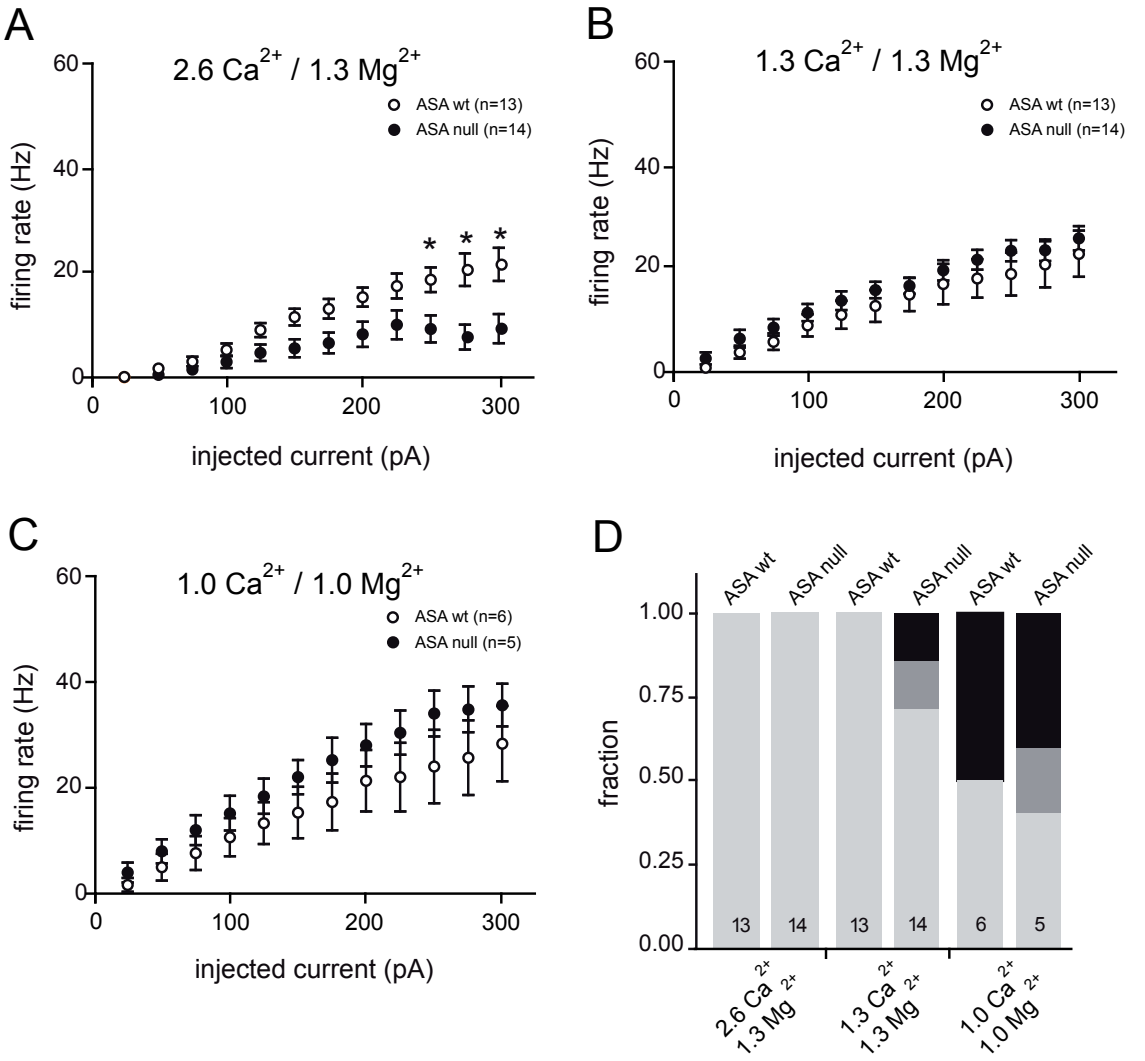

Fig. 3.14.: Firing behavior of CA3 pyramidal cells during long-pulse current injections
A, B and C: Calculated firing rate as a function of injected current (pA) for different bivalent concentrations (in mM). A: 2.6 Ca^{2+} and 1.3 Mg^{2+}, B: 1.3 Ca^{2+} and 1.3 Mg^{2+},C: 1.0 Ca^{2+} and 1.0 Mg^{2+}. D: Classification of all wildtype-control (ASA wt) and null (ASA null) cells in regular firing (light gray), doublet firing (dark gray) and burst firing (black) cells during different extracellular bivalent concentrations. All graphs show mean values ± SEM, n-numbers shown in D. $*$, $**$ and $***$ indicate $p < 0.05$, 0.01 and 0.001, respectively.

CA1 pyramidal cell firing behavior

Firing behavior was also investigated in CA1 pyramidal cells while injecting long current injections of 500 ms duration with increasing amplitudes (50 pA steps). Input-output relations were obtained and the firing rate was plotted as a function of stimulation amplitude (Fig. 3.15 A and B). For CA1 pyramidal cells we did not find any differences

between ASA wildtype-control or null cells, neither for young animals (8-12 weeks), nor for the older animals (5-6 months, Fig. 3.15 B).

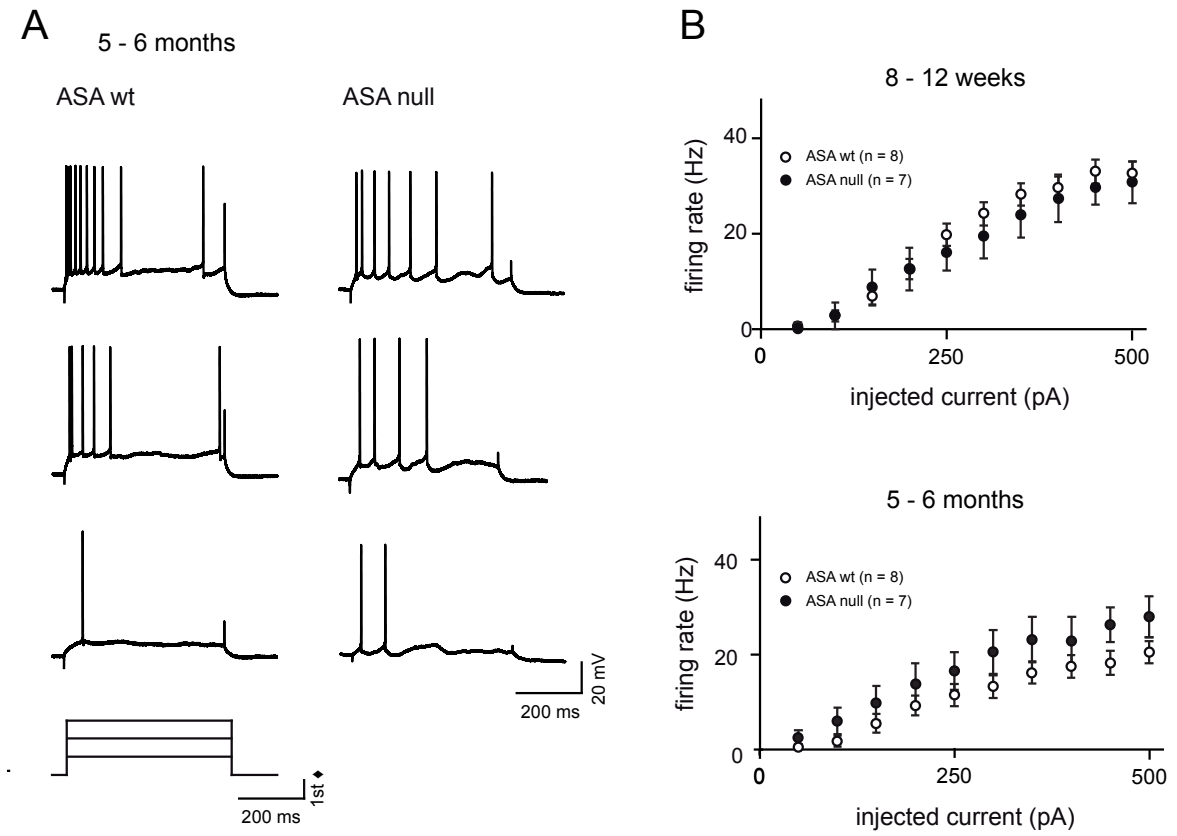

Fig. 3.15.: Firing behavior in CA1 pyramidal cells during long current injections
A. Example traces for wildtype-control (left) and null (right) cells during triple- (uppermost), double- (second) and single- (third) threshold current injection. B: Calculated firing rate as a function of injected current (pA) for different ages. top: 8-12 weeks, bottom: 5-6 months. All graphs show mean values ± SEM, n-numbers are shown within graphs.

Spike adaptation in CA3

Unlike other hippocampal neurons, pyramidal cells most often show regular firing patterns. To investigate if ASA null pyramidal cells show different firing pattern in comparison to ASA wildtype-control cells we investigated spike adaptation within hippocampal pyramidal cells at different extracellular bivalent concentrations. To this end we applied the jitter stimulation protocol (Fig. 3.16 A). The timepoint of firing was examined while injecting long current pulses to calculate firing adaptation at least eight times with a constant stimulation amplitude which evoked six to seven APs. The calculated values for the jitter were tested for each ISI with Mann-Whitney U test.

ASA wildtype-control cells as well as ASA null cells show regular firing patterns, the minimum ISI values were small for the first evoked APs and increased with ongoing AP-number. No differences in jitter, independent of outer bivalent concentration, could be detected (Fig. 3.16 B).

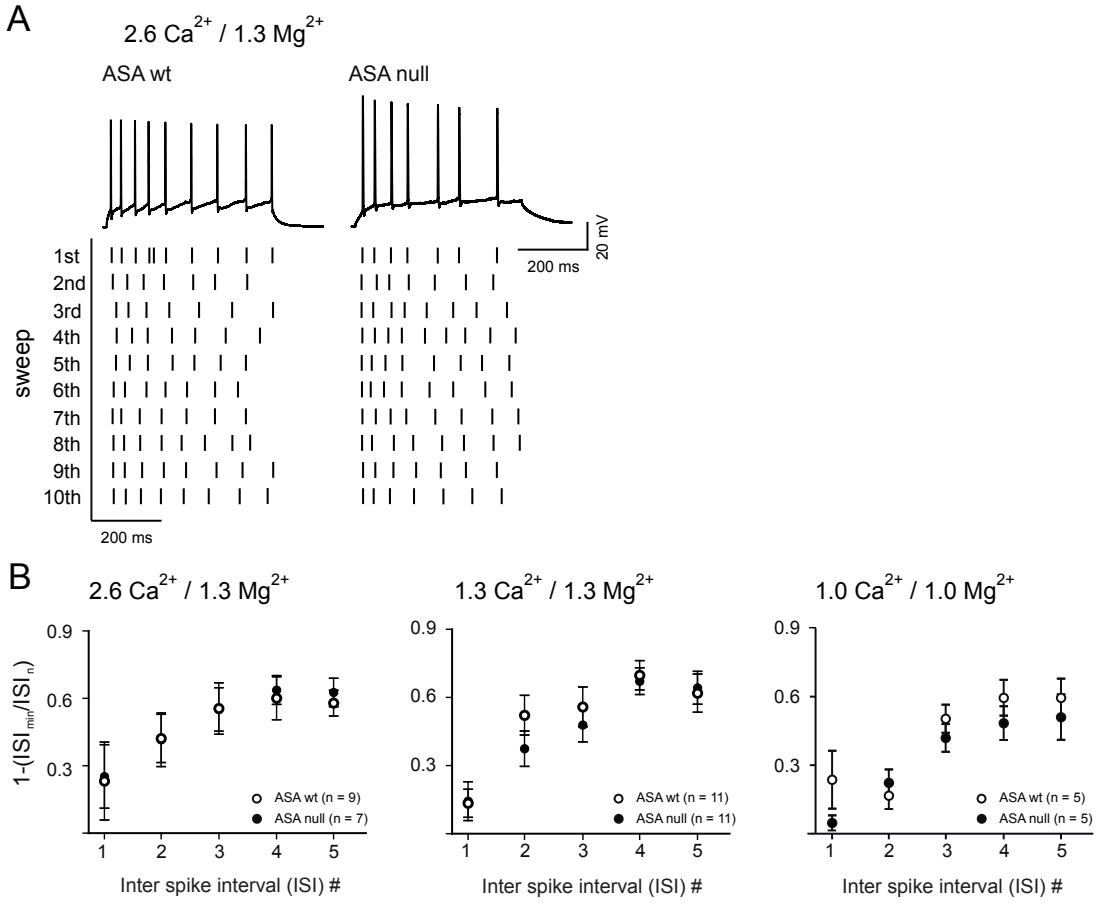

Fig. 3.16.: Spike adaptation during repetitive long (500 ms) current injections
A. Original recordings of firing CA3 pyramidal cells in ASA wildtype-control (left panel) and null cells (right panel). Below each recording, raster plots of AP timepoints due to each injection sweep is shown for all ten sweeps. B. Adaptation index as a function of ISI number. Data are shown for extracellular bivalent concentrations of 2.6 Ca^{2+} and 1.3 Mg^{2+} (left), 1.3 Ca^{2+} and 1.3 Mg^{2+}(middle) and 1.0 Ca^{2+} and 1.0 Mg^{2+} (right) for ASA wildtype-control (white circles) and ASA null cells (black circles).

Spike adaptation in CA1

To calculate spike adaptation, firing was examined while injecting long current pulses at least eight times with a constant stimulation amplitude which evoked seven to eight APs. The calculated ISI adaptation index increased with ongoing pulse duration. This was the case for all measured cells independent of genotype and age (Fig. 3.17). The

calculated values for the jitter were tested for each ISI with Mann-Whitney U test.

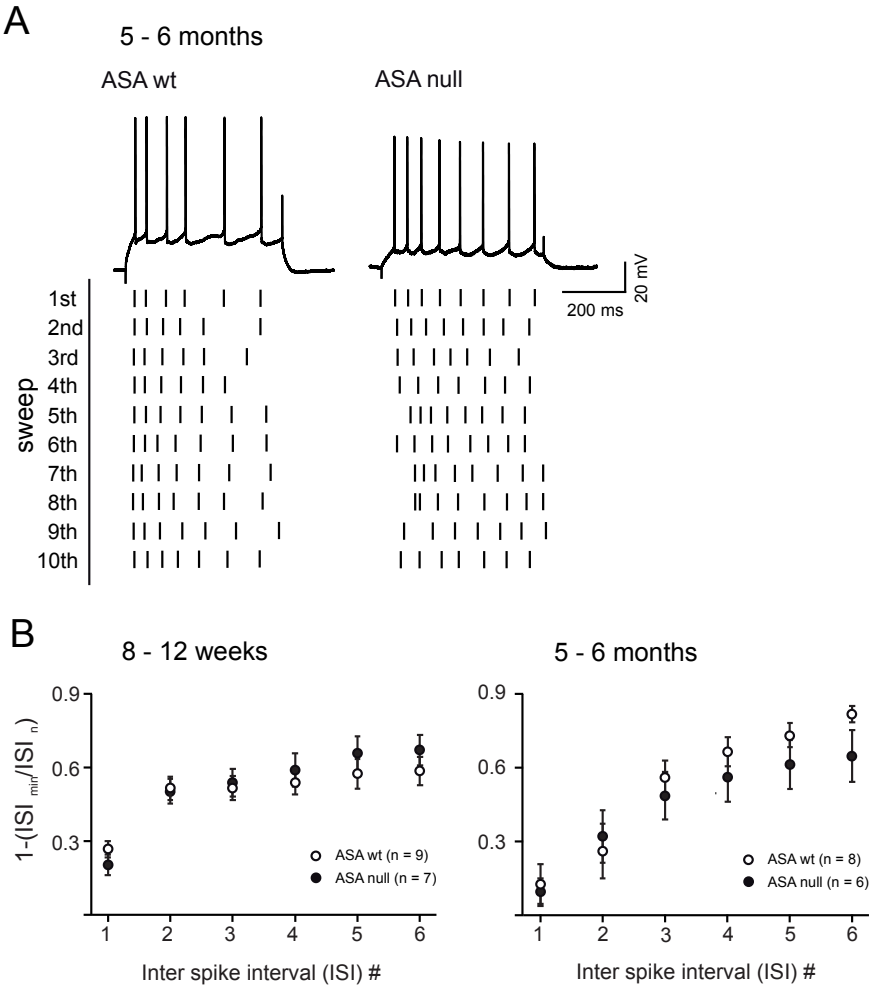

Fig. 3.17.: Spike adaptation in CA1 pyramidal cells during long (500 ms) current injections
A. Original recordings of firing CA1 pyramidal cells in ASA wildtype-control and ASA null tissue during 500 ms current injection. Below each recording, raster plots of AP timepoints due to each injection sweep are shown for ten sweeps. B. As a value of spiketime adaptation the minimum ISI was divided by the interspike interval given by the x-axis labeling, the result was substracted from 1. These data were shown for cells measured in tissue from either animals of an age of 8-12 weeks (left) or 5-6 months (right) for ASA wildtype-control (white circles) and ASA null cells (black circles). N-numbers are shown within the graphs.

Maximal firing rate of CA1 pyramidal cells

To investigate the maximal firing rate, ramp-like current injections were performed (Fig. 3.18 A, schematic ramp at the bottom). To this end 2 s lasting currents were injected via the recording pipette. The slope of the ramp was increased until the evoked AP

frequency did no longer increase (Fig. 3.18 A, bottom, middle and upper recording). Offline, the minimal interval (ms) between two consecutive APs was calculated. Data were plotted as minimal interval per cell related to animal genotype and age (Fig. 3.18 B). After statistical analysis with Mann-Whitney U test no significant differences could be found (8-12 weeks: p=0.396, 5-6 months: p=0.282). We conclude that CA1 pyramidal cells in ASA null animals do not fire with higher frequencies compared to ASA wildtype-control animals.

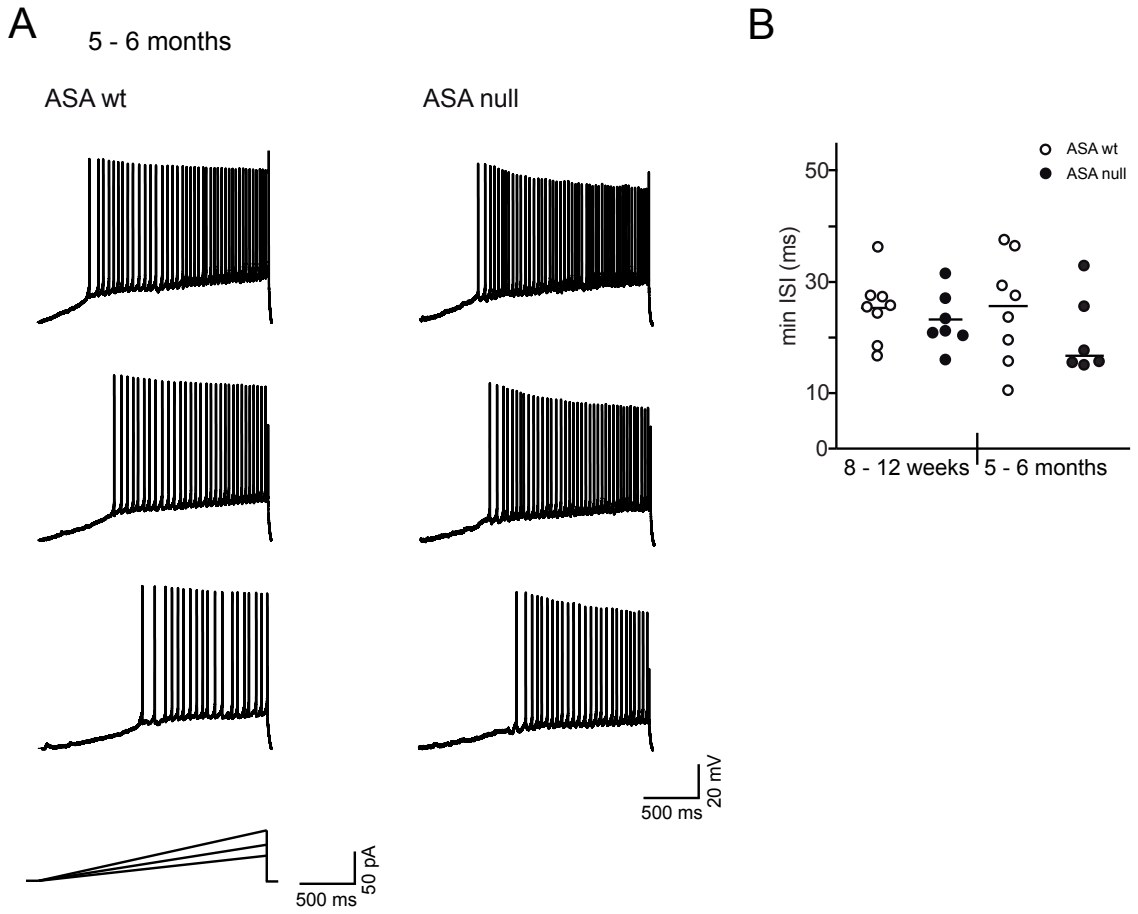

Fig. 3.18.: Maximal firing frequency of CA1 pyramidal cells
A. Recordings of CA1 pyramidal cells in ASA wildtype-control (left traces) and ASA null tissue (right traces) of 5-6 months old animals. Traces show firing behavior during 35 pA (lowermost), 55 pA (middle) and 75 pA (uppermost) ramp-like current injection. B. The minimum ISI (ms) calculated for wildtype-control and null cells at an age of either 8-12 weeks (left scatterplots) or of 5-6 months (right two scatterplots). Single cells were plotted as circles (white circles for wildtype-control and black circles for null cells).

4. Discussion

Main findings

This is the first study on hippocampal network oscillatory activity and the putatively underlying cellular properties in ASA-deficient animals. Given the findings of increased high-frequency network activity in the cortical EEG of ASA null mice (Eckhardt et al., 2007) and the importance of oscillatory network activity in the hippocampus (Colgin, 2016), the aim was to investigate hippocampal network activity and single cell physiology in ASA null vs. wild type mice.

The main findings of this work are summarized as follows:

- Alcian blue staining revealed sulfatide-accumulations within the DG, CA3 and CA1 region of the hippocampus as well as within the fimbria and adjacent cortical regions of ASA null compared to ASA wildtype-control mice.
- With means of Electrospray ionization mass spectroscopy (ESI-MS) an increase of sulfatide storage in ASA null mice within neuronal compartments of the DG and CA1 as well as in corpus callosum could be measured.
- ASA null mice show an increased fraction of SPWs that are superimposed with ripple activity.
- This increase in high-frequency activity does not appear to be caused by changes of intrinsic properties of principal neurons within hippocampal CA3 or CA1 subregions in ASA null mice.
- The revealed synaptic properties of principal neurons within the CA3 subregion of the hippocampus did not correlate with the measured increase in high frequency activity. These main findings will be discussed in the following sections.

4.1. Sulfatide accumulation

ASA is an enzyme needed for lipid metabolism, specifically for the degradation of sulfatides (von Figura et al., 2001; Eckhardt et al., 2007). Thus, a hallmark of ASA deficiency is the accumulation of sulfatides, especially in lysosomes (von Figura et al., 2001; Wittke et al., 2004; Eckhardt et al., 2007; Ballabio and Gieselmann, 2009). A first set of experiments was performed to investigate if young ASA null mice with an age of 8-12 weeks show sulfatide accumulation within the hippocampal formation and adjacent neuronal areas. To this end histochemical methods were applied to investigate the cellular distribution of sulfatides.

4.1.1. Validation of the applied staining method

The polyanionic character of sulfatide aggregates enables staining with cationic dyes for histochemical detection. To detect accumulated sulfatides, staining with cationic dyes such as toluidine blue at acidic pH was applied (Résibois, 1971). This technique makes use of metachromasia (the accumulation of an acidic lipid causes the change in the color of staining) exhibited by this dye when it is bound to densely arranged anionic sites, e. g. in sulfatide aggregates. Due to the lipid nature of the stored material the usual techniques can be performed with frozen pre-embedded tissue blocks (Schott et al., 2001).

The Alcian blue molecule is a tetravalent basic (cationic) dye that preferably stains acidic glycosaminoglycans. Alcian blue staining is specific for polysulfated material, because sulfate residues remain available for binding of tetracationic dye. Therefore, this staining was recommended for the histochemical detection of sulfatides in human and murine tissue samples of ASA-deficient material (Schott et al., 2001). The procedure yields a blue to bluish-green staining of sulfatide-containing structures and can be combined with various other standard staining methods like PAS reaction (periodic acid Schiff stain) which is used for staining polysaccharides in plasma membranes, cytosol and the nucleus. Another staining method which can be combined is the H&E stain (haematoxylin and eosin stain) which uses a cationic dye to stain previously the nucleus (blue) and the cytoplasm (red, Lüllmann-Rauch and Asan (2015)). Within our experiments we used NeuN-staining to dye specifically neurons and get an overview of the cellular layers within the hippocampus. As a result of these two staining methods we believe that we were

able to specifically and robostly detect sulfatide accumulation within the analyzed brain slices.

4.1.2. Sulfatide storage in ASA null mice

Our histochemical results support the idea that even in young ASA null mice (8-12 weeks of age) sulfatides are significantly accumulated within the hippocampal and adjacent areas. We observed Alcian blue staining within the DG, CA3- and CA1-region of the hippocampus as well as in the fimbria and adjacent cortical areas in ASA null mice, whereas healthy littermates did not show this staining pattern. In past experiments Alcian blue stainings have been performed at different age stages. Hess et al. (1996) performed stainings in animals at an age of 11-24 months, leading to the observation of alcianophilic material within the white matter, specifically corpus callosum, the hippocampal fimbria and the internal capsule. They differentiated between two different accumulation patterns: Small granules adjacent to myelinated fibers were interpreted as sulfatide accumulations within the processes of oligodendrocytes, whereas clusters of large granules within the white matter were thought to be accumulations in swollen astrocytes (Hess et al., 1996). In addition, they reported an increase in sulfatide accumulation with ongoing age and unaffected myelin sheaths within the hippocampal areas. In 2004 Wittke et al. performed experiments with ASA null mice at an age of a few postnatal days up to an age of 26 months, using age-matched wildtype mice as control. This led to the finding that in oligodendrocytes within the spinal cord, of mice at an age of P2, show numerous sulfatide accumulations which proliferate with ongoing age. At an age of one month, some brain nuclei within the mid- and forebrain showed sulfatide accumulations and astrocytes had small sulfatide inclusions. Wittke et al. (2004) assumed that oligodendrocytes as well as certain neurons are the first cell types which show sulfatide storage. Sulfatide storage was most prominent in oligodendrocytes and neuronal perikarya in certain nuclei as well as in microglial cells. At an age of 1-2 years most cell types within the central nervous system were affected to different degrees and neuronal perikarya revealed alcianophilic material. At this age alcianophilic material, assumed to be sulfatide, could be found in white matter as well as in many nuclei, mainly in perikarya. Investigations of the DG and the pyramidal cell layer revealed that they were remarkably pale in contrast to other brain regions (Wittke et al., 2004). ASA null mice at an age of 24 months were marked by sulfatide inclusions within the CA3 region and the fimbria which was densely packed with alcianophilic inclusions. Further evident

storage at an age of 6 months in contrast to ASA wildtype control animals has been reported (Faldini et al., 2011). Focusing at the telencephalon and diencephalon in mice at six or 24 months, a weak staining of the hippocampus and prominent pattern of sulfatide storage within the corpus callosum was found in younger animals. In older animals, at an age of 24 months, ASA null mice exhibited storage throughout the telencephalon and diencephalon. Hippocampal regions also appeared to be pale but the CA3 region as well as the hippocampal regions were in contrast to wildtype control animals, marked by sulfatide accumulations in pyramidal cell layers (Faldini et al., 2011). Comparison of theses studies with our results indicate that sulfatide storage increases age dependent and is present even in younger animals. However, as hippocampal areas did not show numerous sulfatide inclusions throughout the lifespan of the animals, the physiological effects in this region may be subtle.

4.1.3. Sulfatide storage in other mouse models

Additionally, further mouse models for sulfatide storage have been subjected to histological analysis. In 2007 Eckhardt et al. investigated sulfatide storage in ASA null mice overexpressing either CST or CGT. These transgenic knockout animals showed a severe sulfatide storage (Eckhardt et al., 2007) at an age of 5-6 months compared to mere ASA null animals. Both enzymes account for an increase of sulfatide molecules, which could not be metabolized due to the lack of ASA. Therefore an increase of stored material and alcianophilic material was found in Alcian blue stainings. In addition, sulfatide inclusions were prominent within CA1 and CA3. In CST/CGT/ASA null mice intraneuronal sulfatide storage was found throughout the entire CNS (Eckhardt et al., 2007). These experiments nicely show the effects of artificial sulfatide increase on hippocampal and neuronal sulfatide inclusions. To validate sulfatide accumulation at an early age within this severe phenotype (CST or CGT overexpressing ASA null mouse), stable breeding conditions and appropriate survival rates of the breeding were required. Due to problems with these two parameters (personal communications with Dr. Matthias Eckhardt), we were not able to perform these experiments in those models.
Another method to characterize sulfatide accumulation immunohistochemical stainings with means of anti-Sulph I antibodies (Fredman et al., 1988; Molander-Melin et al., 2004). These antibodies recognize the ASA substrates sulfatide, seminolipid and lactosylceramide sulfate. Applying this method, Molander-Melin found sulfatide accumulation in neurons and astrocytes of ASA null mice older than twelve months (Molander-Melin

et al., 2004).
Alcian blue staining is a suitable method to selectivly stain sulfated lipids like sulfatide. However to detect sulfolipid differentiation this method is unfeasable. To distinguish between the different sulfatide-subtypes (neuronal C18:0 sulfatide and glial C24:1 sulfatide), we used ESI-MS which allows a quantification of accumulated material. The analysis of different brain areas showed increased neuronal sulfatide storage within CA1, dentate gyrus and corpus callosum, but unchanged sulfatide levels in CA3, fimbria and cortex. Comparing our results in young (8-10 weeks old) with older (5-6 months) ASA null mice, it appears that sulfatide storage increases with age, but is already significant in young animals when compared with wildtype littermates.

4.1.4. The pathological role of accumulated material in ASA null mice

In our experiments we were able to show that ASA null mice are marked by an increase in stored neural sulfatide compared to their healthy littermates. However the effects of lysosomal and endosomal stored sulfatides on neuronal function remains unclear. In previous experiments the murine model of MLD has been studied in detail (Hess et al., 1996; van Zyl et al., 2010; Eckhardt et al., 2007).
Additionally to neuronal storage, storage of sulfatides within white matter like oligodendrocytes and microglia was described. It was hypothesized that this storage correlates with human demyelinisation within the CNS and PNS, a hallmark symptom of this disease. However, experiments using ASA null mice revealed that neural sulfatide storage in mice is not correlated with demyelinisation since ASA null mice were lacking demyelinisation despite sulfatide storage (Hess et al., 1996; Gieselmann et al., 1998; Wittke et al., 2004). Within the cerebellum, animals showed neuronal degeneration but no sulfatide storage. Additionally the mice showed only a mild phenotype even in old animals. Importantly the affected neural cell types seem to tolerate relatively large amounts of sulfatide inclusions (Eckhardt et al., 2007). Therefore one could suggest that the symptoms in MLD might not be a result of cell death and demyelinisation alone but could result directly from neuronal sulfatide storage. In 2010 Zyl et al. pointed out that sulfatide levels within plasma membranes of neurons increase and therefore also might affect the excitability of these cells (van Zyl et al., 2010). Sulfatides are negatively charged molecules. If sulfatides are enriched within the outer leaflet of neuronal plasma

membrane, the charges might affect adjacent channels like voltage-gated potassium channels. It has also been shown that sulfatide increase the open probability of calcium and voltage-gated potassium channels (Chi and Qi, 2006) and affect intracellular calcium concentrations and protein C activity (Hannun and Bell, 1987; Dyer and Benjamins, 1991). Furthermore, sulfatides are located within lipid rafts, cholesterol- and sphingomyelin-enriched microdomains (Eckhardt et al., 2007). Therefore an increase in sulfatides might influence the localization and the transport of lipid-raft associated proteins on the outer plasma membrane (Saravanan et al., 2004).
The pathological role of stored material has been discussed in several studies on other LSDs. Like in studies on murine models of LSDs, e.g. hexa null mouse, as model for Tay-Sachs disease (Miklyaeva et al., 2004), one might assume that the absence of a severe phenotype (and the unchanged mortality rate) in ASA null mice might be due to compensatory processes which also prevent demyelinisation within CNS and PNS.
The outcome of sulfatide storage in Parkinson's disease is unclear, while a study on Parkinson's disease initially showed that sulfatide levels in the superior frontal and cerebellar gray matter were increased (Cheng et al., 2003), whereas another study revealed a decrease of sulfatide within brain tissue of Parkinson patients (Fabelo et al., 2011).
Additionally to demyelinisation, some MLD-patients suffer from epileptic seizures. The tendency for generating high frequency activity has also been described in adult ASA null mice. Despite lacking demyelinisation, this suggests that neuronal sulfatide storage might result in toxic effects, which accounts for certain aspects of disease pathology (Yaghootfam et al., 2005).
Electrophysiological measurements could be performed to investigate whether intrinsic passive and active properties of neurons within the effected areas changes in ASA null mice compared to their healthy littermates. Additionally, field recordings in young mice might show if sulfatide storage found in our ASA null mice correlates the degree of high-frequency activity.

4.2. Altered SPW-R activity in ASA null mice

To investigate effects of sulfatide accumulation on neuronal network oscillatory activity, we performed field potential recordings within CA3 and CA1 of ASA null and wildtype-control mice. Because recurrent spontaneous cortical EEG discharges have been described in ASA-KO mice (Eckhardt et al., 2007), we hypothesized an increase in

hippocampal network activity. Our recordings in CA3 and CA1 s.r. showed increased values for SPW-R activity in ASA null compared to ASA wildtype-control slices. These data support our hypothesis that ASA null mice are prone to an increase in high-frequency activity within the hippocampal region.

4.2.1. Altered high frequency oscillations in diseases

High frequency oscillations (HFOs) are a hallmark of epilepsy, a family of neurological disorders that are summarized by the increased propensity of the CNS to generate recurrent epileptic seizures (Engel et al., 2009). HFOs are synchronous neuronal oscillations with frequencies above 100 Hz. Whereas non-pathologic ripple oscillations show frequencies of 100-200 Hz in rats (Bragin et al., 2010), animal models of epilepsy and patients with mesial temporal lobe epilepsy (mTLE; Engel et al. (2009) are marked by pathologic high frequency oscillations (250-600 Hz). These so-called fast ripples are pathologic (pHFO) and are thought to be caused by fields of hyper synchronized APs and bursts of population spikes within small discrete neuronal clusters (Bragin et al., 2010). In mTLE they occur during the onset of hippocampal seizures. It has been shown that the number of fast ripples correlates with the rate of seizures (Bragin et al., 2010). It is also known that mTLE patients show high correlations of pHFOs and a hippocampal atrophy (Staba et al., 2007).
Many studies on epilepsy concentrate on an unbalanced ratio of inhibition to excitation. In mTLE the loss of interneurons leads to a local reorganization of neuronal circuits and highly active epileptic foci occur (Menendez de la Prida and Trevelyan, 2011). In contrast to ripples occurring in non-pathologic tissue within the hippocampal formation, pHFOs are spatically restricted. Those pHFOs seemed to be associated with regions capable of generating spontaneous seizures, among them hippocampal region CA3 (Bragin et al., 2010). In several studies pHFOs are discussed as reliable biomarkers for epileptogenesis (Engel et al., 2009; Bragin et al., 2010).
A prime target of Alzheimer's disease (AD) is the hippocampal formation, which causes progressive memory impairments (Blennow et al., 2006). Beside this, patients suffering from AD are known to have an increased incidence of epileptic seizures (Blennow et al., 2006; Amatniek et al., 2006; Lozsadi and Larner, 2006). In a mouse model of AD, Busche et al. (2008) focused on the effects of Amyloid-beta ($A\beta$) on cortical neuronal activity. They were able to reveal an increase in neuronal activity in the direct vicinity of $A\beta$ plaques (Busche et al., 2008). In another murine model for AD it has been

reported that these mice show spontaneous nonconvulsive seizure activity in cortical and hippocampal networks (Palop et al., 2007). Additionally, many studies investigated behavioral phenotypes in AD models. Taken findings of these models together it can be stated that AD mice showed deficits in learning and memory. Their performance in experiments of object recognition, T-maze and Y-maze were poor. Beside these tests they are marked by general hyperactivity (Dodart et al., 1999; Chapman et al., 1999; Kobayashi and Chen, 2005). These behavioural features are similar to those known from AD patients. In contrast, the effects on SPW-R activity have so far not been investigated, but a link between pHFO, an affected hippocampus and deficits in learning and memory appears plausible.

The neuropsychiatric disorder of schizophrenia is associated with abnormal social behavior, confusion thinking and other cognitive symptoms, such as learning deficits. In a murine model of this disorder the animals have an increased SPW-R activity *in vivo* correlating to learning deficits (Suh et al., 2013). This correlation suggests that learning deficits could also result from increased SPW-R activity. However, the cellular basis of this mechanism is not fully understood.

Neuronal mechanisms of seizure activity have so far not been identified in GM1- and GM2-Gangliosidose, Morbus Krabbe and Morbus Gaucher. Generalized convulsive seizures belong to the striking neural symptoms of these diseases (Hoffmann and Grau, 2004). Cortical or even hippocampal high frequency activity has not been studied in these LSDs until now. Up to this point it is known that some LSDs involve neuronal symptoms. Our experiments suggest a link between neurological symptoms like seizure and high-frequency activity within the murine hippocampal formation and the genotype of ASA enzyme loss.

4.2.2. Detection of SPW-Rs in vivo and in vitro

SPW-R activity occurs during periods of rest and slow wave sleep. Several studies have been performed to validate the method of extracellular SPW-R recordings *in vivo* (O'Keefe and Conway, 1978; Buzsáki, 1986; Csicsvari et al., 1999, 2000) in behaving and sleeping animals. To this end, either silicon probes or multielectrode arrays were implanted within the hippocampal formation and were therefore used to record field potentials permanently and under different behavioral states (O'Keefe and Conway, 1978; Buzsáki, 1986; Csicsvari et al., 1999, 2000). The measured SPW-R activity *in vivo* consists of field potential transients accompanied by high frequency oscillations.

To evaluate an *in vitro* model for SPW-R measurements several studies have been performed on field electrode measurements in murine hippocampal slices (Pais et al., 2003; Maier et al., 2003; Nimmrich et al., 2005; Behrens et al., 2005). *In vitro* SPW-R activity also consists of rhythmically recurring field potential transients accompanied by high frequency oscillations and increased neuronal firing, showing striking similarities with SPW-Rs occurring *in vivo* . In comparison, both methods offer advantages and disadvantages. Whereas *in vivo* measurements offer the opportunity to record behavior associated neuronal activity in animals within an artificial or even natural environment, *in vitro* experiments offer pharmacological accessibility. Due to the similarity of SPW-R measured *in vitro* compared to those measured *in vivo* , we decided to record SPW-R in ASA null and wildtype-control animals *in vitro* . In contrast to SPW-R activity *in vivo* , recordings *in vitro* additionally ensure regularly occurring events with stable amplitudes (Buzsáki and Chrobak, 2005). An easy way to study this HFO is therefore given by the use of acute brain slice preparations taking into account that these oscillations need a minimum network size and/or connectivity (Schlingloff et al., 2014). Since our experiments aimed at differences in several basic SPW-R features.
While others reported a SPW frequency of about 2-3 Hz in CA3 and CA1 (Maier et al., 2002), we measured different frequencies in both areas. In ASA null animals we found a SPW frequency of 3.11 Hz in CA3 and of 0.895 Hz in CA1. The recorded frequencies in ASA wildtype-control animals were 2.209 Hz within CA3 and 0.688 Hz within the CA1 area. Whereas the frequencies measured within the CA3 region agree with values in comparable experimental subsets (Maier et al., 2002), the recordings in the CA1 region showed lower values in both genotypes. Besides similar slicing procedure and recording chambers minimal differences regarding cutting angle and oxigenation as well as the composition of the extracellular solution might influence the network connectivity and the probability of generating SPWs and ripples. Therefore we conclude that despite these differences our methodology is appropiate.

4.2.3. The cellular mechanisms regulating SPWs and ripples

SPWs

SPWs reflect compound excitatory postsynaptic activity and are thought to be generated within the hippocampal principal cell layer (Buzsáki et al., 1992). Measured within the s.r. they represent a sink of net current due to synchronous AP generation of the

principal cells, which are thought to be synchronized via local interneurons.
Due to its multiple mutual excitatory connections between the principal cells, the CA3 region contains many recurrent connections which are capable of triggering synchronized activation (Miles and Wong, 1986; Hasselmo et al., 1995). This recurrent synchronized activity might generate the described SPW-R pattern. A lower density of recurrent connections in CA1 could be the reason for a lower SPW incidence in CA1 compared to SPW-R in CA3 (Maier et al., 2003). Another mechanism which ensures synchronous activity of principal cells is a synchronous Gamma-Aminobutyric acid (GABA) release from electrically coupled interneurons (Traub and Miles, 1995; Avoli, 1996; Traub and Bibbig, 2000). SPW-Rs have slower propagation velocity than field EPSPs and additionally show backward propagation. Therefore a clear discrimination between field EPSPs and SPW-R is apparent (Buzsáki, 1986; Maier et al., 2003). An increase of SPW activity might hint towards an altered neuronal network and a potential modification of the recurrent neuronal connections.

Ripples

Ripples as part of SPW-R activity can occur *in vivo* and *in vitro* without underlying slow field potentials (Ylinen et al., 1995; Draguhn et al., 1998). In the past, three different models for ripple-generation were discussed but the true mechanism remains disrupted. Potential mechanisms are:

- electrical coupling of neurons via gap junctions
- feedback-loop among pyramidal cell and interneurons
- local inhibition among interneurons

The first possible mechanism for high frequency oscillation generation, like ripples, which occur more or less spontaneously might be the synchronized activity of neurons via axonal gap junctions (Draguhn et al., 1998). The idea of electrical synapses within the transduction pathway of hippocampal high frequency oscillations has been proposed (MacVicar and Dudek, 1981; Taylor and Dudek, 1982). Electrical synapses, also called gap junctions, consist of two hemichannels, which themselves are hexameres of connexins and are arranged to form a pore between two cells. Therefore, they function as electrical synapses and mediate electrical coupling of neurons or glial cells (Evans and Martin, 2002). Around 20 highly homologous products of connexin genes have been

identified in humans and mice (Willecke et al., 2002). It is known that gap junctions occur in various cell types within many organs including the CNS. They are also found within the hippocampal formation, where most of them are expressed in glial cells or in interneurons (Fukuda and Kosaka, 2000; Connors and Long, 2004). The predominant connexin within the hippocampus is Connexin36 which occurs in mature interneurons (Spruston, 2001). Other connexins like Connexin43, Connexin47 and Connexin50 are thought to play important roles in pyramidal cells (Spruston, 2001; Behrens et al., 2011). These electrical synapses, which are thought to be situated within the axons of neighboring neurons (Jensen and Yaari, 1997), might play a role in the generation of rapid transmembrane potentials like epileptiform discharges and ripple oscillations during SPW-R activity (Jensen and Yaari, 1997; Draguhn et al., 1998; Spruston, 2001; Schmitz et al., 2001; Behrens et al., 2011). For instance Draguhn et al. (1998) hypothesized that synaptic mechanisms might be too slow for ripple generation. In a series of experiments they found ripples to be neither affected by GABAA-receptor antagonists nor by a block of total synaptic transmission by either omitting extracellular Ca^{2+} concentration or increasing extracellular concentration of Mg^{2+}. However, block of gap junctions led to a disruption of high-frequency ripple activity.

With means of computer simulations Draguhn et al. (1998) showed that 1-2 electrical synapses per CA1 pyramidal cell are needed to generate ripple activity. The model assumed a high densitiy of Na^{2+} channels within the axonal compartments which prevents the postjunctional membrane from filtering the incoming signals and allows antidromic propagation of APs is (Draguhn et al., 1998). Therefore, for a long time, they were thought to be suitable candidates to mediate fast oscillations like the SPW associated ripple oscillations (Draguhn et al., 1998; Traub and Bibbig, 2000; Pais et al., 2003). However, the mechanism remains controversial. In a recent study, Schlingloff et al. (2014) argue against the idea of gap junction mediated ripple generation due to gap junction localization within the apical and basal dendritic tufts (Fukuda and Kosaka, 2000) a widespread block of ripples during GABAzine application and the fact that presently available gap-junction blockers are highly non-specific (Connors and Long, 2004).

As a second mechanism, a feedback loop between pyramidal cells and interneurons. has been proposed to be capable of generating HFOs like gamma oscillations (Ylinen et al., 1995; Buzsáki et al., 1992; Klausberger et al., 2003). This mechanism, also known as PING mechanism (Pyramidal cell Inhibitory Network Gamma mechanism), produces net-

work oscillations with a range between 20-80 Hz (Gulyás and Freund, 2014; Schlingloff et al., 2014). Therefore this mechanism does not fit the achieved ripple frequencies of 150-200 Hz.

As a last mechanism Schlingloff et al. (2014) showed that SPW-R in CA3 are initiated through a combined refractory and stochastic mechanism (Schlingloff et al., 2014). When coincidental firing in a set of spontaneously active pyramidal cells occurs, these cells trigger a gradual, exponential built-up of activity in the recurrent CA3 network and SPWs are initiated. This tonic excitation of the pyramidal cells drives firing of PV^+ BCs. Afterward PV^+ BCs show phasic inhibitory activity which synchronizes at ripple frequency and leads to phase-modulated firing of the pyramidal cells. Therefore PV^+ BCs synchronize and promote pyramidal cell firing and seem to be an essential pace-keeper during ripple activity. This mechanism (Fig. 4.1) is called FINO (fast inhibitory neuronal oscillation) and does not seem to rely on to be due to CCK^+ BC activity (Schlingloff et al., 2014; Gulyás and Freund, 2014). During ripple activity pyramidal cells fire sparsely (Behrens et al., 2005), and a part of those cells fire action potentials in tight synchrony to the SPW-Rs (Buzsáki et al., 1992; Csicsvari et al., 1999). This mechanism needs a specific and rapid interaction between participating cells in order to secure the precise phase-coupling in the range of milliseconds.

A total of 80-90 % of pyramidal neurons within the hippocampal formation underlie SPW-R initiated inhibition (Ylinen et al., 1995; Grenier et al., 2001) which might help to sharpen synchrony (Traub and Bibbig, 2000) or suppress AP generation in principal cells outside the SPW-R network. The firing activity of inhibitory interneurons within the CA3 network can follow ripple activity nearly in a 1:1 fashion (Ylinen et al., 1995; Csicsvari et al., 1998). Additionally the role of interneurons in this hippocampal network activity was part of further studies (Ellender et al., 2010; Hájos et al., 2013). Interneuron activity during SPW-R activity varies among the different interneuron classes. The role of interneurons in oscillogenesis has been frequently studied before (Buzsáki, 1984; Ylinen et al., 1995) and revealed the important role for perisomatic inhibition in rhythm generation. For instance perisomatic inhibition is involved in the generation of gamma rhythms and therefore might also contribute to faster field oscillations, such as ripple oscillations, or pHFOs (Ellender et al., 2010). The role of interneurons to synchronize large populations of pyramidal cells has also been discussed for hippocampal oscillations with lower frequencies like theta oscillations (Cobb et al., 1995). Taken together, SPW incidence and the fraction of SPWs associated with ripples may depend on a va-

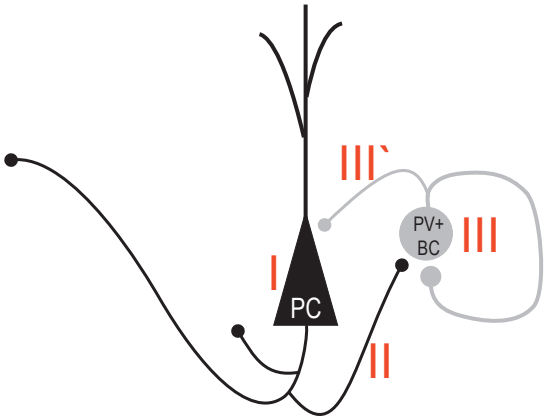

Fig. 4.1.: Scheme of FINO mechanism within the CA3 region showing one pyramidal cell (PC, black) on the left and one PV+ BC (gray) on the right side. The mechanism depends on tonic PC-activity, indicated as I (red), which drives excitation of PV+ BC (red II). The activated PV+ BC drives phasic inhibition of PC and itself (red III, III'.

riety of cellular and network properties. To identify possible mechanisms underlying our findings of increased ripple-associated SPWs in ASA-deficient mice we set out to characterize intrinsic properties of hippocampal pyramidal neurons and synaptic properties of the excitatory-inhibitory micronetwork. Changes in intrinsic properties might lead to increased excitability and therefore an increase in ripple activity. Additionally changed synaptic properties could influence the network activity and lead to an increase in excitation over inhibition or vice versa (Ellender and Paulsen, 2010). The implications of my results will be discussed in the next section.

4.3. Intrinsic electrophysiological properties of hippocampal CA3 and CA1 pyramidal neurons

SPW-R events are thought to be initiated by the synchronous discharge of CA3 cells, that in turn promotes both ripple oscillations and the synchronous discharge of cells in the CA1 (O'Neill et al., 2010). *In vivo* intrinsic bursting of CA3 pyramidal cells might promote high-frequency activity. However CA3 and CA1 pyramidal neurons in slices do not show this firing pattern. Bursting behavior depends on a variety of ionic currents and on different membrane properties like membrane resistance, membrane potential and the distribution of ion channels within the plasma membrane.
It has been speculated that the loss of ASA enzyme function leads to an accumulation

of sulfatides within glial and even neuronal membranes. Sulfatides are located in the outer leaflet of the plasma membrane (Simons and Ikonen, 1997; Simons and Toomre, 2000), probably leading to higher asymmetry of surface charges (Eckhardt, 2008; van Zyl et al., 2010). An excess of negatively loaded substances at the outer leaflet of the plasma membrane may influence the cellular charge screening abilities of the neuron. If charge modifications next to ion channels arise, the cellular environment will be polarized leading to an electrostatic potential and if important functional sites of the ion channels lie within this environment the channel function could be modulated and single channel conductance might be influenced, resulting in a changed channel sensitivity to toxins, blocking ions and agonists (Green and Andersen, 1991; Chi and Qi, 2006; van Zyl et al., 2010). This effect also may affect general channel open probability in voltage-gated ion channels which are opened through a gating charge (Catterall et al., 1993).
To investigate possible effects of neuronal sulfatide accumulations within the somatic plasma membrane to neuronal currents we performed whole cell measurements in CA3 and CA1 pyramidal cells of ASA wildtype-control and ASA null mice.

4.3.1. Intrinsic properties of pyramidal cells in ASA null mice

The passive properties of measured CA3 pyramidal cells via patch-clamp technique were in good agreement with values measured in other studies (Spruston and Johnston, 1992; Major et al., 1994; Hemond et al., 2009). Additionally, we recorded data to assess the passive properties of CA1 pyramidal cells with sharp-microelectrodes. Those values did not show striking differences to values of other studies (Wong and Prince, 1981; Jensen et al., 1994; Opitz et al., 1995). We could not detect any differences between ASA wildtype-control and ASA null pyramidal cells.
It has been speculated that high-frequency activity might be generated by bursting excitatory neurons (Engel et al., 2009; Bragin et al., 2010; Menendez de la Prida and Trevelyan, 2011). In MLE Yaari et al. (2007) revealed that mechanisms of low-threshold bursting occur within in the CA1 pyramidal cell layer after inducing a pilocarpine status epilepticus in rats. They assume that these bursts are caused by back propagating sodium spikes and calcium current driven depolarizations in distal apical dendrites (Yaari et al., 2007). Additionally, low-threshold calcium channels may generate burst discharges (Huguenard, 1996; Beck and Yaari, 2012).
To investigate the firing behavior of pyramidal cells within different hippocampal regions (CA3, CA1), we performed single cell measurements in ASA wildtype-control and null

mice. Applying somatic current injections, we analyzed APs, spike ADPs and firing patterns of these cells. Our experiments did not reveal any differences between pyramidal cells of ASA wildtype-control and ASA null animals, neither for CA3 nor for CA1 pyramidal cells.

The missing differences in AP properties between the two genotypes suggest that the characteristics of the I_{NAT} and I_K are neither changed in CA3 nor in CA1 pyramidal cells in ASA null mice. Changed AP properties can hint towards changes in ionic currents. Whereas the INAT is responsible for AP-generation, the delayed rectifier IK mediates AP repolarisation and therefore controls AP half width. To investigate the single current properties of either INAT or IK, single channel measurements would be required.

Investigations of CA1 pyramidal cell firing mode and the influence of spike ADP (Wong and Prince, 1981; Jung et al., 2001; Yue, 2004; Metz et al., 2005), led to the finding that the somatic spike ADP-height in CA1 pyramidal is critically correlated to bursting behavior. The cellular mechanisms underlying this depolarization are mainly carried by I_{NAP} and I_M arising at ion channels located in the neuron soma (Yue, 2004; Yue et al., 2005; Yue, 2006; Golomb et al., 2006). Our experiments revealed no differences between genotypes in either CA3 or CA1 pyramidal cells while comparing spike ADP amplitudes and areas. These findings suggest that this interplay of these currents and their responsible channels are not altered by neuronal sulfatide accumulation either. Further patch-clamp experiments might reveal whether the single ionic currents in pyramidal cells are impaired. This would require additional voltage-clamp measurements.

In vivo most CA1 pyramidal cells either fire single APs or show burst-firing behavior (Su et al., 2001). This is different to firing behavior in slices where most CA1 pyramidal cells have a regular firing pattern (Su et al., 2001). The tendency of a pyramidal cell to fire APs in bursts depends on the nature of ionic conductances in its plasma membrane as well as on the ionic composition of the extracellular surrounding. Regular firing CA1 pyramidal cells can generate AP bursts if the extracellular Ca^{2+} concentration is lowered or the K^+- concentration is raised (Jensen et al., 1994; Su et al., 2001; Golomb et al., 2006). In CA3 pyramidal cells intrinsic bursting requires the activation of Ca^{2+} channels by sodium spikes and the spike ADP seems to play an important role for this firing mode (Wong and Prince, 1981).

In the following mechanisms for this behavior are discussed for CA1 pyramidal cells. It was observed that a decrease of the extracellular calcium ion concentration while depolarizing the measured cell leads to an increase in burst firing propensity. Su et al.

(2001) hypothesized that calcium ions decreases the INAP . This might happen due to selective binding of calcium ions to G-protein coupled calcium-sensing receptors such as metabotropic glutamate-receptors. In epilepsy a decrease of calcium (down to 0.2 mM) during seizures is consistent with this mechanism (Su et al., 2001).
In an additional set of experiments, a systematic decrease of the Ca^{2+} concentration within the extracellular solution (down to 1 mM) led to an increase in AP firing and burst firing behavior in pyramidal cells. However, this effect did not differ between ASA null cells and ASA wildtype-control cells. In further experiments lower calcium concentrations (<1 mM) mimicking seizure activity can be performed to investigate whether the two genotypes still do not show differences in bursting behavior. Our experiments suggest that bursting mechanisms are not altered within murine ASA null cells, of least within the range of calcium concentration measured.
In summary our experiments indicate that neuronal sulfatide accumulation within membranes did not affect passive or active properties in CA3 and CA1 pyramidal cells. Although hippocampal slices of ASA null mice seemed to be prone to high-frequency activity, our experiments revealed that during somatic current injections CA3 pyramidal cells did not show an increased tendency to fire APs in contrast to wildtype-control cells. These results appear to be in conflict to the measured increase in SPW-R fraction within ASA null hippocampal slices. This can be explained by discrepancies using two slightly different recording conditions, implying 450 $^{+}$m slices for field potential recordings (SPW-R experiments) and 300 $^{+}$m for patch-clamp studies. Therefore our single cell measurements were performed using slices which contain reduced neuronal network activity. Additionally, our slice preparation procedure might promote cutting CA3 axons and therefore one source of SPW-R generation.

4.3.2. Possible effects on peripheral, neuronal compartments

Our histochemical sulfatide stainings did not reveal the exact cellular compartment in which sulfatides has been accumulated. Beside the apparent cytoplasmic sulfatide storage within lysosoms and endosoms and the somatic accumulations within the plasma membrane, there might be additional functionally important sulfatide storage in neurons. Sulfatide accumulations in peripheral, neuronal regions like axons and dendrites might directly impact neuronal intrinsic properties. Our experiments did not allow to uncover the effects on sulfatide accumulations within these areas.
Beside orthodromic AP discharges at the axon initial segment towards the axonal presy-

naptic sites, antidromic APs may be generated within the axon. Such events are called ectopic APs and show backpropagation towards the soma (Pinault, 1995). Ectopic APs also exist within neurons of the hippocampus (Perreault and Avoli, 1989; Stasheff and Wilson, 1990). Their role for synchronization of bursting neurons (Pinault and Pumain, 1989; Pinault, 1995) has been discussed in a couple of studies. A correlation between ectopic APs and epileptic seizures has been shown as well (Stasheff and Wilson, 1990). A study focusing on the role of ectopic APs for SPW-R generation (Papatheodoropoulos, 2008) revealed that 20 % of CA1 pyramidal cells fire putative ectopic APs phase-coupled to SPW-Rs. This study further suggested correlations of the ectopic AP discharge probability and the maximal amplitude of the ripple oscillation and during IPSPs measured in pyramidal cells, which were shown to be correlated with the SPW-R event (Papatheodoropoulos, 2008).

To what extent the function of pyramidal cell axons for generating ectopic APs might be affected has to be evaluated and the possible modifications due to sulfatide storage have to be investigated in further studies. We assume that within our experiments ectopic APs could not be recorded due to possible axon-cutting severing during our slice preparation.

At synapses on the dendritic tree, when EPSP arrive temporally and spatially distributed. The integration of the incoming events will follow a linear fashion (Mueller, 2011). Dendrites of CA1 pyramidal neurons have the ability of a supra linear integration of spatially clustered, synchronous excitatory inputs. This postsynaptic response is caused by the recruitment of dendritic voltage-gated sodium, calcium and NMDA channels and a dendritic spike is generated locally on the dendrite (Schiller et al., 2000; Ariav et al., 2003; Losonczy and Magee, 2006). This integration mode of pyramidal cell dendrites mediated by dendritic spikes is thought to increase the information storage capacity of neuronal dendrites. In former experiments dendritic spikes have been shown to trigger neuronal output with high temporal precision (Softky, 1994; Golding and Spruston, 1998; Poirazi and Mel, 2001; Ariav et al., 2003). The role of dendritic spikes within the CA1 region for synaptic plasticity in the hippocampus by providing dendritic CA^{2+} influx and depolarization was part of previous studies (Golding et al., 2002; Remy and Spruston, 2007). The accumulation of sulfatides within neuronal membranes of the dendritic tree could not be addressed in our investigations. How the generation of dendritic spikes might be influenced by these accumulations and to what extend stored sulfatides might alter the charge of the plasma membrane and therefore effect voltage-gated channels at the

postsynaptic side have to be investigated in future studies.
The fact that the measured intrinsic properties did not show alterations in ASA null slices led us to perform additional experiments concerning the synaptic function of CA3 pyramidal neurons and feed-back inhibition within the hippocampal CA3 network. In further experiments we investigated on parts of inhibitory circuitry within this neuronal network and wanted to specify the role of perticular interneurons for local networks within the hippocampus.

4.4. Inhibition and Excitation in hippocampal CA3 network

Although GABAergic interneurons only make up about 10 % of all neurons in the hippocampal formation (Freund and Buzsáki, 1996) ,they are essential for the control of neuronal activity in hippocampal circuits, and to delicately counterbalance hippocampal output.
Interneurons within the CA3 region of the hippocampus respectively mediate two kinds of inhibition by either participating in feed forward or in feed back inhibition. The feed back circuitry is solely activated when CA3 pyramidal cells fire APs and thus constrains excitation of CA3 pyramidal cells (Miles, 1990).
The dynamic range of the postsynaptic target cells is thought to be increased by feed forward inhibition preventing the excitatory inputs to become saturated. Furthermore, feed forward inhibition reduces the time-window for summation of excitatory inputs in the pyramidal cells and increases the temporal precision of firing in their principal cell targets (Pouille and Scanziani, 2001; Pouille et al., 2009; Bartos et al., 2011). If feed forward inhibition is impaired, a subsequent change in SPW-R formation is a putative consequence. Since SPW-generation depends on a precise timing on principal cell firing, this oscillation pattern is thought to reflect a synchronous discharge of pyramidal cells. Therefore alterations in feed forward inhibition could lead to a disruption of SPW generation, bearing on shifted SPW incidence and amplitude.
To study cellular mechanisms for an increase in SPW activity in ASA null hippocampal slices, we investigated different cellular mechanisms which are thought to play a role in SPW generation. Our initial studies therefore aimed at at spontaneous, AP-independent synaptic events in CA3 pyramidal cells in order to provide an overview whether basic synaptic properties within the CA3 region are affected.

4.4.1. Inhibitory and excitatory synaptic events in CA3 PCs

Spontaneous transmitter release can be measured as single, quantal events at the postsynaptic site. While suppressing action potential generation by TTX (Nakajima et al., 1962), each measured miniature postsynaptic current (mPSC), inhibitory or excitatory, represents a full collapse fusion of one synaptic vesicle (Wang, 2010). Analyzing kinetic properties like decay and rise times of these mPSCs can yield information about filter mechanisms arising at the dendritic tree towards the somatically located electrode (Edwards et al., 1990).
Miniature PSC characteristics like frequency and amplitude can differ, dependent on presynaptic properties like bouton size, active zone size, number of readily releasable vesicles, calcium homeostasis and recycling of vesicular membranes (Schikorski and Stevens, 1997; Reimer et al., 1998; Murthy et al., 2001; Atwood and Karunanithi, 2002; Branco et al., 2010; Holderith et al., 2012) as well as recycling of neurotransmitters within the synaptic cleft (Edwards et al., 1990). Investigation of mPSC properties of either inhibitory or excitatory events can be applied to identify potential synaptic differences between the two genotypes. Therefore, measuring mPSCs provides a meaningful experimental tool to get a first impression whether inhibitory synapses within the local network of the CA3 region are altered.
In 8-12 weeks old ASA null and wildtype-control cells, we found that spontaneous postsynaptic currents neither of excitatory nor of inhibitory nature differed between genotypes. Amplitude and frequency did not show any changes, which led to the conclusion that presynaptic and the postsynaptic properties responsible for miniature PSC generation were not altered within ASA null cells.

4.4.2. Excitation-Inhibition balance in disease pattern of epilepsy

The role of inhibition for neuronal networks can be studied applying models which imply an altered inhibition.
Disturbed inhibition may lead to neuronal dysfunction and especially to the disease pattern of epilepsy in a complex way. It is widely believed that decreased inhibition is at least partly responsible for hyperexcitability. However, the role of inhibitory interneurons exceeds the control of neuronal excitability and involves synchronization of large populations of pyramidal cells like in HFOs (Cobb et al., 1995). Changes in the spatiotemporal pattern of inhibition might further disturb the neuronal balance. In some forms

of epilepsy pathologically increased inhibition may support the generation of seizures (Mann and Mody, 2008). For instance in one model a modulation in the excitation-inhibition ratio occurs in the feed forward pathway of the mossy fiber input to CA3 which led to an alteration of CA3 firing behavior (Treviño et al., 2011). In healthy hippocampus DG granule cells innervate more CA3 interneurons than pyramidal cells (Acsády et al., 1998). Thus, feed forward inhibition plays a role in preventing CA3 cells to fire in bursts and to generate plateau potentials (Torborg et al., 2010).

4.4.3. Excitation-Inhibition balance in ASA null mice

To investigate the role of interneurons for CA3 pyramidal cell activity, we studied interneuron mediated feed back inhibition. Our aim was to investigate excitation-inhibition balance in CA3 feed back inhibition loops and thereby gain more information about the role of CA3 interneurons. To this end, we measured inhibitory and excitatory postsynaptic currents in CA3 pyramidal cells elicited by Schaffer collateral stimulation. Our measurements revealed a strong postsynaptic inhibitory current after Schaffer collateral stimulation. Excitatory currents could only be seen after blocking the dominant inhibitory current. The ratio between EPSC and IPSC amplitudes and areas was not altered between the two genotypes. These data suggest that the balance of recurrent excitatory and feedback inhibitory inputs to CA3 pyramidal cells is not affected by the loss of ASA enzyme activity and sulfatide storage.

Our methods address the question if feed back inhibition is affected at all. The function of single interneuron types within this feed back loop or mechanisms of feed forward inhibition was not investigated further.

The interaction of inhibition and excitation during hippocampal rhythmic activity is still not fully understood. The detailed mechanism of ripple initiation in CA3 is unknown, but an involvement of interneurons in shaping this network pattern is likely. CA3 interneurons have been the subject of several studies concerning SPW-R activity (Buzsáki et al., 1992; Ylinen et al., 1995; Csicsvari et al., 1999; Klausberger et al., 2003; Ellender et al., 2010; Ellender and Paulsen, 2010). A role of perisomatic targeting interneurons (PTIs) for SPW incidence has been shown several times (Ellender et al., 2010; Ellender and Paulsen, 2010; Hájos et al., 2013). To reveal the mechanism, Ellender et al. performed a set of experiments (Ellender and Paulsen, 2010) to study the activation of a subset of individual PTIs. During activation SPW-R were suppressed but following activation local SPW generation was enhanced. They also investigated the mechanisms by which this

subset of PTIs could initiate SPW generation. The ability of single PTIs to suppress or enhance SPW-R generation could be explained by a transient increase in excitation over inhibition (Ellender et al., 2010). A study published by Hájos et al. (2013)s revealed that the three types of PTIs behave differently during SPW-R activity. PV^+ BC receive larger synaptic excitation before and after the peak of SPW-Rs than axo-axonic cells or CCK^+ BCs. In comparison to pyramidal cells, this hints towards a direct participation in SPW-R generation. Dendritic targeting interneurons do seem to mediate minor effects in SPW-R initiation or propagation but are not part of major mechanisms.
Although it has been shown that cortical slow oscillations exert an influence on SPW-R activity (Sirota et al., 2003; Battaglia et al., 2004), generation of SPW takes place in the recurrent neuronal network of CA3 (Buzsáki, 1986). Therefore we hypothesized that perisomatic feed back inhibition plays a more important role in SPW-R generation than DG-mediated feed forward inhibition. To reveal if PTI modalities are modified due to sulfatide storage and whether affected PTIs do influence ripple generation, those interneurons have to be part of further characterizing studies.

4.4.4. Synaptic changes in ASA null and sulfatide accumulating mice

We hypothesized that a potential sulfatide storage within neuronal membranes might lead to a disruption of proper synaptic function by influencing synaptic release mechanisms. A change in postsynaptic current frequency mainly depends on the number of presynaptic transmitter release sites whereas the postsynaptic current amplitude depends on transmitter receptor density.
ASA null mice showed no impairment of synaptic function in CA3 pyramidal cells. We hypothesize that sulfatate membrane accumulations in ASA null mice might not influence mechanisms of synapses at the dendritic tree or the axon of this particular cell type. To complete our knowledge of synaptic functions in ASA null mice synaptical properties of other hippocampal neurons like CA1 pyramidal cells and interneurons have to be evaluated.

4.5. Summary

Our study revealed some peculiarities within the hippocampal region of ASA null mice. On one side we were able to show that within young animals of 8-12 weeks, sulfatide accumulations arise within gray and white matter of the hippocampus and adjacent areas. Additionally, the neuronal network within the CA3 and CA1 region of the hippocampus showed an increase in SPW-R activity. This goes along with the results of Eckhardt et al. (2007) who reported an increase of cortical burst like EEG activity in ASA null mice of the same age.

However we were not able to identify the cellular mechanism underlying these changes. Intrinsic properties of both CA1 and CA3 pyramidal neurons did not show any differences compared to those of ASA wildtype-control mice. Additionally, our characterization of the synaptic features in CA3 pyramidal cells did not reveal any changes. Finally, the excitation-inhibition ratio did not show any alterations between the two genotypes.

This suggest that the alterations in ASA null mice are due to more subtle effects.The sum of tiny alterations, which might be hard to detect for each separately, could be an explanation for the increase of SPW-R activity. These might include subtle physiological changes in certain subtypes of interneurons, which were not the prime subject of this work. Furthermore, our experiments were performed in slices and not *in vivo* , which might limit the detection of some network mechanisms.

Interestingly our experiments supported the *in vivo* measurements of Eckhardt et al. (2007) and fit the behavioral phenotype measured in various cognitive tests (Hess et al., 1996; D'Hooge et al., 2001). Those experiments showed that ASA null mice of three, six and twelve months of age develop hyperactivity within their cages. With ongoing age the animals performed worse in the rotarod test and the passive avoidance test. In all age groups the Morris water maze test revealed that ASA null mice showed a reduced swimming velocity and performed worse compared to the ASA wildtype-control mice (D'Hooge et al., 2001).

Our measured data in young animals hint towards an increase in hippocampal network activity which might lead to a cognitive impairment in older animals (Hess et al., 1996; Gieselmann et al., 1998). It has been proposed that SPW-R activity is essential for memory consolidation and retrieval (Buzsáki, 1998). Thus one might speculate that the impairment of SPW-R generation plays a role in these deficits. However, these behavioral investigations have been performed in older animals than those used for our

SPW-R measurements.

Cognitive decline is a characteristic feature of all forms of MLD. Adult patients often display behavior characteristic of frontal dementia and white matter dysfunction (Shapiro et al., 1994, 1995). From older studies it is known that aged ASA null mice display some of the biochemical, neuropathological, EEG and behavioral hallmarks of the human disorder MLD (Gieselmann et al., 1998). Our experiments revealed that even in young ASA null mice some neuronal network properties are affected and the course for cognitive decline might be set. However the cellular mechanisms underlying these network alterations appear to be subtle and require further study.

List of Figures

List of Tables

•

A. Abbreviations

ACSF	artificial cerebrospinal fluid
ADP	after depolarization
AMPA	alpha-amino-3-hydroxy-5-methyl-4-isoxazolepropionic acid
AP-V	(2R)-amino-5-phosphonovaleric acid
ASA	arylsulfatase A
AP	action potential
BBB	blood brain barrier
Ca^{2+}	calcium
CA1	cornu ammonis (Ammon's horn), subregion 1
CA3	cornu ammonis (Ammon's horn), subregion 3
cDNA	complementary DNA
Cl^{-}	chloride
CNS	central nervous system
CNQX	6-cyano-7-nitroquinoxaline-2,3-dione
DG	dentate gyrus
EC	entorhinal cortex
EGTA	ethylene glycol tetraacetic acid
EPSP	excitatory postsynaptic potential
GABA	γ-Aminobutyric acid
GalCer	galactosylceramid
GAG	glycosaminglycan
GC	granule cell
HEPES	4-(2-hydroxyethyl)-1-piperazineethanesulfonic acid
HSTC	hematopoietic stem cells-therapy
IPSP	inhibitory postsynaptic potential
K^{+}	potassium
LTP	long term potentiation
LSD	lysosomal storage disorder
MLD	metachromatic leukodystrophy

MRI	magnetic resonance image
mEPSC	miniature excitatory postsynaptic current
mIPSC	miniature inhibitory postsynaptic current
mRNA	messenger RNA
Na^+	sodium
ns	not significant
p	probability
PBS	phosphate buffer salt solution
PC	pyramidal cell
PFA	paraformaldehyde
PLP	proteolipidprotein
PNS	peripheral nervous system
PPF	paired-pulse facilitation
PP	perforant path
rhASA	recombinant human arylsulfatase A
SC	Schaffer-collateral
SEM	standard error of mean
SWP	sharp wave
SWP-ripple	sharp wave ripple complex
slm	stratum lacunosum moleculare
so	stratum oriens
sp	stratum pyramidale
sr	stratum radiatum
t	time
TBS	tris-buffer salt solution
TTX	tetrodotoxin

B. Contributors

The experiments, which were focused on sulfatide-accumulation in hippocampus were performed by Dr. Matthhias Eckhardt (Alcian-blue stainings) and by Klaudia Brysch (ESI-MS measurement) (AG Prof. Volkmar Gieselmann/ Department of Biochemistry, University Clinic Bonn). All biocytin stainings for cell reconstruction were performed by Olivia Steffan.

Bibliography

Acsády L, Kamondi A, Sík A, Freund T, Buzsáki G (1998) GABAergic cells are the major postsynaptic targets of mossy fibers in the rat hippocampus. *The Journal of Neuroscience* 18:3386–403.

Ahmed OJ, Mehta MR (2012) Running Speed Alters the Frequency of Hippocampal Gamma Oscillations. *Journal of Neuroscience* 32:7373–7383.

Alberts B, Johnson A, Lewis J, Raff M, Roberts K, Walter P (2004) *Molekularbiologie der Zelle* Wiley-VCH Verlag GmbH & Co. KGaA, Weinheim, 4th edition.

Alzheimer A (1910) Beiträge zur Kenntnisse der pathologischen Neuroglia und ihrer Beziehungen zu den Abbauvorgängen im Nervengewebe. *Nissl-Alzheimer's Histol Histopathol Arb* 3.

Amaral DG, Dolorfo C, Alvarez-Royo P (1991) Organization of CA1 projections to the subiculum: a PHA-L analysis in the rat. *Hippocampus* 1:415–35.

Amaral DG, Ishizuka N, Claiborne B (1990) Neurons, numbers and the hippocampal network. *Progress in Brain Research* 83:1–11.

Amaral DG, Lavenex P (2007) Hippocampal Neuroanatomy In Andersen, P. M, R., Amaral, D., Bliss, T., O'Keefe J, editors, *The Hippocampus Book*, pp. 37–117. Oxford University Press, New York.

Amaral DG, Witter MP (1989) The three-dimensional organization of the hippocampal formation: a review of anatomical data. *Neuroscience* 31:571–91.

Amatniek JC, Hauser WA, DelCastillo-Castaneda C, Jacobs DM, Marder K, Bell K, Albert M, Brandt J, Stern Y (2006) Incidence and predictors of seizures in patients with Alzheimer's disease. *Epilepsia* 47:867–72.

Ariav G, Polsky A, Schiller J (2003) Submillisecond precision of the input-output transformation function mediated by fast sodium dendritic spikes in basal dendrites of CA1 pyramidal neurons. *The Journal of Neuroscience* 23:7750–8.

Atwood HL, Karunanithi S (2002) Diversification of synaptic strength: presynaptic elements. *Nature Reviews. Neuroscience* 3:497–516.

Austin J, McAfee D, Armstrong D, O'Rourke M, Shearer L, Bachhawat B (1964) Low sulfatase activities in metachromatic leukodystrophy (MLD). A controlled study of enzymes in 9 living and 4 autopsied patients with MLD. *Transactions of the American Neurological Association* 89:147–50.

Avoli M (1996) GABA-mediated synchronous potentials and seizure generation. *Epilepsia* 37:1035–42.

Ballabio A, Gieselmann V (2009) Lysosomal disorders: from storage to cellular damage. *Biochimica et Biophysica Acta* 1793:684–96.

Bartos M, Alle H, Vida I (2011) Role of microcircuit structure and input integration in hippocampal interneuron recruitment and plasticity. *Neuropharmacology* 60:730–739.

Battaglia FP, Sutherland GR, McNaughton BL (2004) Hippocampal sharp wave bursts coincide with neocortical "up-state" transitions. *Learning & Memory (Cold Spring Harbor, N.Y.)* 11:697–704.

Beck H, Yaari Y (2012) *Antiepileptogenesis, Plasticity of AED Targets, Drug resistance, and Targeting the Immature Brain in Jasper's Basic Mechanisms of the Epilepsies* Oxford University Press, USA, 4th edition.

Beck M (2010) Therapy for lysosomal storage disorders. *IUBMB life* 62:33–40.

Behrens CJ, Ul Haq R, Liotta a, Anderson ML, Heinemann U (2011) Nonspecific effects of the gap junction blocker mefloquine on fast hippocampal network oscillations in the adult rat in vitro. *Neuroscience* 192:11–9.

Behrens CJ, van den Boom LP, de Hoz L, Friedman A, Heinemann U (2005) Induction of sharp wave-ripple complexes in vitro and reorganization of hippocampal networks. *Nature Neuroscience* 8:1560–7.

Belluscio MA, Mizuseki K, Schmidt R, Kempter R, Buzsaki G (2012) Cross-Frequency Phase-Phase Coupling between Theta and Gamma Oscillations in the Hippocampus. *Journal of Neuroscience* 32:423–435.

Bennett MR, Gibson WG, Robinson J (1994) Dynamics of the CA3 pyramidal neuron autoassociative memory network in the hippocampus. *Philosophical Transactions of the Royal Society of London. Series B, Biological Sciences* 343:167–87.

Berger H (1929) Über das Elektrenkephalogramm des Menschen. *Arch. Psychaitr. Nervenkr.* 87:527–570.

Biffi a, Lucchini G, Rovelli A, Sessa M (2008) Metachromatic leukodystrophy: an overview of current and prospective treatments. *Bone Marrow Transplantation* 42 Suppl 2:S2–6.

Biffi A, De Palma M, Quattrini A, Del Carro U, Amadio S, Visigalli I, Sessa M, Fasano S, Brambilla R, Marchesini S, Bordignon C, Naldini L (2004) Correction of metachromatic leukodystrophy in the mouse model by transplantation of genetically modified hematopoietic stem cells. *The Journal of Clinical Investigation* 113:1118–29.

Biffi A, Montini E, Lorioli L, Cesani M, Fumagalli F, Plati T, Baldoli C, Martino S, Calabria A, Canale S, Benedicenti F, Vallanti G, Biasco L, Leo S, Kabbara N, Zanetti G, Rizzo WB, Mehta NaL, Cicalese MP, Casiraghi M, Boelens JJ, Del Carro U, Dow DJ, Schmidt M, Assanelli A, Neduva V, Di Serio C, Stupka E, Gardner J, von Kalle C, Bordignon C, Ciceri F, Rovelli A, Roncarolo MG, Aiuti A, Sessa M, Naldini L (2013) Lentiviral hematopoietic stem cell gene therapy benefits metachromatic leukodystrophy. *Science* 341:1233158.

Blackstad TW, Brink K, Hem J, Jeune B (1970) Distribution of hippocampal mossy fibers in the rat. An experimental study with silver impregnation methods. *The Journal of Comparative Neurology* 138:433–49.

Blennow K, de Leon MJ, Zetterberg H (2006) Alzheimer's disease. *Lancet* 368:387–403.

Bosch EP, Hart MN (1978) Late adult-onset metachromatic leukodystrophy. Dementia and polyneuropathy in a 63-year-old man. *Archives of Neurology* 35:475–7.

Bragin A, Engel J, Staba RJ (2010) High-frequency oscillations in epileptic brain. *Current Opinion in Neurology* 23:151–156.

Branco T, Marra V, Staras K (2010) Examining size-strength relationships at hippocampal synapses using an ultrastructural measurement of synaptic release probability. *Journal of Structural Biology* 172:203–10.

Brown JT, Randall AD (2009) Activity-dependent depression of the spike after-depolarization generates long-lasting intrinsic plasticity in hippocampal CA3 pyramidal neurons. *The Journal of Physiology* 587:1265–81.

Brown WV, Desnick RJ, Grabowski Ga (2014) JCL Roundtable: Enzyme replacement therapy for lipid storage disorders. *Journal of Clinical Lipidology* 8:463–472.

Brun VH, Otnass MK, Molden S, Steffenach HA, Witter MP, Moser MB, Moser EI (2002) Place cells and place recognition maintained by direct entorhinal-hippocampal circuitry. *Science* 296:2243–6.

Bunsey M, Eichenbaum H (1996) Conservation of hippocampal memory function in rats and humans. *Nature* 379:255–7.

Busche MA, Eichhoff G, Adelsberger H, Abramowski D, Wiederhold KH, Haass C, Staufenbiel M, Konnerth A, Garaschuk O (2008) Clusters of hyperactive neurons near amyloid plaques in a mouse model of Alzheimer's disease. *Science* 321:1686–9.

Buzsáki G (1984) Feed-forward inhibition in the hippocampal formation. *Progress in Neurobiology* 22:131–53.

Buzsáki G (1986) Hippocampal sharp waves: their origin and significance. *Brain Research* 398:242–52.

Buzsáki G (1989) Two-stage model of memory trace formation: a role for "noisy" brain states. *Neuroscience* 31:551–70.

Buzsáki G (1998) Memory consolidation during sleep: a neurophysiological perspective. *Journal of Sleep Research* 7 Suppl 1:17–23.

Buzsáki G, Horváth Z, Urioste R, Hetke J, Wise K (1992) High-frequency network oscillation in the hippocampus. *Science* 256:1025–7.

Buzsáki G, Rappelsberger P, Kellényi L (1985) Depth profiles of hippocampal rhythmic slow activity ('theta rhythm') depend on behaviour. *Electroencephalography and Clinical Neurophysiology* 61:77–88.

Buzsáki G, Chrobak JJ (2005) Synaptic plasticity and self-organization in the hippocampus. *Nature Neuroscience* 8:1418–20.

Cartier N, Hacein-Bey-Abina S, Bartholomae CC, Veres G, Schmidt M, Kutschera I, Vidaud M, Abel U, Dal-Cortivo L, Caccavelli L, Mahlaoui N, Kiermer V, Mittelstaedt D, Bellesme C, Lahlou N, Lefrère F, Blanche S, Audit M, Payen E, Leboulch P, L'Homme B, Bougnères P, Von Kalle C, Fischer A, Cavazzana-Calvo M, Aubourg P (2009) Hematopoietic stem cell gene therapy with a lentiviral vector in X-linked adrenoleukodystrophy. *Science* 326:818–23.

Catterall WA, Catterall W, Numa S, Jan L, Jan Y, Armstrong C, Guy H, Conti F, Stühmer W, et Al., Papazian D, Timpe L, Jan Y, Jan L, Liman E, Hess P, Logothetis D, Movahedi S, Salter C, Lindpaintner K, Nadal-Ginard B, Auld V, et Al., McCormack K, et Al., Lopez G, Jan Y, Jan L, Tytgat J, Hess P, Hille B, Noda M, Suzuki H, Numa S, Stühmer W, Terlau H, et Al., Satin J, et Al., Backx P, Yue D, Lawrence J, Marban E, Tomaselli G, Heinemann S, Terlau H, Imoto K, MacKinnon R, Miller C,

MacKinnon R, Heginbotham L, Abramson T, MacKinnon R, Yellen G, Heginbotham L, MacKinnon R, Kavanaugh M, et Al., Striessnig J, Glossmann H, Catterall W, Catterall W, Striessnig J, Yellen G, Jurman M, Abramson T, MacKinnon R, Choi K, Mossman C, Aubé J, Yellen G, Hartmann H, et Al., Yool A, Schwarz T, Kirsch G, et Al., Heginbotham L, Abramson A, MacKinnon R, Heinemann S, Terlau H, Stühmer W, Imoto K, Numa S, Vassilev P, Scheuer T, Catterall W, Vassilev P, Scheuer T, Catterall W, Moorman J, Kirsch G, Brown A, Joho R, Patton D, West J, Catterall W, Goldin A, West J, et Al., Scheuer T, West J, Wang Y, Catterall W, Hoshi T, Zagotta W, Aldrich R, Zagotta W, Hoshi T, Aldrich R, Demo S, Yellen G, Isacoff E, Jan Y, Jan L, Hoshi T, Zagotta W, Aldrich R, Bezanilla F, Perozo E, Papazian D, Stefani E, Rudy B, Patton D, Isom L, Catterall W, Goldin A (1993) Structure and function of voltage-gated ion channels. *Trends in Neurosciences* 16:500–506.

Chapman PF, White GL, Jones MW, Cooper-Blacketer D, Marshall VJ, Irizarry M, Younkin L, Good MA, Bliss TV, Hyman BT, Younkin SG, Hsiao KK (1999) Impaired synaptic plasticity and learning in aged amyloid precursor protein transgenic mice. *Nature Neuroscience* 2:271–6.

Cheng H, Xu J, McKeel DW, Han X (2003) Specificity and potential mechanism of sulfatide deficiency in Alzheimer's disease: an electrospray ionization mass spectrometric study. *Cellular and Molecular Biology (Noisy-le-Grand, France)* 49:809–18.

Chi S, Qi Z (2006) Regulatory effect of sulphatides on BKCa channels. *British Journal of Pharmacology* 149:1031–8.

Chrobak JJ, Buzsáki G (1994) Selective activation of deep layer (V-VI) retrohippocampal cortical neurons during hippocampal sharp waves in the behaving rat. *The Journal of Neuroscience* 14:6160–70.

Chrobak JJ, Lörincz A, Buzsáki G (2000) Physiological patterns in the hippocampo-entorhinal cortex system. *Hippocampus* 10:457–65.

Cobb SR, Buhl EH, Halasy K, Paulsen O, Somogyi P (1995) Synchronization of neuronal activity in hippocampus by individual GABAergic interneurons. *Nature* 378:75–8.

Colgin LL (2016) Rhythms of the hippocampal network. *Nature Reviews Neuroscience* 17:239–249.

Colgin LL, Denninger T, Fyhn M, Hafting T, Bonnevie T, Jensen O, Moser MB, Moser EI (2009) Frequency of gamma oscillations routes flow of information in the hippocampus. *Nature* 462:353–7.

Connors BW, Gutnick MJ (1990) Intrinsic firing patterns of diverse neocortical neurons. *Trends in Neurosciences* 13:99–104.

Connors BW, Long Ma (2004) Electrical synapses in the mammalian brain. *Annual Review of Neuroscience* 27:393–418.

Consiglio A, Quattrini A, Martino S, Bensadoun JC, Dolcetta D, Trojani A, Benaglia G, Marchesini S, Cestari V, Oliverio A, Bordignon C, Naldini L (2001) In vivo gene therapy of metachromatic leukodystrophy by lentiviral vectors: correction of neuropathology and protection against learning impairments in affected mice. *Nature Medicine* 7:310–6.

Csicsvari J, Hirase H, Czurko A, Buzsáki G (1998) Reliability and state dependence of pyramidal cell-interneuron synapses in the hippocampus: an ensemble approach in the behaving rat. *Neuron* 21:179–89.

Csicsvari J, Hirase H, Czurkó A, Mamiya A, Buzsáki G (1999) Oscillatory coupling of hippocampal pyramidal cells and interneurons in the behaving Rat. *The Journal of Neuroscience* 19:274–87.

Csicsvari J, Hirase H, Mamiya A, Buzsáki G (2000) Ensemble patterns of hippocampal CA3-CA1 neurons during sharp wave-associated population events. *Neuron* 28:585–94.

Csicsvari J, Jamieson B, Wise KD, Buzsáki G (2003) Mechanisms of gamma oscillations in the hippocampus of the behaving rat. *Neuron* 37:311–22.

de Duve C (1963) The lysosome. *Scientific American* 208:64–72.

Deconinck N, Messaaoui A, Ziereisen F, Kadhim H, Sznajer Y, Pelc K, Nassogne MC, Vanier MT, Dan B (2008) Metachromatic leukodystrophy without arylsulfatase A deficiency: a new case of saposin-B deficiency. *European Journal of Paediatric Neurology* 12:46–50.

D'Hooge R, Van Dam D, Franck F, Gieselmann V, De Deyn PP (2001) Hyperactivity, neuromotor defects, and impaired learning and memory in a mouse model for metachromatic leukodystrophy. *Brain Research* 907:35–43.

Diba K, Buzsáki G (2007) Forward and reverse hippocampal place-cell sequences during ripples. *Nature Neuroscience* 10:1241–2.

Dierks T, Schlotawa L, Frese MA, Radhakrishnan K, von Figura K, Schmidt B (2009) Molecular basis of multiple sulfatase deficiency, mucolipidosis II/III and Niemann-Pick C1 disease - Lysosomal storage disorders caused by defects of non-lysosomal proteins. *Biochimica et Biophysica Acta* 1793:710–25.

Dodart JC, Meziane H, Mathis C, Bales KR, Paul SM, Ungerer A (1999) Behavioral disturbances in transgenic mice overexpressing the V717F beta-amyloid precursor protein. *Behavioral Neuroscience* 113:982–90.

Draguhn A, Traub RD, Schmitz D, Jefferys JG (1998) Electrical coupling underlies high-frequency oscillations in the hippocampus in vitro. *Nature* 394:189–92.

Dupret D, O'Neill J, Pleydell-Bouverie B, Csicsvari J (2010) The reorganization and reactivation of hippocampal maps predict spatial memory performance. *Nature Neuroscience* 13:995–1002.

Dyer C, Benjamins J (1991) Galactocerebroside and sulfatide independently mediate Ca2+ responses in oligodendrocytes. *Journal of Neuroscience Research* 30:699–711.

Eckhardt M (2008) The role and metabolism of sulfatide in the nervous system. *Molecular Neurobiology* 37:93–103.

Eckhardt M, Hedayati KK, Pitsch J, Lüllmann-Rauch R, Beck H, Fewou SN, Gieselmann V (2007) Sulfatide storage in neurons causes hyperexcitability and axonal degeneration in a mouse model of metachromatic leukodystrophy. *The Journal of Neuroscience* 27:9009–21.

Edwards FA, Konnerth A, Sakmann B (1990) Quantal analysis of inhibitory synaptic transmission in the dentate gyrus of rat hippocampal slices: a patch-clamp study. *The Journal of Physiology* 430:213–49.

Ellender TJ, Nissen W, Colgin LL, Mann EO, Paulsen O (2010) Priming of hippocampal population bursts by individual perisomatic-targeting interneurons. *The Journal of Neuroscience* 30:5979–91.

Ellender TJ, Paulsen O (2010) The many tunes of perisomatic targeting interneurons in the hippocampal network. *Frontiers in Cellular Neuroscience* 4:1–11.

Engel J, Bragin A, Staba R, Mody I (2009) High-frequency oscillations: what is normal and what is not? *Epilepsia* 50:598–604.

Evans WH, Martin PEM (2002) Gap junctions: structure and function (Review). *Molecular Membrane Biology* 19:121–36.

Fabelo N, Martín V, Santpere G, Marín R, Torrent L, Ferrer I, Díaz M (2011) Severe alterations in lipid composition of frontal cortex lipid rafts from Parkinson's disease and incidental Parkinson's disease. *Molecular Medicine (Cambridge, Mass.)* 17:1107–18.

Faldini E, Stroobants S, Lüllmann-Rauch R, Eckhardt M, Gieselmann V, Balschun D, D'Hooge R (2011) Telencephalic histopathology and changes in behavioural and neural plasticity in a murine model for metachromatic leukodystrophy. *Behavioural Brain Research* 222:309–14.

Foster DJ, Wilson MA (2006) Reverse replay of behavioural sequences in hippocampal place cells during the awake state. *Nature* 440:680–3.

Fredman P, Mattsson L, Andersson K, Davidsson P, Ishizuka I, Jeansson S, Månsson JE, Svennerholm L (1988) Characterization of the binding epitope of a monoclonal antibody to sulphatide. *The Biochemical Journal* 251:17–22.

Freund TF, Buzsáki G (1996) Interneurons of the hippocampus. *Hippocampus* 6:347–470.

Fukuda T, Kosaka T (2000) Gap junctions linking the dendritic network of GABAergic interneurons in the hippocampus. *The Journal of Neuroscience* 20:1519–28.

Gieselmann V (1995) Lysosomal storage diseases. *Biochimica et Biophysica Acta* 1270:103–36.

Gieselmann V, Matzner U, Hess B, Lüllmann-Rauch R, Coenen R, Hartmann D, D'Hooge R, DeDeyn P, Nagels G (1998) Metachromatic leukodystrophy: molecular genetics and an animal model. *Journal of Inherited Metabolic Disease* 21:564–74.

Gieselmann V (2008) Metachromatic leukodystrophy: genetics, pathogenesis and therapeutic options. *Acta Paediatrica (Oslo, Norway : 1992). Supplement* 97:15–21.

Girardeau G, Benchenane K, Wiener SI, Buzsáki G, Zugaro MB (2009) Selective suppression of hippocampal ripples impairs spatial memory. *Nature Neuroscience* 12:1222–3.

Golding NL, Spruston N (1998) Dendritic sodium spikes are variable triggers of axonal action potentials in hippocampal CA1 pyramidal neurons. *Neuron* 21:1189–200.

Golding NL, Staff NP, Spruston N (2002) Dendritic spikes as a mechanism for cooperative long-term potentiation. *Nature* 418:326–331.

Golomb D, Yue C, Yaari Y (2006) Contribution of persistent Na+ current and M-type K+ current to somatic bursting in CA1 pyramidal cells: combined experimental and modeling study. *Journal of Neurophysiology* 96:1912–26.

Grabowski GA (2012) Gaucher disease and other storage disorders. *Hematology / the Education Program of the American Society of Hematology. American Society of Hematology. Education Program* 2012:13–8.

Green JD, Arduini AA (1954) Hippocampal electrical activity in arousal. *Journal of Neurophysiology* 17:533–57.

Green WN, Andersen OS (1991) Surface charges and ion channel function. *Annual Review of Physiology* 53:341–59.

Grenier F, Timofeev I, Steriade M (2001) Focal synchronization of ripples (80-200 Hz) in neocortex and their neuronal correlates. *Journal of Neurophysiology* 86:1884–98.

Gulyás AI, Freund TT (2014) Generation of physiological and pathological high frequency oscillations: the role of perisomatic inhibition in sharp-wave ripple and interictal spike generation. *Current Opinion in Neurobiology* 31C:26–32.

Gustavson KH, Hagberg B (1971) The incidence and genetics of metachromatic leucodystrophy in northern Sweden. *Acta Paediatrica Scandinavica* 60:585–90.

Hafting T, Fyhn M, Molden S, Moser MB, Moser EI (2005) Microstructure of a spatial map in the entorhinal cortex. *Nature* 436:801–6.

Hagberg B (1971) Clinical aspects of globoid cell and metachromatic leukodystrophies. *Birth Defects Original Article Series* 7:103–12.

Hájos N, Karlócai MR, Németh B, Ulbert I, Monyer H, Szabó G, Erdélyi F, Freund TF, Gulyás AI (2013) Input-output features of anatomically identified CA3 neurons during hippocampal sharp wave/ripple oscillation in vitro. *The Journal of Neuroscience* 33:11677–91.

Hannun YA, Bell RM (1987) Lysosphingolipids inhibit protein kinase C: implications for the sphingolipidoses. *Science* 235:670–4.

Hannun YA, Bell RM (1989) Functions of sphingolipids and sphingolipid breakdown products in cellular regulation. *Science* 243:500–7.

Hasselmo ME, Schnell E, Barkai E (1995) Dynamics of learning and recall at excitatory recurrent synapses and cholinergic modulation in rat hippocampal region CA3. *The Journal of Neuroscience* 15:5249–62.

Heim P, Claussen M, Hoffmann B, Conzelmann E, Gärtner J, Harzer K, Hunneman DH, Köhler W, Kurlemann G, Kohlschütter A (1997) Leukodystrophy incidence in Germany. *American Journal of Medical Genetics* 71:475–8.

Hemond P, Migliore M, Ascoli GA, Jaffe DB (2009) The membrane response of hippocampal CA3b pyramidal neurons near rest: Heterogeneity of passive properties and the contribution of hyperpolarization-activated currents. *Neuroscience* 160:359–70.

Henze DA, Cameron WE, Barrionuevo G (1996) Dendritic morphology and its effects on the amplitude and rise-time of synaptic signals in hippocampal CA3 pyramidal cells. *The Journal of Comparative Neurology* 369:331–44.

Hers HG (1965) Inborn lysosomal diseases. *Gastroenterology* 48:625–33.

Hess B, Saftig P, Hartmann D, Coenen R, Lüllmann-Rauch R, Goebel HH, Evers M, von Figura K, D'Hooge R, Nagels G, De Deyn P, Peters C, Gieselmann V (1996) Phenotype of arylsulfatase A-deficient mice: relationship to human metachromatic leukodystrophy. *Proceedings of the National Academy of Sciences of the United States of America* 93:14821–6.

Hoffmann G, Grau A (2004) *Stoffwechselerkrankungen in der Neurologie* Georg Thieme Verlag KG, Stuttgart, 1st edition.

Holderith N, Lorincz A, Katona G, Rózsa B, Kulik A, Watanabe M, Nusser Z (2012) Release probability of hippocampal glutamatergic terminals scales with the size of the active zone. *Nature Neuroscience* 15:988–97.

Holtzman E (1989) *Lysosomes (Cellular Organelles)* Springer, Plenum Press,, New York, 1 edition.

Huckfinne (2010) *Inborn errors of metabolism* Wikimedia Commons; http://upload.wikimedia.org/wikipedia/commons/0/0e/Inborn_errors_of_metabolism.svg.

Huguenard JR (1996) Low-threshold calcium currents in central nervous system neurons. *AnnuaL Review of Physiology* 58:329–48.

Huizing M, Helip-Wooley A, Westbroek W, Gunay-Aygun M, Gahl WA (2008) Disorders of lysosome-related organelle biogenesis: clinical and molecular genetics. *Annual Review of Genomics and Human Genetics* 9:359–86.

Ishizuka N, Cowan WM, Amaral DG (1995) A quantitative analysis of the dendritic organization of pyramidal cells in the rat hippocampus. *The Journal of Comparative Neurology* 362:17–45.

Ishizuka N, Weber J, Amaral DG (1990) Organization of intrahippocampal projections originating from CA3 pyramidal cells in the rat. *The Journal of Comparative Neurology* 295:580–623.

Jadhav SP, Kemere C, German PW, Frank LM (2012) Awake hippocampal sharp-wave ripples support spatial memory. *Science* 336:1454–8.

Jatana M, Giri S, Singh AK (2002) Apoptotic positive cells in Krabbe brain and induction of apoptosis in rat C6 glial cells by psychosine. *Neuroscience Letters* 330:183–7.

Jeewajee A, Lever C, Burton S, O'Keefe J, Burgess N (2008) Environmental novelty is signaled by reduction of the hippocampal theta frequency. *Hippocampus* 18:340–8.

Jensen MS, Azouz R, Yaari Y (1994) Variant firing patterns in rat hippocampal pyramidal cells modulated by extracellular potassium. *Journal of Neurophysiology* 71:831–9.

Jensen MS, Yaari Y (1997) Role of intrinsic burst firing, potassium accumulation, and electrical coupling in the elevated potassium model of hippocampal epilepsy. *Journal of Neurophysiology* 77:1224–33.

Jouvet M (1969) Biogenic amines and the states of sleep. *Science* 163:32–41.

Jouvet M, Michel F, Courjon J (1959) Electric activity of the rhinencephalon during sleep in cats. [L'activité électrique du rhinencéphale au cours du sommeil chez le chat.]. *Comptes rendus des Séances de la Société de Biologie et de ses Filiales* 153:101–105.

Jung HY, Staff NP, Spruston N (2001) Action potential bursting in subicular pyramidal neurons is driven by a calcium tail current. *The Journal of Neuroscience* 21:3312–21.

Kacher Y, Golan A, Pewzner-Jung Y, Futerman AH (2007) Changes in macrophage morphology in a Gaucher disease model are dependent on CTP:phosphocholine cytidylyltransferase alpha. *Blood Cells, Molecules & Diseases* 39:124–9.

Kanamori N (1986) Hippocampal minispindle wave in the cat: the different distribution of two types of waves. *Neuroscience Research* 4:152–6.

Kano T, Inaba Y, Avoli M (2005) Periodic oscillatory activity in parahippocampal slices maintained in vitro. *Neuroscience* 130:1041–53.

Kemppainen S, Jolkkonen E, Pitkänen A (2002) Projections from the posterior cortical nucleus of the amygdala to the hippocampal formation and parahippocampal region in rat. *Hippocampus* 12:735–55.

Klausberger T, Magill PJ, Márton LF, Roberts JDB, Cobden PM, Buzsáki G, Somogyi P (2003) Brain-state- and cell-type-specific firing of hippocampal interneurons in vivo. *Nature* 421:844–8.

Klausberger T, Somogyi P (2008) Neuronal diversity and temporal dynamics: the unity of hippocampal circuit operations. *Science* 321:53–7.

Klein D, Yaghootfam A, Matzner U, Koch B, Braulke T, Gieselmann V (2009) Mannose 6-phosphate receptor-dependent endocytosis of lysosomal enzymes is increased in sulfatide-storing kidney cells. *Biological Chemistry* 390:41–8.

Knowles WD, Schwartzkroin PA (1981) Axonal ramifications of hippocampal Ca1 pyramidal cells. *The Journal of Neuroscience* 1:1236–41.

Kobayashi DT, Chen KS (2005) Behavioral phenotypes of amyloid-based genetically modified mouse models of Alzheimer's disease. *Genes, Brain, and Behavior* 4:173–96.

Kohlschütter A (2013) Lysosomal leukodystrophies: Krabbe disease and metachromatic leukodystrophy. *Handbook of Clinical Neurology* 113:1611–8.

Korkotian E, Schwarz A, Pelled D, Schwarzmann G, Segal M, Futerman AH (1999) Elevation of intracellular glucosylceramide levels results in an increase in endoplasmic reticulum density and in functional calcium stores in cultured neurons. *The Journal of Biological Chemistry* 274:21673–8.

Krägeloh-Mann I, Groeschel S, Kehrer C, Opherk K, Nägele T, Handgretinger R, Müller I (2013) Juvenile metachromatic leukodystrophy 10 years post transplant compared with a non-transplanted cohort. *Bone Marrow Transplantation* 48:369–75.

Kretz KA, Carson GS, Morimoto S, Kishimoto Y, Fluharty AL, O'Brien JS (1990) Characterization of a mutation in a family with saposin B deficiency: a glycosylation site defect. *Proceedings of the National Academy of Sciences of the United States of America* 87:2541–4.

Kreysing J, von Figura K, Gieselmann V (1990) Structure of the arylsulfatase A gene. *European Journal of Biochemistry / FEBS* 191:627–31.

Kubota D, Colgin LL, Casale M, Brucher FA, Lynch G (2003) Endogenous waves in hippocampal slices. *Journal of Neurophysiology* 89:81–9.

Kudoh T, Wenger DA (1982) Diagnosis of metachromatic leukodystrophy, Krabbe disease, and Farber disease after uptake of fatty acid-labeled cerebroside sulfate into cultured skin fibroblasts. *The Journal of Clinical Investigation* 70:89–97.

Lacaille JC, Schwartzkroin PA (1988) Stratum lacunosum-moleculare interneurons of hippocampal CA1 region. I. Intracellular response characteristics, synaptic responses, and morphology. *The Journal of Neuroscience* 8:1400–10.

Lachmann RH (2011) Enzyme replacement therapy for lysosomal storage diseases. *Current Opinion in Pediatrics* 23:588–93.

Landrieu P, Blanche S, Vanier MT, Metral S, Husson B, Sandhoff K, Fischer A (1998) Bone marrow transplantation in metachromatic leukodystrophy caused by saposin-B deficiency: a case report with a 3-year follow-up period. *The Journal of Pediatrics* 133:129–32.

Lawrence JJ, McBain CJ (2003) Interneuron diversity series: containing the detonation–feedforward inhibition in the CA3 hippocampus. *Trends in Neurosciences* 26:631–40.

Li XG, Somogyi P, Ylinen A, Buzsáki G (1994) The hippocampal CA3 network: an in vivo intracellular labeling study. *The Journal of Comparative Neurology* 339:181–208.

Lieberman AP, Puertollano R, Raben N, Slaugenhaupt S, Walkley SU, Ballabio A (2012) Autophagy in lysosomal storage disorders. *Autophagy* 8:719–30.

Lingwood D, Fisher LJ, Callahan JW, Ballantyne JS (2004) Sulfatide and Na+-K+-ATPase: a salinity-sensitive relationship in the gill basolateral membrane of rainbow trout. *The Journal of Membrane Biology* 201:77–84.

Losonczy A, Magee JC (2006) Integrative properties of radial oblique dendrites in hippocampal CA1 pyramidal neurons. *Neuron* 50:291–307.

Lozsadi DA, Larner AJ (2006) Prevalence and causes of seizures at the time of diagnosis of probable Alzheimer's disease. *Dementia and Geriatric Cognitive Disorders* 22:121–4.

Luca T, Givogri MI, Perani L, Galbiati F, Follenzi A, Naldini L, Bongarzone ER (2005) Axons mediate the distribution of arylsulfatase A within the mouse hippocampus upon gene delivery. *Molecular Therapy : the Journal of the American Society of Gene Therapy* 12:669–79.

Lugowska A, Amaral O, Berger J, Berna L, Bosshard NU, Chabas A, Fensom A, Gieselmann V, Gorovenko NG, Lissens W, Mansson JE, Marcao A, Michelakakis H, Bernheimer H, Ol'khovych NV, Regis S, Sinke R, Tylki-Szymanska A, Czartoryska B (2005) Mutations c.459+1G>A and p.P426L in the ARSA gene: prevalence in metachromatic leukodystrophy patients from European countries. *Molecular Genetics and Metabolism* 86:353–9.

Lüllmann-Rauch R, Asan E (2015) Anhang In *Taschenlehrbuch Histologie*, chapter 27, p. 745. Georg Thieme Verlag KG, Stuttgart, 5th edition.

MacVicar BA, Dudek FE (1981) Electrotonic coupling between pyramidal cells: a direct demonstration in rat hippocampal slices. *Science* 213:782–5.

Maier N, Guldenagel M, Sohl G, Siegmund H, Willecke K, Draguhn a (2002) Reduction of high-frequency network oscillations (ripples) and pathological network discharges in hippocampal slices from connexin 36-deficient mice. *The Journal of Physiology* 541:521–528.

Maier N, Nimmrich V, Draguhn A (2003) Cellular and network mechanisms underlying spontaneous sharp wave-ripple complexes in mouse hippocampal slices. *The Journal of Physiology* 550:873–87.

Major G, Larkman A, Jonas P, Sakmann B, Jack J (1994) Detailed passive cable models of whole-cell recorded CA3 pyramidal neurons in rat hippocampal slices. *The Journal of Neuroscience* 14:4613–4638.

Mann EO, Mody I (2008) The multifaceted role of inhibition in epilepsy: seizure-genesis through excessive GABAergic inhibition in autosomal dominant nocturnal frontal lobe epilepsy. *Current Opinion in Neurology* 21:155–160.

Matzner U, Hartmann D, Lüllmann-Rauch R, Coenen R, Rothert F, Månsson JE, Fredman P, D'Hooge R, De Deyn PP, Gieselmann V (2002) Bone marrow stem cell-based gene transfer in a mouse model for metachromatic leukodystrophy: effects on visceral and nervous system disease manifestations. *Gene Therapy* 9:53–63.

Matzner U, Herbst E, Hedayati KK, Lüllmann-Rauch R, Wessig C, Schröder S, Eistrup C, Möller C, Fogh J, Gieselmann V (2005) Enzyme replacement improves nervous system pathology and function in a mouse model for metachromatic leukodystrophy. *Human Molecular Genetics* 14:1139–52.

Meikle PJ, Hopwood JJ, Clague AE, Carey WF (1999) Prevalence of lysosomal storage disorders. *JAMA : the Journal of the American Medical Association* 281:249–54.

Menendez de la Prida L, Trevelyan AJ (2011) Cellular mechanisms of high frequency oscillations in epilepsy: on the diverse sources of pathological activities. *Epilepsy Research* 97:308–17.

Metz AE, Jarsky T, Martina M, Spruston N (2005) R-type calcium channels contribute to afterdepolarization and bursting in hippocampal CA1 pyramidal neurons. *The Journal of Neuroscience* 25:5763–73.

Miklyaeva EI, Dong W, Bureau A, Fattahie R, Xu Y, Su M, Fick GH, Huang JQ, Igdoura S, Hanai N, Gravel RA (2004) Late onset Tay-Sachs disease in mice with targeted disruption of the Hexa gene: behavioral changes and pathology of the central nervous system. *Brain Research* 1001:37–50.

Miles R (1990) Synaptic excitation of inhibitory cells by single CA3 hippocampal pyramidal cells of the guinea-pig in vitro. *The Journal of Physiology* 428:61–77.

Miles R, Wong RK (1986) Excitatory synaptic interactions between CA3 neurones in the guinea-pig hippocampus. *The Journal of Physiology* 373:397–418.

MLD Foundation (2013) *Homepage* 21345 Miles Drive West Linn, OR 97068-2878 USA, http://mld edition.

Molander-Melin M, Pernber Z, Franken S, Gieselmann V, Månsson JE, Fredman P (2004) Accumulation of sulfatide in neuronal and glial cells of arylsulfatase A deficient mice. *Journal of Neurocytology* 33:417–27.

Mölle M, Yeshenko O, Marshall L, Sara SJ, Born J (2006) Hippocampal sharp wave-ripples linked to slow oscillations in rat slow-wave sleep. *Journal of Neurophysiology* 96:62–70.

Moser EI, Kropff E, Moser MB (2008) Place cells, grid cells, and the brain's spatial representation system. *Annual Review of Neuroscience* 31:69–89.

Moser MB, Rowland DC, Moser EI (2015) Place cells, grid cells, and memory. *Cold Spring Harbor Perspectives in Medicine* 5:a021808.

Mueller C (2011) Control of neuronal input-output coupling by recurrent inhibition in the hippocampus Ph.D. diss., Universität Bonn.

Murthy VN, Schikorski T, Stevens CF, Zhu Y (2001) Inactivity produces increases in neurotransmitter release and synapse size. *Neuron* 32:673–82.

Nakajima S, Iwasaki S, Obata K (1962) Delayed rectification and anomalous rectification in frog's skeletal muscle membrane. *The Journal of General Physiology* 46:97–115.

Nakazawa K, Quirk MC, Chitwood RA, Watanabe M, Yeckel MF, Sun LD, Kato A, Carr CA, Johnston D, Wilson MA, Tonegawa S (2002) Requirement for hippocampal CA3 NMDA receptors in associative memory recall. *Science* 297:211–8.

Nguyen HN, Wang C, Perry DC (2002) Depletion of intracellular calcium stores is toxic to SH-SY5Y neuronal cells. *Brain Research* 924:159–66.

NIH Publication No 03-5115 (2014) *Homepage* NIH Publication No. 03-5115; Office of Communications and Public Liaison National Institute of Neurological Disorders and Stroke National Institutes of Health Bethesda, MD 20892.

NIH Publication No 05-2628 (2005) *Homepage* NIH Publication No. 05-2628; Office of Communications and Public Liaison National Institute of Neurological Disorders and Stroke National Institutes of Health Bethesda, MD 20892.

Nimmrich V, Maier N, Schmitz D, Draguhn A (2005) Induced sharp wave-ripple complexes in the absence of synaptic inhibition in mouse hippocampal slices. *The Journal of Physiology* 563:663–70.

Nishino I (2006) Autophagic vacuolar myopathy. *Seminars in Pediatric Neurology* 13:90–5.

Nixon RA, Cataldo AM (1995) The endosomal-lysosomal system of neurons: new roles. *Trends in Neurosciences* 18:489–496.

Norton W, Cammer W (1984) Isolation and charaterization of myelin In Morell P, editor, *Myelin Plenum*, pp. 147–195, New York.

O'Keefe J (1976) Place units in the hippocampus of the freely moving rat. *Experimental Neurology* 51:78–109.

O'Keefe J, Conway DH (1978) Hippocampal place units in the freely moving rat: why they fire where they fire. *Experimental Brain Research. Experimentelle Hirnforschung. Expérimentation cérébrale* 31:573–90.

O'Keefe J, Dostrovsky J (1971) The hippocampus as a spatial map. Preliminary evidence from unit activity in the freely-moving rat. *Brain Research* 34:171–5.

O'Keefe J, Recce ML (1993) Phase relationship between hippocampal place units and the EEG theta rhythm. *Hippocampus* 3:317–30.

Ólafsdóttir HF, Carpenter F, Barry C (2016) Coordinated grid and place cell replay during rest. *Nature Neuroscience* 19:792–4.

O'Neill J, Pleydell-Bouverie B, Dupret D, Csicsvari J (2010) Play it again: reactivation of waking experience and memory. *Trends in Neurosciences* 33:220–9.

O'Neill J, Senior T, Csicsvari J (2006) Place-selective firing of CA1 pyramidal cells during sharp wave/ripple network patterns in exploratory behavior. *Neuron* 49:143–55.

Opitz T, Richter P, Carter A, Kozikowski A, Shinozaki H, Reymann K (1995) Metabotropic glutamate receptor subtypes differentially influence neuronal recovery from in vitro hypoxia/hypoglycemia in rat hippocampal slices. *Neuroscience* 68:989–1001.

Pais I, Hormuzdi SG, Monyer H, Traub RD, Wood IC, Buhl EH, Whittington MA, LeBeau FEN (2003) Sharp wave-like activity in the hippocampus in vitro in mice lacking the gap junction protein connexin 36. *Journal of Neurophysiology* 89:2046–54.

Palop JJ, Chin J, Roberson ED, Wang J, Thwin MT, Bien-Ly N, Yoo J, Ho KO, Yu GQ, Kreitzer A, Finkbeiner S, Noebels JL, Mucke L (2007) Aberrant excitatory neuronal activity and compensatory remodeling of inhibitory hippocampal circuits in mouse models of Alzheimer's disease. *Neuron* 55:697–711.

Papatheodoropoulos C (2008) A possible role of ectopic action potentials in the in vitro hippocampal sharp wave-ripple complexes. *Neuroscience* 157:495–501.

Papatheodoropoulos C, Kostopoulos G (2002) Spontaneous, low frequency (approximately 2-3 Hz) field activity generated in rat ventral hippocampal slices perfused with normal medium. *Brain Research Bulletin* 57:187–93.

Parton RG, Dotti CG (1993) Cell biology of neuronal endocytosis. *Journal of Neuroscience Research* 36:1–9.

Parton RG, Simons K, Dotti CG (1992) Axonal and dendritic endocytic pathways in cultured neurons. *The Journal of Cell Biology* 119:123–37.

Pavlides C, Winson J (1989) Influences of hippocampal place cell firing in the awake state on the activity of these cells during subsequent sleep episodes. *The Journal of Neuroscience* 9:2907–18.

Perreault P, Avoli M (1989) Effects of low concentrations of 4-aminopyridine on CA1 pyramidal cells of the hippocampus. *Journal of Neurophysiology* 61:953–70.

Pikkarainen M, Rönkkö S, Savander V, Insausti R, Pitkänen A (1999) Projections from the lateral, basal, and accessory basal nuclei of the amygdala to the hippocampal formation in rat. *The Journal of Comparative Neurology* 403:229–60.

Pinault D, Pumain R (1989) Antidromic firing occurs spontaneously on thalamic relay neurons: triggering of somatic intrinsic burst discharges by ectopic action potentials. *Neuroscience* 31:625–37.

Pinault D (1995) Backpropagation of action potentials generated at ectopic axonal loci: hypothesis that axon terminals integrate local environmental signals. *Brain Research Reviews* 21:42–92.

Poirazi P, Mel BW (2001) Impact of active dendrites and structural plasticity on the memory capacity of neural tissue. *Neuron* 29:779–96.

Poorthuis BJ, Wevers RA, Kleijer WJ, Groener JE, de Jong JG, van Weely S, Niezen-Koning KE, van Diggelen OP (1999) The frequency of lysosomal storage diseases in The Netherlands. *Human Genetics* 105:151–6.

Pouille F, Scanziani M (2001) Enforcement of temporal fidelity in pyramidal cells by somatic feed-forward inhibition. *Science* 293:1159–63.

Pouille F, Marin-Burgin A, Adesnik H, Atallah BV, Scanziani M (2009) Input normalization by global feedforward inhibition expands cortical dynamic range. *Nature Neuroscience* 12:1577–85.

Poupetová H, Ledvinová J, Berná L, Dvoráková L, Kozich V, Elleder M (2010) The birth prevalence of lysosomal storage disorders in the Czech Republic: comparison with data in different populations. *Journal of Inherited Metabolic Disease* 33:387–96.

Rafi MA, Zhang XL, DeGala G, Wenger DA (1990) Detection of a point mutation in sphingolipid activator protein-1 mRNA in patients with a variant form of metachromatic leukodystrophy. *Biochemical and Biophysical Research Communications* 166:1017–23.

Reimer RJ, Fon EA, Edwards RH (1998) Vesicular neurotransmitter transport and the presynaptic regulation of quantal size. *Current Opinion in Neurobiology* 8:405–12.

Remy S, Spruston N (2007) Dendritic spikes induce single-burst long-term potentiation. *Proceedings of the National Academy of Sciences of the United States of America* 104:17192–7.

Résibois A (1971) Electron microscopic studies of metachromatic leucodystrophy. IV. Liver and kidney alterations. *Pathologia Europaea* 6:278–98.

Sandhoff K, Kolter T, Harzer K (2001) Sphingolipid activator proteins In Scriver C, Beaudet A, Sly W, Valle D, Childs B, Kinzler K, Vogelstein B, editors, *The Metabolic and Molecular Bases of Inherited Diseases*, pp. 3371–3388. New York, McGraw-Hill, 8th edition.

Sandhoff R, Hepbildikler ST, Jennemann R, Geyer R, Gieselmann V, Proia RL, Wiegandt H, Grone HJ (2002) Kidney sulfatides in mouse models of inherited glycosphingolipid disorders: determination by nano-electrospray ionization tandem mass spectrometry. *The Journal of Biological Chemistry* 277:20386–98.

Saravanan K, Schaeren-Wiemers N, Klein D, Sandhoff R, Schwarz A, Yaghootfam A, Gieselmann V, Franken S (2004) Specific downregulation and mistargeting of the lipid raft-associated protein MAL in a glycolipid storage disorder. *Neurobiol Dis.* 16:396–406.

Scharfman HE (2007) The CA3 "backprojection" to the dentate gyrus. *Progress in Brain Research* 163:627–37.

Schikorski T, Stevens CF (1997) Quantitative ultrastructural analysis of hippocampal excitatory synapses. *The Journal of Neuroscience* 17:5858–67.

Schiller J, Major G, Koester HJ, Schiller Y (2000) NMDA spikes in basal dendrites of cortical pyramidal neurons. *Nature* 404:285–9.

Schlingloff D, Káli S, Freund TF, Hájos N, Gulyás AI (2014) Mechanisms of sharp wave initiation and ripple generation. *The Journal of Neuroscience* 34:11385–98.

Schmandt T, Goßrau G, Kischlat T, Opitz T, Brüstle O (2006) Animal models for cell and gene therapy in myelin disease. *Drug Discovery Today: Disease Models* 3:349–358.

Schmidt-Hieber C, Jonas P, Bischofberger J (2008) Action potential initiation and propagation in hippocampal mossy fibre axons. *The Journal of Physiology* 586:1849–57.

Schmitz D, Schuchmann S, Fisahn A, Draguhn A, Buhl EH, Petrasch-Parwez E, Dermietzel R, Heinemann U, Traub RD (2001) Axo-axonal coupling. a novel mechanism for ultrafast neuronal communication. *Neuron* 31:831–40.

Schott I, Hartmann D, Gieselmann V, Lüllmann-Rauch R (2001) Sulfatide storage in visceral organs of arylsulfatase A-deficient mice. *Virchows Archiv : an international Journal of Pathology* 439:90–6.

Schwartzkroin PA, Prince DA (1977) Penicillin-induced epileptiform activity in the hippocampal in vitro prepatation. *Annals of Neurology* 1:463–9.

Schwartzkroin PA, Prince DA (1978) Cellular and field potential properties of epileptogenic hippocampal slices. *Brain Research* 147:117–30.

Schwartzkroin PA, Prince DA (1980) Changes in excitatory and inhibitory synaptic potentials leading to epileptogenic activity. *Brain Research* 183:61–76.

Sekerli M, Del Negro CA, Lee RH, Butera RJ (2004) Estimating action potential thresholds from neuronal time-series: new metrics and evaluation of methodologies. *IEEE transactions on Bio-Medical Engineering* 51:1665–72.

Sevin C, Benraiss A, Van Dam D, Bonnin D, Nagels G, Verot L, Laurendeau I, Vidaud M, Gieselmann V, Vanier M, De Deyn PP, Aubourg P, Cartier N (2006) Intracerebral adeno-associated virus-mediated gene transfer in rapidly progressive forms of metachromatic leukodystrophy. *Human Molecular Genetics* 15:53–64.

Shapiro EG, Lockman LA, Balthazor M, Krivit W (1995) Neuropsychological outcomes of several storage diseases with and without bone marrow transplantation. *Journal of Inherited Metabolic Disease* 18:413–29.

Shapiro EG, Lockman LA, Knopman D, Krivit W (1994) Characteristics of the dementia in late-onset metachromatic leukodystrophy. *Neurology* 44:662–5.

Shapiro LJ, Aleck KA, Kaback MM, Itabashi H, Desnick RJ, Brand N, Stevens RL, Fluharty AL, Kihara H (1979) Metachromatic leukodystrophy without arylsulfatase A deficiency. *Pediatric Research* 13:1179–81.

Shirvalkar PR, Rapp PR, Shapiro ML (2010) Bidirectional changes to hippocampal theta-gamma comodulation predict memory for recent spatial episodes. *Proceedings of the National Academy of Sciences of the United States of America* 107:7054–9.

Siapas AG, Wilson MA (1998) Coordinated interactions between hippocampal ripples and cortical spindles during slow-wave sleep. *Neuron* 21:1123–8.

Simons K, Ikonen E (1997) Functional rafts in cell membranes. *Nature* 387:569–72.

Simons K, Toomre D (2000) Lipid rafts and signal transduction. *Nature Reviews. Molecular Cell Biology* 1:31–9.

Simons K, Vaz WLC (2004) Model systems, lipid rafts, and cell membranes. *Annual Review of Biophysics and Biomolecular Structure* 33:269–95.

Sirota A, Csicsvari J, Buhl D, Buzsáki G (2003) Communication between neocortex and hippocampus during sleep in rodents. *Proceedings of the National Academy of Sciences of the United States of America* 100:2065–9.

Softky W (1994) Sub-millisecond coincidence detection in active dendritic trees. *Neuroscience* 58:13–41.

Somogyi P (1977) A specific 'axo-axonal' interneuron in the visual cortex of the rat. *Brain Research* 136:345–50.

Souillet G, Guffon N, Maire I, Pujol M, Taylor P, Sevin F, Bleyzac N, Mulier C, Durin A, Kebaili K, Galambrun C, Bertrand Y, Froissart R, Dorche C, Gebuhrer L, Garin C, Berard J, Guibaud P (2003) Outcome of 27 patients with Hurler's syndrome transplanted from either related or unrelated haematopoietic stem cell sources. *Bone Marrow Transplantation* 31:1105–17.

Spruston N, Johnston D (1992) Perforated patch-clamp analysis of the passive membrane properties of three classes of hippocampal neurons. *Journal of Neurophysiology* 67:508–29.

Spruston N (2001) Axonal Gap Junctions Send Ripples through the Hippocampus. *Neuron* 31:669–671.

Spruston N (2008) Pyramidal neurons: dendritic structure and synaptic integration. *Nature Reviews. Neuroscience* 9:206–21.

Squire LR (1992) Memory and the hippocampus: a synthesis from findings with rats, monkeys, and humans. *Psychological Review* 99:195–231.

Squire LR, Stark CEL, Clark RE (2004) The medial temporal lobe. *Annual Review of Neuroscience* 27:279–306.

Staba RJ, Frighetto L, Behnke EJ, Mathern GW, Fields T, Bragin A, Ogren J, Fried I, Wilson CL, Engel J (2007) Increased fast ripple to ripple ratios correlate with reduced hippocampal volumes and neuron loss in temporal lobe epilepsy patients. *Epilepsia* 48:2130–8.

Staff NP, Jung HY, Thiagarajan T, Yao M, Spruston N (2000) Resting and active properties of pyramidal neurons in subiculum and CA1 of rat hippocampus. *Journal of Neurophysiology* 84:2398–408.

Stasheff SF, Wilson WA (1990) Increased ectopic action potential generation accompanies epileptogenesis in vitro. *Neuroscience Letters* 111:144–50.

Steffenach HA, Sloviter RS, Moser EI, Moser MB (2002) Impaired retention of spatial memory after transection of longitudinally oriented axons of hippocampal CA3 pyramidal cells. *Proceedings of the National Academy of Sciences* 99:3194–3198.

Steward O, Scoville SA (1976) Cells of origin of entorhinal cortical afferents to the hippocampus and fascia dentata of the rat. *The Journal of Comparative Neurology* 169:347–70.

Stroobants S, Leroy T, Eckhardt M, Aerts JM, Berckmans D, D'Hooge R (2008) Early signs of neurolipidosis-related behavioural alterations in a murine model of metachromatic leukodystrophy. *Behavioural Brain Research* 189:306–16.

Su H, Alroy G, Kirson ED, Yaari Y (2001) Extracellular calcium modulates persistent sodium current-dependent burst-firing in hippocampal pyramidal neurons. *The Journal of Neuroscience* 21:4173–82.

Suh J, Foster DJ, Davoudi H, Wilson MA, Tonegawa S (2013) Impaired hippocampal ripple-associated replay in a mouse model of schizophrenia. *Neuron* 80:484–93.

Suzuki M, Sugimoto Y, Ohsaki Y, Ueno M, Kato S, Kitamura Y, Hosokawa H, Davies JP, Ioannou YA, Vanier MT, Ohno K, Ninomiya H (2007) Endosomal accumulation of Toll-like receptor 4 causes constitutive secretion of cytokines and activation of signal transducers and activators of transcription in Niemann-Pick disease type C (NPC) fibroblasts: a potential basis for glial cell activation in. *The Journal of Neuroscience* 27:1879–91.

Suzuki SS, Smith GK (1988) Spontaneous EEG spikes in the normal hippocampus. II. Relations to synchronous burst discharges. *Electroencephalography and Clinical Neurophysiology* 69:532–40.

Tanaka K, Webster HD (1993) Effects of psychosine (galactosylsphingosine) on the survival and the fine structure of cultured Schwann cells. *Journal of Nuropathology and Experimental Neurology* 52:490–8.

Taylor CP, Dudek FE (1982) Synchronous neural afterdischarges in rat hippocampal slices without active chemical synapses. *Science* 218:810–2.

Taylor C, Marta C, Bansal R, Pfeiffer S (2004) The transport, assembly, and function of myelin lipids In Lazzarini R, editor, *Myelin Biology and Disorders. vol. 1. Academic*, pp. 57–88, New York.

Tempesta MC, Salvayre R, Levade T (1994) Functional compartments of sulphatide metabolism in cultured living cells: evidence for the involvement of a novel sulphatide-degrading pathway. *The Biochemical Journal* 297 (Pt 3:479–89.

Thome C, Kelly T, Yanez A, Schultz C, Engelhardt M, Cambridge SB, Both M, Draguhn A, Beck H, Egorov AV (2014) Axon-carrying dendrites convey privileged synaptic input in hippocampal neurons. *Neuron* 83:1418–30.

Toda Ki, Kobayashi T, Goto I, Ohno K, Eto T, Inui S, Okada S (1990) Lysosulfatide (Sulfogalactosylsphingosine) Accumulation in Tissues from Patients with Metachromatic Leukodystrophy. *Neurochemistry* 55:1585–1591.

Torborg CL, Nakashiba T, Tonegawa S, McBain CJ (2010) Control of CA3 output by feedforward inhibition despite developmental changes in the excitation-inhibition balance. *The Journal of Neuroscience* 30:15628–37.

Traub RD, Bibbig A (2000) A model of high-frequency ripples in the hippocampus based on synaptic coupling plus axon-axon gap junctions between pyramidal neurons. *The Journal of Neuroscience* 20:2086–93.

Traub RD, Miles R (1995) Pyramidal cell-to-inhibitory cell spike transduction explicable by active dendritic conductances in inhibitory cell. *Journal of Computational Neuroscience* 2:291–8.

Treves A, Rolls ET (1992) Computational constraints suggest the need for two distinct input systems to the hippocampal CA3 network. *Hippocampus* 2:189–199.

Treviño M, Vivar C, Gutiérrez R (2011) Excitation-inhibition balance in the CA3 network–neuronal specificity and activity-dependent plasticity. *The European Journal of Neuroscience* 33:1771–85.

Tsukita S, Ishikawa H (1980) The movement of membranous organelles in axons. Electron microscopic identification of anterogradely and retrogradely transported organelles. *The Journal of Cell Biology* 84:513–30.

Tukker JJ, Fuentealba P, Hartwich K, Somogyi P, Klausberger T (2007) Cell Type-Specific Tuning of Hippocampal Interneuron Firing during Gamma Oscillations In Vivo. *Journal of Neuroscience* 27:8184–8189.

Vainio S, Bykov I, Hermansson M, Jokitalo E, Somerharju P, Ikonen E (2005) Defective insulin receptor activation and altered lipid rafts in Niemann-Pick type C disease hepatocytes. *The Biochemical Journal* 391:465–72.

van Zyl R, Gieselmann V, Eckhardt M (2010) Elevated sulfatide levels in neurons cause lethal audiogenic seizures in mice. *Journal of Neurochemistry* 112:282–95.

Vanderwolf CH (1969) Hippocampal electrical activity and voluntary movement in the rat. *Electroencephalography and Clinical Neurophysiology* 26:407–18.

von Figura K, Gieselmann V, Jaeken J (2001) Metachromatic Leukodystrophy In Scriver C, Beaudet A, Valle D, Sly W, Childs B, Kinzler K, Vogelstein B, editors, *The Metabolic and Molecular Bases of Inherited Diseases*, chapter 148, pp. 2693–2740. New York, McGraw-Hill, 8th edition.

Walkley SU, Sikora J, Micsenyi M, Davidson C, Dobrenis K (2010) Lysosomal compromise and brain dysfunction: examining the role of neuroaxonal dystrophy. *Biochemical Society Transactions* 38:1436–41.

Wang ZW (2010) Origin of quantal size variation and high-frequency miniature postsynaptic currents at the Caenorhabditis elegans neuromuscular junction. *The Journal of Neuroscience Research* 88:3425–32.

Wenger DA, Luzi P, Rafi MA (2013) Lysosomal storage diseases: heterogeneous group of disorders. *BioImpacts : BI* 3:145–7.

Westenbroek RE, Ahlijanian MK, Catterall WA (1990) Clustering of L-type Ca2+ channels at the base of major dendrites in hippocampal pyramidal neurons. *Nature* 347:281–4.

Willecke K, Eiberger J, Degen J, Eckardt D, Romualdi A, Güldenagel M, Deutsch U, Söhl G (2002) Structural and functional diversity of connexin genes in the mouse and human genome. *Biological Chemistry* 383:725–37.

Williams S, Samulack DD, Beaulieu C, LaCaille JC (1994) Membrane properties and synaptic responses of interneurons located near the stratum lacunosum-moleculare/radiatum border of area CA1 in whole-cell recordings from rat hippocampal slices. *Journal of Neurophysiology* 71:2217–35.

Wilson MA, McNaughton BL (1994) Reactivation of hippocampal ensemble memories during sleep. *Science* 265:676–9.

Witte F (1921) Ueber pathologische Abbauvorgaenge im Zentralnervensystem. *Muench Med Wochenschr* 68:69.

Witter MP (1993) Organization of the entorhinal-hippocampal system: a review of current anatomical data. *Hippocampus* 3 Spec No:33–44.

Witter MP, Groenewegen HJ, Lopes da Silva FH, Lohman AH (1989) Functional organization of the extrinsic and intrinsic circuitry of the parahippocampal region. *Progress in Neurobiology* 33:161–253.

Wittke D, Hartmann D, Gieselmann V, Lüllmann-Rauch R (2004) Lysosomal sulfatide storage in the brain of arylsulfatase A-deficient mice: cellular alterations and topographic distribution. *Acta neuropathologica* 108:261–71.

Wong RK, Prince DA (1978) Participation of calcium spikes during intrinsic burst firing in hippocampal neurons. *Brain Research* 159:385–90.

Wong RK, Prince DA (1981) Afterpotential generation in hippocampal pyramidal cells. *Journal of Neurophysiology* 45:86–97.

Wouterlood FG, Saldana E, Witter MP (1990) Projection from the nucleus reuniens thalami to the hippocampal region: light and electron microscopic tracing study in the rat with the anterograde tracer Phaseolus vulgaris-leucoagglutinin. *The Journal of Comparative Neurology* 296:179–203.

Yaari Y, Yue C, Su H (2007) Recruitment of apical dendritic T-type Ca2+ channels by backpropagating spikes underlies de novo intrinsic bursting in hippocampal epileptogenesis. *The Journal of Physiology* 580:435–50.

Yaghootfam A, Gieselmann V, Eckhardt M (2005) Delay of myelin formation in arylsulphatase A-deficient mice. *The European Journal of Neuroscience* 21:711–20.

Yamamoto J, Suh J, Takeuchi D, Tonegawa S (2014) Successful execution of working memory linked to synchronized high-frequency gamma oscillations. *Cell* 157:845–57.

Ylinen A, Bragin A, Nádasdy Z, Jandó G, Szabó I, Sik A, Buzsáki G (1995) Sharp wave-associated high-frequency oscillation (200 Hz) in the intact hippocampus: network and intracellular mechanisms. *The Journal of Neuroscience* 15:30–46.

Yue C (2004) KCNQ/M Channels Control Spike Afterdepolarization and Burst Generation in Hippocampal Neurons. *The Journal of Neuroscience* 24:4614–4624.

Yue C (2006) Axo-Somatic and Apical Dendritic Kv7/M Channels Differentially Regulate the Intrinsic Excitability of Adult Rat CA1 Pyramidal Cells. *Journal of Neurophysiology* 95:3480–3495.

Yue C, Remy S, Su H, Beck H, Yaari Y (2005) Proximal persistent Na+ channels drive spike afterdepolarizations and associated bursting in adult CA1 pyramidal cells. *The Journal of Neuroscience* 25:9704–20.

Zaka M, Wenger DA (2004) Psychosine-induced apoptosis in a mouse oligodendrocyte progenitor cell line is mediated by caspase activation. *Neuroscience Letters* 358:205–9.

Zheng C, Bieri KW, Trettel SG, Colgin LL (2015) The relationship between gamma frequency and running speed differs for slow and fast gamma rhythms in freely behaving rats. *Hippocampus* 25:924–938.

Zlotogora J, Bach G, Bösenberg C, Barak Y, von Figura K, Gieselmann V (1995) Molecular basis of late infantile metachromatic leukodystrophy in the Habbanite Jews. *Human Mutation* 5:137–43.